Cranfield University

School of Applied Sciences

Department of Natural Resources

PhD

2010

Audrey Versteegen

Biotic and Abiotic Controls on Calcium Carbonate Formation in Soils

Supervisors:

Prof. Guy Kirk (Cranfield University)

Prof. Karl Ritz (Cranfield University)

Dr. Antoni Milodowski (British Geological Survey)

Abstract

Over half of the carbon (C) taking part in the global C cycle is held in terrestrial systems. Because of the sensitivity of the C cycle to changes in such soil-based pools of carbon, it is important to understand the basic mechanisms by which soil C is stored and cycled between the range of different pools which occur belowground. In the context of climate change mitigation, it is considered that increasing soil-based stocks of C, either by reducing losses from soils, or by actively sequestering new carbon, is a potentially important strategy . Organic carbon is the main form of carbon in soil and as such has received most focus. However, significant amounts of carbon occur in an inorganic form, mainly as calcium carbonate ($CaCO_3$). $CaCO_3$ is one of the most widespread minerals on Earth, it covers over 13% of its surface and is involved in many environmental biogeochemical cycles. However, to use $CaCO_3$ formation to "geoengineer the climate" requires a better understanding of the factors governing $CaCO_3$ precipitation in soils.

Secondary $CaCO_3$ is a common feature of soils in arid and semi-arid regions, where evapotranspiration exceeds rainfall for long periods of the year. The rate of formation of secondary $CaCO_3$ in temperate soils is much slower, but there is potential to increase it. This study aimed to quantitatively understand the mechanisms of $CaCO_3$ formation in temperate soils and the role played by soil microbes in mediating such processes: the morphology of some contemporary $CaCO_3$ deposits in temperate soils indicates a biological origin, including network-like structures that suggest a fungal basis. Such observations also suggest that $CaCO_3$ precipitation may affect

other soil properties such as porosity, structural stability and biotic activity.

The rate of $CaCO_3$ precipitation in soils depends on: (i) the concentration of reactants in the soil solution; (ii) the presence and concentration of potential inhibitors of the reaction; (iii) the presence and availability of suitable nucleation sites for precipitation; (iv) the rate of delivery of the reactants and inhibitors to precipitation sites by diffusion through the soil structure.

Each of these factors may depend on biological processes in the soil as well as physicochemical conditions, and was studied in controlled experimental systems. Rates of $CaCO_3$ precipitation were first measured in shaken suspensions of four soils under controlled CO_2 partial pressures. Concentration-distance profiles of Ca^{2+} (in solution and as precipitated $CaCO_3$) and pH were then measured in columns of moist soil exposed to a source of HCO_3^- ions at one end, to account for diffusion through the soil structure. The results of the experiments were used to validate a model of $CaCO_3$ formation, which allows for movement of Ca^{2+} and OH^- ions to a nucleation site by acid-base transfer, mainly from atmospheric CO_2 dissolved in solution. It was found that the precipitation of $CaCO_3$ in soils obeyed the same basic principles as in aqueous media, and the movement of ions in a zone of $CaCO_3$ precipitation could be explained by a diffusion model with the physicochemical properties of the soils studied as parameters. The rate of $CaCO_3$ precipitation was influenced by the constraints put on the diffusion of reactants through the soil pore network, but possibly even more so by the availability of suitable reaction sites. This study highlighted the important role played by soil microbes in the transport of reactants through respiratory production of CO_2, but also potentially in providing nucleation surfaces.

To investigate the effects of soil microbial communities on $CaCO_3$ formation, the same measurements were made in the grassland soil containing manipulated communities, either by sterilisation or in which either eukaryotes or prokaryotes were inhibited using specific biocides. The amount of precipitation was found to be affected by the presence of either microbial community compared to a sterile system, stipulated to be both due to the presence of CO_2 facilitating acid-base transfers, and the availability of microbial surfaces playing the role of heterogeneous

nucleation sites for the formation of $CaCO_3$ crystals in the presence of DOC inhibiting homogeneous crystal growth. The predominance of either bacterial of fungal communities was also found to affect the morphology of crystal formed, potentially due to different spatial distribution of CO_2 and availability of nucleation surfaces between the two systems, leading to competition for reactants and thus different rates of $CaCO_3$ precipitation.

This study demonstrates the crucial roles that CO_2 partial pressure, soil structure and texture, and microbial communities play in governing $CaCO_3$ precipitation in soils.

Acknowledgements

Along the three years the production of this document took, a myriad of people advised, encouraged, interfered and helped.

First and foremost, my supervisors of course, for the continued support and guidance, professionally as well as in times of moral wobble. Tony, a special thank you for making the British Geological Survey laboratories so easily available, microbiology would not have been or looked as thrilling without the days of ESEM exploration.
Equally, many grateful thanks to Richard, Maria, Sue and Jan, the Soil and Water laboratory staff here in Cranfield, for being so helpful, accommodating and sometimes downright entertaining on those long slicing days.

With less scientific input, but of equal importance, I have to mention Tony and the whole Campus Security team, for rescuing me from many blaring alarms, locked doors and immobilised cars. To the guys in the CSA for providing much needed escapism throughout, Kartik and Akarsh in particular for curries and Himalayan dreams.

In the last few months especially, I can't be thankful enough to those who stuck around, whether they understood or not. To Graham, for never letting me go without a treat and some brain food, Jenny and Richard for the warm welcomes and reassuring conversations.
Jack, always there, thank you for reminding me of what is to come, and continuously dreaming forward. Mel and Laura for the never-failing abundance of smiles, hugs and kind words. Pup&Mum for always having time to worry about me, and Neirou and Maud my amazing sisters for egging me on quietly, applying subatomic hindsight to my crystals..

Contents

List of Figures

List of Tables

Chapter 1

Introduction

1.1 Inorganic carbon in soils

The global carbon cycle conveys ca. 210 Gt of carbon per year, of which more than 120 Gt are transported between the atmosphere and the terrestrial system, where it is mainly held in soils (Dupre et al., 2003). The global carbon balance is thus sensitive to any changes in soil carbon (Royal Society, 2001). There is currently much effort to increase soil carbon, whether by reducing emissions or by actively sequestering new carbon (Royal Society, 2001). This has focused on organic forms of carbon, they being the main forms in most soils. However, significant amounts also occur in inorganic forms, mainly as various calcium carbonate ($CaCO_3$) and calcium magnesium carbonates ($CaMg(CO_3)_2$) (Burford et al., 2006).

Carbonates are amongst the most common and most reactive minerals on Earth (Warren et al., 2001; Lin and Singer, 2005a). As well as forming an important reservoir of the Earth's carbon, they play a vital role in the cycling and transport of numerous elements between the oceans, soils and the atmosphere. In the soil environment, they are present on over 13% of the Earth's surface, and there is now interest in how that might be manipulated.

The possibility of increasing the sequestration of atmospheric CO_2 in soils by increasing inorganic carbon precipitation is one of the main ideas in "geoengineering the climate" (Royal Society, 2009). Weathering of silicates to carbonates is the main control on atmospheric CO_2 on geological timescales. Thus the idea is to enhance weathering of silicate rocks by applying finely-divided silicate rocks to soils in excess of acidifying processes, so that the base (i.e. Brønsted base, capable of neutralizing H^+ ions) in the silicates is transformed to carbonates in the soil, or ultimately in the deep ocean. For example, for the simple olivine Mg_2SiO_4:

$$Mg_2SiO_4 + 4CO_2 + 4H_2O = 2Mg^{2+} + 4HCO_3^- + H_4SiO_4 = 2MgCO_3 + 2CO_2 + SiO_2 + 4H_2O$$

or for $CaSiO_3$:

$$CaSiO_3 + 2CO_2 + 3H_2O = Ca^{2+} + 2HCO_3^- + H_4SiO_4 = CaCO_3 + CO_2 + SiO_2 + 3H_2O$$

The potential scope for this on a wide scale is debated (Schuiling and Krijgsman, 2006; Hartmann and Kempe, 2008). That aside, its ecological consequences for soils, the land surface and seas are highly uncertain.

However, on a smaller scale, there may be a significant potential for avoiding carbon emissions from soils by replacing agricultural lime applications with ground silicates (Whitmore et al., 2010). Liming to balance soil acidity releases one mole of CO_2 to the atmosphere per two moles of acid (i.e. H^+) neutralised:

$$CaCO_3 + 2H^+ = Ca^{2+} + CO_2 + H_2O$$

Whereas, with silicates there would be no CO_2 release, e.g. for Mg_2SiO_4:

$$Mg_2SiO_4 + 4H^+ = 2Mg^{2+} + H_4SiO_4$$

Whitmore et al. (2010) estimate that substituting silicates for lime in England and Wales could save close to 1 million t CO_2-C per annum. Data compiled by Manning (2008) and Renforth et al. (2009) indicate there are many times the required amounts of silicate wastes available from various sources across England and Wales, including wastes from igneous rock quarry fines, concrete demolition, slags and fly ash.

However, the mechanisms and controls on carbonate formation in soils are poorly understood.

The role of microorganisms in $CaCO_3$ transformation and weathering, leading to calcium carbonate secondary depositions, is becoming increasingly acknowledged (Verrecchia and Verrechia, 1994; Gadd, 2007). The structure and morphology of recent $CaCO_3$ deposits in soils suggest a biological origin, and in many cases, calcium carbonate structures have been associated with biological activity, in the vicinity of plant roots in particular.

Quantitatively describing the conditions of secondary calcium carbonate formation will be of further significance to better understand the mechanisms involved in soils adaptation to environmental changes and the role they could play in eventual mitigation scenarios.

Biomineralisation is also suggested as having potential applications as a soil improvement technique in civil engineering and soil erosion control. Bacterially induced carbonate precipitation in aqueous environments has also recently risen interest because of its possible interest to bioremediate contaminated groundwaters and aquifers. Indeed, the ability of microorganisms to start the precipitation of geochemically reactive minerals can have potential for contaminant bioremediation through sequestration of divalent minerals or radionucleides, such as Cu^{2+} and Sr^{2+} (Fujita et al., 2000; Warren et al., 2001; Ettler et al., 2006).

However, the consequences of precipitated calcium carbonate on the structure of contemporary soils has been reported in the literature (DeJong et al., 2006; Whiffin et al., 2007), so that efforts to stimulate $CaCO_3$ precipitation in soils to sequester carbon, or other beneficial ends, may affect other soil properties such as porosity, structural stability and biotic activity.

1.2 The chemistry of calcium carbonate precipitation

1.2.1 The carbonate system

The principal form of soil inorganic carbon are the compounds of the carbonate system, namely carbon dioxide ($CO_{2_{(g)}}$ and $CO_{2_{(aq)}}$), carbonic acid (H_2CO_3), and bicarbonate ($H_2CO_3^-$) and carbonate (CO_3^{2-}) ions. Carbonate ions are essential to the cycling of major and trace elements, in that they associate with a wide range of other metallic ions such as calcium, magnesium, sodium or potassium, as well as protons in the acid forms, bicarbonate and carbonic acid. Carbonate minerals are found everywhere on Earth and influence major environmental biogeochemical processes.

Atmospheric CO_2 is soluble in water: at room temperature, the solubility of carbon dioxide is about 90 cm^3 of CO_2 in 100 ml water. $CO_{2_{(g)}}$ in air equilibrates with atmospheric CO_2 partial pressure more or less rapidly, and the equilibrium distribution between air and solution is described by Henry's law:

$$[CO_{2_{(aq)}}] = K_H P_{CO_2}$$

where K_H is Henry's law constant. Dissolved CO_2 then reacts with water to form carbonic acid according to Equation (1.b). Depending on the solution pH (see Figure 1.1), carbonic acid deprotonates to HCO_3^- or CO_3^{2-}, following Equations (1.c) and (1.d).

$$CO_2 + H_2O \rightleftharpoons H_2CO_3 \tag{1.a}$$

$$H_2CO_3 \rightleftharpoons HCO_3^- + H^+ \qquad K_1 = \frac{(H^+)(HCO_3^-)}{(H_2CO_3)} \tag{1.b}$$

$$HCO_3^- \rightleftharpoons CO_3^{2-} + H^+ \qquad K_2 = \frac{(H^+)(CO_3^{2-})}{(HCO_3^-)} \tag{1.c}$$

where K_1 and K_2 are equilibrium constants.

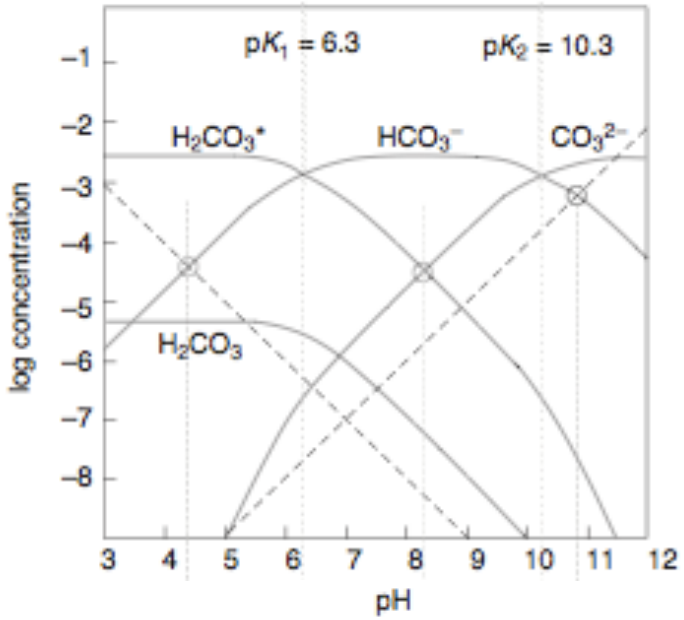

Figure 1.1: *Logarithmic concentration diagram of carbonate species distribution given pH in a closed natural system, showing curve for both actual H_2CO_3 and total aqueous CO_2, $H_2CO_3^*$ (adapted from Stumm and Morgan (1996)).*

1.2.2 Forms and precipitation of calcium carbonate

Calcium carbonate is one of the most common carbonate minerals. Its precipitation is often catalysed by living organisms (McConnaughey and Whelan, 1997). It can precipitate as any of six anhydrous polymorphs and hydrates: in decreasing stability calcite, aragonite, vaterite, calcium carbonate hexahydrate, calcium carbonate monohydrate and amorphous calcium carbonate (Table 1.1). The first five forms listed are crystalline. To better understand or predict which phase will be precipitating under which conditions, some properties of the precipitating solution and possible mineral phases need to be known. Authors generally agree that the most influential parameters are the level of supersaturation in the medium and the solubility of the possible phases for a given set of conditions (Lioliou et al., 2007; Brecevic and Kralj, 2007).

Table 1.1: *Solubility products at 25℃ of the six calcium carbonate polymorphs (source: Brecevic and Nielsen (1989); Brecevic and Kralj (2007); Warren et al. (2001))*

Polymorph	$\log(K_{sp})$
Amorphous calcium carbonate	-6.393
Calcium carbonate monohydrate	-7.195
Calcium carbonate hexahydrate	-7.461
Vaterite	-7.913
Aragonite	-8.340
Calcite	-8.480

Amorphous calcium carbonate

Amorphous calcium carbonate is the least thermodynamically stable of the six possible forms of calcium carbonate. It appears at high supersaturation levels and switches rapidly to a more stable anhydrous phase (calcite, aragonite or vaterite). It is quite common to find metastable and unstable mineral phases precipitating in the initial phases of the precipitation process, to then

undergo rapid changes into a more stable polymorph. Such unstable solid phases, as amorphous calcium carbonate, are often qualified as "precursors" (Brecevic and Nielsen, 1989).

Precipitated amorphous calcium carbonate takes the shape of spheres between 50 and 400 nm in diameter (Brecevic and Kralj, 2007). It is a hydrated phase, and contains less than one molecule of water per molecule of $CaCO_3$.

Amorphous calcium carbonate is the only hydrated phase that has been found in calcified biological systems. Living organisms can catalyse the precipitation of this phase as a precursor to a more stable crystalline polymorph (Koga et al., 1998). The amorphous solid phase is stabilised inside living organisms to store calcium and carbonate temporarily (Aizenberg et al., 1996; Raz et al., 2002). The solubility of amorphous calcium carbonate being much higher than that of the other mineral phases, the ions are easily available for crystallization after contact with water. This process is common in plants such as *Ficus microcarpa*, and in several crustaceans and sea creatures, such as sea tulips or sponges, where unstable amorphous calcium carbonate co-exists with calcite (Addadi et al., 2003). In the latter organisms, the amorphous phase is stabilised through the joint action of Mg^{2+} and glycoproteins generally rich in glutamic acid, glutamine, serine or glycine (Lee et al., 2005; Han and Aizenberg, 2008), while proteins rich in aspartic acid or asparagine favour calcite formation (Aizenberg et al., 1996).

Further to a storage strategy, forming such composite structures fulfils biological roles still not completely understood. These include gravity sensing and navigation in the Earth's magnetic field using the density of the precipitated crystalline phases (Addadi et al., 2003).

Calcium carbonate hexahydrate and calcium carbonate monohydrate

The two hydrated crystalline forms of calcium carbonate are slightly more stable than the amorphous phase. With higher solubilities, both phases precipitate before the more stable mineral polymorphs, calcite, aragonite and vaterite. Calcium carbonate monohydrate exists as a mineral called monohydrocalcite in sediments; its formation results from an interaction with

magnesium ions or organic matter, or the presence of microorganisms (Brecevic and Kralj, 2007).

Vaterite

Vaterite is the least stable of the anhydrous crystalline forms of calcium carbonate. Its structure is hexagonal in spherulitic precipitates (Warren et al., 2001), and its high solubility causes it to be unstable under standard conditions (Rodriguez-Navarro et al., 2007). However, under specific circumstances, vaterite can be stabilised, and it is present in several calcareous sediments, metamorphic rocks, cements, mortars and plasters, mollusc and bird egg shells (Brecevic and Kralj, 2007). Its precipitation is aided by organic activity, and there are some examples of vaterite being precipitated rather than calcite if organic macromolecules are present (Rodriguez-Navarro et al., 2007). The exact mechanisms by which organic molecules stabilize vaterite are still discussed, and whether they act as templates to facilitate the precipitation of vaterite, or inhibit its conversion to calcite or aragonite is controversial (Rodriguez-Navarro et al., 2007).

Vaterite nucleation has been shown to be heterogeneous (Brecevic and Kralj, 2007), i.e. the first crystal forms and become properly oriented on the surface of a different substance, such as a dust particle. Vaterite has also been qualified of "precursor phase"; in particular in the formation of geological calcium carbonate, since it spontaneously and rapidly shifts to calcite, which is thermodynamically more stable (Xyla et al., 1991).

Aragonite

Aragonite is the second most stable and widely found anhydrous phase of calcium carbonate. Its crystals are orthorhombic, most often occurring as needles. Although aragonite forms naturally during the making of many organisms' shells, these are biologically controlled processes, and it is uncommon to obtain inorganically precipitated aragonite at the Earth's surface standard

temperature and pressure (Beruto and Giordani, 1993). It does shift to calcite eventually, but more slowly than vaterite.

Calcite

Under standard conditions of temperature and pressure at the Earth's surface, all unstable phases of precipitated calcium carbonate eventually transform to calcite, which is the most thermodynamically stable polymorph. Calcite is thus the most common of the calcium carbonate polymorphs (Lin and Singer, 2005b); it is also thought to be the most widespread mineral at the Earth's surface (Flugel, 2009). Its crystals have an hexagonal-rhombohedral structure (Warren et al., 2001).

Buczynski and Chafetz (1991) succeeded in making marine bacteria precipitate both calcite and aragonite in the laboratory, but only in different cultures. They explained this by differences in precipitation rates between the cultures. Aragonite formed preferentially when precipitation proceeded quickly. Aragonite is however less stable than calcite at normal surface temperature and pressure. If temperature alone is increased, aragonite spontaneously transforms into calcite. Aragonite is thus most commonly found in warm aqueous conditions, while calcite can be precipitated in media with slower ion diffusion rates (Buczynski and Chafetz, 1991). Because vaterite is less stable and more soluble than both calcite and aragonite, it easily shifts to one of its polymorphs when in contact with water.

1.2.3 Kinetics of precipitation

Calcium carbonate precipitates according to one of the following reactions:

$$Ca^{2+} + CO_3^{2-} \rightleftharpoons CaCO_3 \quad 1.d$$

$$Ca^{2+} + HCO_3^{-} \rightleftharpoons CaCO_3 + H^{+} \quad 1.e$$

An increase in the concentration in solution of calcium or any ion of the carbonate system would push the equilibrium to the right and precipitate calcium carbonate. The precipitation of $CaCO_3$ would not only have an immediate effect on pH by reducing the alkalinity of the solution, it would also pull carbon dioxide from the atmosphere, further acidifying the solution due to the reaction

$$Ca^{2+} + CO_2 + H_2O \rightleftharpoons CaCO_3 + 2H^{+} \quad 1.f$$

Because carbonate minerals, and particularly calcium carbonate, are so widespread and influence important processes at the surface of the Earth, the mechanisms involved in the precipitation-dissolution cycle have been extensively studied. The kinetics of calcite precipitation in particular, owing to its position as the most stable $CaCO_3$ polymorph and the end product of all the transition reactions from unstable to stable forms, have received the most interest.

Calcium carbonate precipitation in aqueous systems has been shown to be a kinetically rather than thermodynamically controlled process (Lebron and Suarez, 1998). With the three mineral polymorphs described above as three possible products for the precipitation reaction, Xyla et al. (1991) identified vaterite, the least stable of the three, as the product forming first for temperatures ranging from 25 to 80°C and pH 8.0 to 9.0 in aqueous conditions. Vaterite has thus been qualified as a "precursor phase", since it then spontaneously and rapidly shifts to calcite, which is thermodynamically more stable. As explained above, amorphous calcium carbonate in

biological systems is another illustration of this; its transformation into more stable crystalline forms is not only thermodynamically but also kinetically favoured (Aizenberg et al., 1996).

The change in Gibbs free energy in precipitation determines which polymorph is precipitated (Manoli et al., 1997). The change in the Gibbs free energy ΔG_x for polymorph x is given by (Lioliou et al., 2007)

$$\Delta \mathrm{G_x} = -\frac{\mathrm{R_g T}}{2} ln \mathrm{SI_x} \tag{1.1}$$

where R is the gas constant, T the absolute temperature, and SI is the degree of supersaturation with respect to x

$$\mathrm{SI_x} = \frac{(\mathrm{Ca^{2+}})(\mathrm{CO_3^{2-}})}{\mathrm{K_{sp,x}}} \tag{1.2}$$

where $\mathrm{K_{sp,x}}$ is the solubility product of x.

Nucleation is the most energetically demanding process in precipitation (Brecevic and Kralj, 2007) and the presence of a suitable nucleation site is the most important factor governing the rate of the precipitation. *In vitro* the most effective sites for further crystal growth are calcite crystals already formed, or "seeds" . Dust particles or bacteria may also act as nucleation sites. However, such "heterogeneous" nucleation reactions are less efficient, especially when the solution is less saturated (Lebron and Suarez, 1998).

The degree of supersaturation and hence rate of calcium carbonate precipitation is directly linked to the partial pressure of carbon dioxide in the system. An increased pressure of CO_2 will lead to an increase in the concentration of carbonate ions, depending on the alkalinity of the solution. The higher the alkalinity for a given CO_2 pressure, the higher will be the concentration of carbonate and the saturation index SI.

1.2.4 Catalysers and inhibitors

The two most commonly recognised inhibitors of calcium carbonate precipitation and crystal growth in the natural environment are orthophosphate (PO_4^{3-}) and soluble organic ligands or other organic matter (Lebron and Suarez, 1998). However, the inhibition mechanisms are not all fully understood. For instance, when organic molecules are sorbed onto a mineral surface, depending on the saturation conditions, they can either induce dissolution or impair crystal growth (Lin et al., 2005). Supersaturated conditions generally coincide with high levels of dissolved organic matter, whether because of high biological activity producing high pressures of CO_2, or pH effects on the solubility of organic matter. While calcium carbonate precipitation is then thermodynamically favoured, organic ligands may act as inhibitors.

Inhibition occurs because of competition for adsorption onto a nucleation site (Inskeep and Bloom, 1986b; Lebron and Suarez, 1996, 1998; Lin and Singer, 2005a, 2006). The efficiency of an inhibitor depends then on its characteristics. In the case of organic matter, important properties include the molecule's hydrophobicity, molecular weight and chemistry. Inskeep and Bloom (1986b) highlighted carbon aromaticity as the most influential chemical property for an efficient inhibitor. The inhibitor hydrophobicity favours better coverage of mineral surfaces, while a higher molecular weight more efficiently blocks the access to nucleation sites through stereochemical effects (Lin et al., 2005). These properties may counterbalance each other to the extent that two molecules with different properties can end up having the same inhibitory effect.

Zavarin and Doner (2005) found that 0.2 mg L^{-1} of inorganic phosphate was enough to completely inhibit the precipitation reaction in aqueous solution super-saturated with respect to $CaCO_3$. In simulated soil solutions, Huang (1990) found that at P concentrations greater than ca. 1 μM, P was co-precipitated with $CaCO_3$, altering its surface properties and inhibiting further $CaCO_3$ precipitation. But at P concentrations greater than ca. 100 μM, precipitation

was stimulated, possibly because the accumulated Ca phosphate now provided suitable nucleation sites. Likewise, while DOC is generally thought to inhibit precipitation, some substances produced by living organisms, such as glycoproteins, stabilise amorphous calcium carbonate for instance (Han and Aizenberg, 2008). Amino-acids seem to have two antithetic roles: as calcium carbonate precipitation inhibitors as mentioned above, and as stabilisers of vaterite, the least stable anhydrous calcium carbonate polymorph, in supersaturated conditions (Manoli et al., 2002).

Most studies of catalysers and inhibitors of $CaCO_3$ precipitation have been made in aquatic conditions; there will be further complications under soil conditions.

1.3 Calcium carbonate precipitation in soils

The same basic chemical principles govern calcium carbonate precipitation in soils as in simple aqueous systems. However, in addition to differences in the composition of soil air and solution compared with the atmosphere and natural waters, the presence of solid phase minerals and organic matter means the kinetics of precipitation and rate-limiting processes are quite different. Because soils are structured and have a pore network in which water is distributed, diffusion of reacting solutes to reaction sites is slower than in bulk water, and so is more likely to be rate-limiting.

1.3.1 Factors influencing precipitation

Soil type

Calcium carbonate structures have been found in both topsoil and subsoil and in a wide range of different soil types, including sands (Wright, 1986), clayey soils (Kemp, 1995; Clarke et al., 2006), and alluvial soils (Schmittner and Giresse, 1999). The form (hydrated/anhydrous) and morphology of calcium carbonate in soils varies with soil texture, available moisture content,

vegetation cover and the availability of calcium and carbonate.

Climate

Soil calcium carbonate is most associated with areas with a defined alternation of wet and dry periods. Calcareous layers at depth, and small secondary calcite structures through the soil profile in places such as Ivory Coast (Cailleau et al., 2005), or Spain (Freytet et al., 1997; Alonso-Zarza et al., 1998) are often described in the literature. These areas are generally characterised as arid to semiarid, or Mediterranean, with an evapotranspiration rate exceeding the rainfall for at least eight months of the year (Schmittner and Giresse, 1999). Wet-dry cycles make the soil solution supersaturated with calcium and carbonate ions, leading to precipitation (Birkeland, 1974). Such climates were thought to be *sine qua non* for the precipitation of $CaCO_3$. However, the observation of precipitated calcium carbonate in temperate areas such as North Yorkshire, England (Lebron and Suarez, 1998; Milodowski, pers.communication,2008) questions the argument that an arid climate is necessary to their presence.

Further questions are raised on the actual factors triggering the accumulation of calcite in arid regions, and whether these mechanisms have shifted or spread to temperate areas of the Earth. Cerling (1984) has suggested calcium carbonate is also favoured by the concentrating of soil solution during soil freezing. However, this is unlikely to be a widespread phenomenon, otherwise secondary calcium carbonate structures should be more widespread in cold regions.

1.3.2 Diffusion as a rate-limiting process

Chemical reactions in soils are modulated by the soil structure. The soil pore network resulting from soil structure influences the kinetics of a reaction principally by regulating the diffusion of reactants to reaction sites and by providing reaction surfaces.

The diffusion of a solute in solution depends on its concentration gradient, and, for charged solutes, to some extent on the concentration gradients of other ions present: because the electroneutrality of the solution has to be conserved at every point, an ion will not travel independently. The factors governing solute diffusion in soils are quantified as follows.

The relation between the flux F of a solute through a volume of soil of length dx and its concentration gradient $\frac{\mathrm{d}C}{\mathrm{d}x}$ through that length of soil is given by Fick's first law:

$$F = -D\frac{\mathrm{d}C}{\mathrm{d}x} \tag{1.3}$$

where D is the ion diffusion coefficient in the soil. For most conditions, the soil diffusion coefficient of a particular solute is given by Nye (1979)

$$D = -D_L\theta f\frac{\mathrm{d}C_L}{\mathrm{d}C} \tag{1.4}$$

where D_L is the diffusion coefficient of the solute in free solution, θ is the soil volume fraction occupied by water, f an impedance factor for tortuosity effects in the soil pore network, C_L the soil solution concentration in solute, and C the total solute concentration in the soil.

The derivative $\frac{\mathrm{d}C_L}{\mathrm{d}C}$ in Equation 1.4 indicates the distribution of the solute between the soil solid on which it may be sorbed and the soil solution in which it is free to diffuse. The inverse of this derivative ($\frac{\mathrm{d}C}{\mathrm{d}C_L}$) is termed the soil buffer power for the particular solute considered. Its value ranges from θ for non-adsorbed solutes such as Cl^-, to 10-100 for simple exchangeable ions such as Ca^{2+}, to over 1000 for strongly sorbed solutes such as $H_2PO_4^-$ (Tinker and Nye, 2000).

The impedance factor f varies strongly with the soil moisture content θ. Soil moisture content thus has a major influence on solutes diffusion in soils. Because ions diffuse in the soil solution, when the soil dries out and water films around soil particles decrease, the diffusion process is greatly impeded.

1.3.3 Effects of biological activity

Plants - Aqueous conditions vs. soils

Biology can play both active and passive roles in calcium carbonate precipitation. Several organisms in fresh- and sea-waters induce calcium carbonate precipitation, either directly to produce shells, or as a consequence of a metabolic processes such as photosynthesis.

Carbon dioxide dissolves in water according to Equation (1.a). In natural waters containing photoautotrophic organisms, removal of CO_2 during daytime photosynthesis tends to raise the water pH as the carbonate equilibria (Equations 1.a to 1.c) shift. If the pH rises too high, photosynthesis may be impaired. Hence it may benefit the water biota to stimulate $CaCO_3$ precipitation so as to limit the rise in pH (Equation 1.e, McConnaughey and Whelan,1997).

While it is common to observe such calcification in aquatic plants and algae (Jaillard et al., 1991), it is not reported as a frequent occurrence in terrestrial plants. A major difference is that, while aquatic photosynthetic organisms draw their CO_2 from the surrounding waters, terrestrial higher plants draw their CO_2 from the surrounding air, without the intervention of carbonate equilibria. Hence there is no equivalent need for terrestrial plants to stimulate calcium carbonate formation (BeczeDeak et al., 1997).

However, some secondary calcium carbonate precipitation is associated with terrestrial plants for other reasons. Coatings of calcite are found associated with plant roots. In preliminary field-work for this thesis, observed calcrete coatings closely associated with plant roots in a calcareous soil developed in chalky deposits at Pegwell Bay, Kent (see Figure 1.2).

Rhizogenic calcretes can develop through several mechanisms, both intracellular and extra-cellular (Freytet et al., 1997). Intracellular calcification describes the calcification of actual cells. This can happen either while the root cell is alive, or as it decays. It starts with the soil solution outside the root becoming saturated with calcium carbonate, causing the concentration of Ca^{2+} and carbonate in the root cell cytoplasm to tend to rise. Calcium ions are then stored in cell vacuoles, and react with carbonate, so restoring the cytoplasmic ionic balance. This mechanism

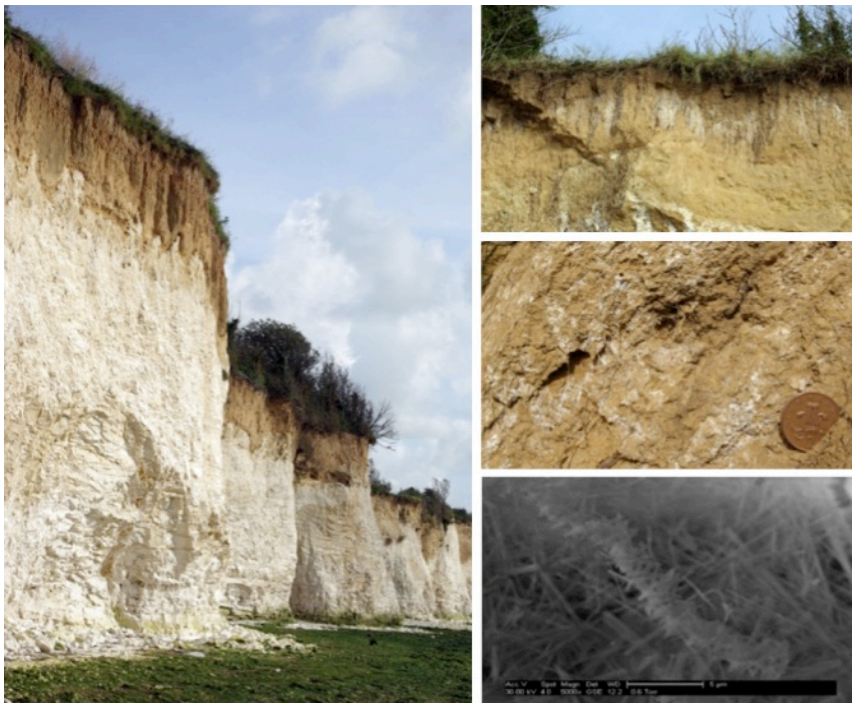

Figure 1.2: *Calcium carbonate deposits at the top of the White cliffs (Pegwell Bay, Kent) and their microscopic filamentous structure.*

is referred to as "active calcification" (McConnaughey and Whelan, 1997). Some authors argue that active calcification is an important mechanism for plants to improve nutrient uptake. The resulting removal of Ca^{2+} and CO_3^{2-} from the soil solution tends to lower the rhizosphere pH, so making nutrients that are less soluble at high pH (e.g. phosphate and some micronutrients) more readily available and assimilable (Jaillard et al., 1991). This happens in living cells. However, as such a cell dies and decays, its walls will generally mineralise also (BeczeDeak et al., 1997).

In extracellular calcification the calcium carbonate accumulates around the roots rather than inside. In regions with a high evapotranspiration rate, plants withdraw water quickly from the soil, excluding calcium, thus concentrating calcium in the soil solution locally around their roots, which triggers calcification. The accumulation of precipitated $CaCO_3$ in soil pores potentially hinders the uptake of nutrients by the root and will also affect local soil structural properties such as strength.

Extracellular calcification of roots can also be due to the association of roots with fungi, in particular Basidiomycetes (Wright, 1986).

Root calcification seems to be a much more widespread phenomenon than previously thought, and an important pedogenic process in some regions at least. It is often associated with arid climates, or at least a pronounced dry season similar to the Mediterranean moisture regime, where evaporation exceeds rainfall for at least 8 months a year (Schmittner and Giresse, 1999). But also occurs in more humid environments (Hassett et al., 1976; Strong et al., 1992; BeczeDeak et al., 1997).

Information on the role of plants in calcium carbonate precipitation can be obtained from the carbonate isotopic composition (Cerling, 1984). The carbon used in the $CaCO_3$ precipitation reaction is mainly derived from soil air, and soil CO_2 depends on the isotopic composition of the soil biomass and what they are assimilating. Soil biomass composition is in turn largely influenced by above-ground vegetation, and more particularly their prevailing photosynthetic pathway. Cerling (1984) found an increase in average $\delta^{13}C$ of 2‰ for a entirely C4 type vegetation compared to a C3 type. The carbon isotopic composition of soil carbonate also depends on respiration rates, as a low rate would increase the fraction of atmospheric CO_2 in the pore network. Bajnoczi and Kovacs-Kis (2006) have highlighted the different isotopic composition of needle fibre calcite and pedogenic carbonate: they found needle fibre calcite to have a higher $\delta^{13}C$ compared to that of pedogenic carbonate, indicating that the carbon in the mineral was the product of the respiration of mainly C4 plants.

Soil fauna

Ellipsoidal biospheroids composed of calcite precipitates up to 1 mm long are sometimes found in soil matrices and earthworm casts (Canti and Piearce, 2003; Carpenter et al., 2007; Lee et al., 2008). Earthworms have calciferous glands where crystallisation of amorphous calcium

carbonate secreted in the epithelium occurs. The resulting biospheroids are then excreted through the earthworm digestive system.

Biomineralisation in earthworms could be a protective mechanism against toxic levels of carbonate in soils around them. However, biospheroids have been produced by earthworms fed leafy vegetable with a high calcium content in non-calcareous soils. Some authors have also argued that precipitation of calcium carbonate helps earthworms buffer their body pH when the CO_2 concentration in soil air increases (BeczeDeak et al., 1997).

Calcium carbonate coatings on the earthworm channels have also been found, supposedly after soil solution evaporation. Finding such evidence of earthworm activity in the soil profile is of particular significance to interpret sedimentary conditions. Indeed, earthworms only survive in moist environmnents, without rapid disturbances.

Microbes

The association of microorganisms and carbonate ions, and microbially-induced calcium carbonate precipitation is now widely acknowledged, and the field of geomicrobiology raises increasing interest (Gadd, 2007). While processes involved in microbially-induced calcite precipitation in soils seem mostly passive, and an indirect consequence of the metabolism of microorganisms on the chemistry of their local environments, several authors argue that not only is microbial metabolism necessary for the precipitation of calcium carbonate (Buczynski and Chafetz, 1991), but also the amount of biological activity is a "key factor" influencing calcrete development (Goudie, 1996; Freytet et al., 1997).

The role of bacteria in precipitation of carbonates particularly has been extensively studied, and applications are found in different disciplines such as civil engineering (DeJong et al., 2006). The influence of fungi however is far less well documented (Burford et al., 2006; Gadd, 2007).

The increase of soil CO_2 due to microbial respiration is one of the most obvious impacts of soil biota on their microenvironment. Carbon dioxide concentrations can be enormously increased

very locally (Lebron and Suarez, 1998). Microaerophilic conditions can develop, where CO_2 concentration can reach 10% of soil air. High CO_2 pressure will favour $CaCO_3$ precipitation. But while the importance of microorganisms in the phenomenon is recognized, the mechanisms by which the interaction between microbes and minerals occur, and their consequences for the type and morphology of the mineral precipitated are not well understood.

Bacteria

Bacteria influence both the nucleation and the crystal growth processes of calcium carbonate precipitation. "Biomineralisation" of calcium carbonate is deemed "common" in bacteria in a wide range of environments (Reith et al., 2009). As for calcification of plant roots, bacterially-induced precipitation can be both active and passive (Warren et al., 2001; Mitchell and Ferris, 2006).

"Active" nucleation takes place when negatively-charged macromolecules on bacterial surface adsorb Ca^{2+} ions, thereby lowering the free energy for $CaCO_3$ precipitation. Hence the bacterial surface mimics a seed of calcium carbonate (Warren et al., 2001). The carboxyl ends of the cell wall macromolecules, whose proton can easily be replaced by cations such as Ca^{2+} share spatial properties with calcite (Mitchell and Ferris, 2006).

In contrast, passive nucleation results from a change in the microbial environment rather than from the properties of bacteria themselves. Such changes, most often promoting the mineral supersaturation of the surrounding medium by increasing its alkalinity, are mainly due to the activity of the bacteria (Fujita et al., 2000; Mitchell and Ferris, 2006). The mechanisms by which microorganisms influence the chemistry of their environments to induce carbonate precipitation raise interest in such fields as wastewater bioremediation (Fujita et al., 2000), soil erosion control (Van der Ruyt and van der Zon, 2009), or even remediation of concrete structures (Achal et al., 2009).

The effects of different organic molecules on both the kinetics and the end product of the precipitation reaction have been extensively studied (Inskeep and Bloom, 1986b; Aizenberg et al.,

1996; Lebron and Suarez, 1998; de Leeuw and Cooper, 2004; Lin et al., 2005; Westin and Rasmuson, 2005). A key mechanism by which biota affect precipitation shared by most bacteria in soils and waters (Warren et al., 2001; Achal et al., 2009), as well as by plants (Bachmeier et al., 2002), is the promotion of urea hydrolysis by the extracellular enzyme urease. In soils, *Bacillus pasteurii* has been noted to produce urease in amounts reaching 1% of its cells' dry weight (Bachmeier et al., 2002). As a result of urea hydrolysis the pH and HCO_3^- concentration localised around the bacteria increase (Equation 1.g). Hence calcium carbonate precipitation is favoured in these micro environments, and the living cell surface acts as a nucleation site (Kemp, 1995). Indeed, CO_2 dissolved in solution as either HCO_3^- or CO_3^{2-} (see Figure 1.1), and accumulate on the alkaline side of the membrane (McConnaughey and Whelan, 1997), thus favouring calcium carbonate precipitation (Warren et al., 2001; Mitchell and Ferris, 2006).

$$CO(NH_2)_2 + H^+ + 2H_2O \overset{urease}{\rightarrow} 2NH_4^+ + HCO_3^- \qquad 1.g$$

The rate of $CaCO_3$ precipitation is in this case directly linked to the rate of urea hydrolysis. In field experiments, Van der Ruyt and van der Zon (2009) found that 100 kg $CaCO_3.m^{-3}$ soil were formed in 24 hours by a culture of *Sporosarcina pasteurii* in sand, flushed with urea and calcium chloride.

Further, some bacteria have been reported to inhibit mineral dissolution. Luttge and Conrad (2004) found that biofilms developed by *Shewanella oneidensis* MR-1 at the surface of calcite crystals prevented CO_2 produced by respiration from being released into solution, where it would decrease pH and provoke dissolution of calcium carbonate.

Fungi

The growth form of the so called eucarpic fungi is a filamentous and branching structure called a mycelium, which is adapted to explore their environment for nutrients. Because the

walls, or septa, compartmenting the hyphae are typically perforated, nutrients can travel along them over long distances (Ritz, 2004). Fungi thus play a very important role in nutrient transport and cycling. As decomposers, they decompose organic matter, taking up and releasing a wide variety of macromolecules.

Fungal growth and metabolic activity influence soil structure. As their mycelia grow, fungi not only physically rearrange soil particles, creating new pores and cracks, but also biochemically modify their environment (Ritz and Young, 2004). As they get coated in the hydrophobic proteins they exude, they change soil response to water (infiltration rates, water repellency) and can thus weaken structure. Fungi however reinforce and stabilise soil pore networks by enhancing soil particle aggregation as their mycelia develop over extended areas (Ritz and Young, 2004), and producing adhesive mucilageus macromolecules and glycoproteins (Ritz, 2004; Masaphy et al., 2009). It has been suggested that fungi "self regulate their own environment" (Ritz and Young, 2004), and while they influence the soil environment through processes such as respiration that can be found in other microorganisms, their influence extends to much wider areas.

Gadd (2007) reviewed the role of fungi in biogeochemical processes. Because of their enwrapping effect, boring and releasing of acidic materials, fungi are potent at dissolving and weathering of a range of minerals, including limestone (Li et al., 2009). Their role in rock formation is less well documented, and only a few studies have looked at the role of fungi in calcium carbonate precipitation (Burford et al., 2006; Masaphy et al., 2009). Symbiotic mycorrhizal fungi wrapped around a root facilitate calcification: as the root then decays, its channel is preserved from collapsing by the calcareous coating, giving the soil a more alveolar structure (Wright, 1986).

Fungi excrete a range of organic acids which have a role in rock weathering and cause the release of calcium and other nutrient ions that can then be assimilated and transported along the hyphae to feed their growing tips. However, hyphae can also sequester solutes, creating supersaturation conditions inside the hyphae, leading to re-precipitation of the solid phase. Crystallisation inside fungal mycelia probably results in acicular shaped calcium carbonate crystals (Verrecchia and Verrechia, 1994). However, most interactions between cations such as Ca^{2+} and fungal cells

happen at their external surfaces. The binding of metal ions onto cell walls can sometimes initiate nucleation and crystal growth of such minerals as calcium carbonate (Burford et al., 2006). Chitin, a polysaccharide rich in nitrogen and the major component of fungal cell walls, has especially been highlighted as a major participant in the binding and further biomineralisation processes (Manoli et al., 1997).

Masaphy et al. (2009) have recently confirmed fungi induce calcification in confined experiments with a fungal mycelium within calcite concretions. The mineral crystals did not directly grow on the hyphae walls, supposedly because of the release of acidic materials, which would indicate that the fungi continues to function despite the mineral coating.

Active precipitation is not the only mechanism through which fungi influence calcium carbonate precipitation, and passive mineral formation may happen on dead fungal biomass, although never to the same extent (Burford et al., 2006). This possibly highlights two different characteristics: first the ability of proteins and polysaccharides at the surface of fungal cell walls to act as nucleation sites despite the absence of an active metabolism; and second the great influence of such an active metabolism on the fungus microenvironment leading to mineral crystal growth.

The paradox of biomineralisation

The above review shows that living organisms play an important role in the precipitation of calcium carbonate. In addition to aquatic and terrestrial plants and soil microbiology discussed above, corals and shellfish have a major influence on carbonate precipitation globally. However, it is not always obvious why calcification should be beneficial; in some cases, it may impair vital functions. Corals and shellfish use solid calcium carbonate for structural purposes, but calcified bacteria or fungal hyphae seem likely to be impeded. McConnaughey and Whelan (1997) have shown that sometimes calcification can happen as an inevitable result of metabolic processes for plants, and facilitate nutrient intake for instance. Such a positive outcome seems far less likely for calcified bacteria and fungal hyphae.

1.3.4 Morphology of calcium carbonate precipitates in soils

Needle fibre

Needle-fibre (acicular) calcite is the most common structural form in soils. They may be frequent in the humiferous horizon and at the transition zone with the subsoil, but not at depth. It seems commonly agreed that needle fibre calcite crystals are associated with fungal mycelia (BeczeDeak et al., 1997), though the mechanism of crystal formation is not yet elucidated. Verrecchia and Verrechia (1994) propose a classification of the acicular crystal morphologies and their formation mechanisms. The needles are formed inside fungal hyphae and released once the walls of the hyphae decompose, and then undergo further precipitation to develop the different morphologies observed. The formation of needle fibre calcite is thus thought to be the result of both biological and physicochemical processes (Wright, 1986).

In contrast to other forms of secondary calcium carbonate precipitation, acicular crystals are associated with certain soil physical properties, in particular large pores, where bundles of needles develop more easily, and such bundles have been noted to develop in desiccation cracks (Bajnoczi and Kovacs-Kis, 2006). They indicate the presence, at the time of their formation, of organic matter and moist conditions, necessary for fungi to develop (BeczeDeak et al., 1997). These conditions are found in the topsoil, where decaying organic matter is abundant.

It was thought that the acicular calcite crystals would only survive in the soil matrix when leaching is limited and the climate semiarid to arid (Bajnoczi and Kovacs-Kis, 2006). Strong et al. (1992) challenged this when they found calcretes in North England. Recent observations in the field across England (Milodowski, BGS, personal communications) also raise questions regarding the origin and conditions of formation of secondary calcium carbonate structures.

Pore coating

Hypocoatings appear in the walls of pores formed in soils by growing roots (BeczeDeak et al., 1997). They develop when calcium carbonate precipitates rapidly, probably mainly due to the

suction applied by roots. They have also been observed in places with alternating dry-moist cycles, or variable water tables. The substrate or parent material does not itself have to be particularly calcareous. In these cases, hypocoatings are likely to appear at depths, where the soil solution has become saturated with calcium while percolating through the soil profile.

In contemporary soils, hypocoatings are most often found in arid to semiarid regions, and they are a pedogenic feature (Kemp et al., 1996). On several occasions they have been found associated with needle-fibre calcite crystals, which indicates the role of vegetation in their formation (BeczeDeak et al., 1997; Bajnoczi and Kovacs-Kis, 2006).

Powdery coatings are at the surface of the ground mass rather than integrated to the soil matrix (hypocoatings). They bear a resemblance with needle fibre calcite at a much smaller scale. Evidence indicates that while needle fibre calcite is contemporary to the surface of the soil in which it is found, powdery coatings happen in the soil once buried and are linked to the overlying layer of soil (BeczeDeak et al., 1997). They probably appear due to a change in the soil solution concentrations and chemistry due to drier conditions rather than percolation through the soil profile.

Calcified root cells

As mentioned above (Section 1.3.3), calcification of terrestrial plants roots is a common phenomenon in calcareous soils. The organic acids and protons excreted by living roots dissolve calcium carbonate present in the soil matrix, thus releasing high levels of calcium which becomes readily available to plants. Plants roots take up Ca^{2+} and lock the ions in the cells vacuoles as precipitated calcium carbonate (BeczeDeak et al., 1997). Calcified root cells take a tubular shape, much like the original root morphology. There do not appear to be any links between the presence of calcified root cells and soil texture, depth in the soil profile, present day terrain or vegetation cover.

1.3.5 Summary

Over the past thirty years, the opinion of the scientific community on what causes calcium carbonate precipitation in soils has been shifting from purely physicochemical considerations to include biological factors. The role played by the rhizosphere microecosystem in the formation of secondary calcium carbonate structures described in this chapter has become more widely recognised. As the phenomenon is studied further, the influence of soil microbiology is becoming clearer, though the exact processes are still not well understood. It is still not clear why soil biota take an active part in the precipitation process, or what are the exact consequences secondary calcium carbonate features have for biotic metabolism, and the soil microenvironment. The literature cites as possible causes protection against element toxicities in lime-rich media, and also a contribution to internal pH regulation (BeczeDeak et al., 1997).

Despite the relatively small quantities of $CaCO_3$ actually used in the structures described above, because they have been proved to form very rapidly, they are important and sensitive environmental markers, to the same extent as direct measurement of atmospheric carbon dioxide levels, or observation of a transition from leaching to non-leaching substrate in the soil profile.

1.4 Thesis objectives

The overall aim of this study is to quantitatively understand and describe the mechanisms involved in calcium carbonate precipitation in temperate soils and the role played by soil microbes in mediating such processes. A good understanding of the mechanisms of $CaCO_3$ formation in soils will lead to the development of a predictive mathematical model of the system, which will then be tested against independent experiments.

Chapter 2

Model of calcium carbonate precipitation in soil

2.1 Introduction

In this chapter, a model of calcium carbonate formation in soil is developed with which to investigate the mechanisms controlling $CaCO_3$ formation in soils under natural conditions. The model is based on underlying physicochemical principles so that it can be applied to soils with varied chemical and biological properties.

The aim was to formulate a predictive mathematical model of the system, allowing for relevant physicochemical and biological processes, which could then be tested against the results produced in independent experiments. The general principles, assumptions and parameters of the model are presented here. The model testing is described in Chapters 3 and 4.

In soils, reactions occur both in the water fraction of the pore network and on the surfaces of minerals and organic matter. The soil structure can influence rates of reactions both through its influence on surface properties and on transport processes. Several chemical speciation software programmes exist, which simulate chemical reactions in aqueous conditions. Examples are PHREEQC and Minteq. PHREEQC also simulates one dimensional transport of solutes. However, such models are not sufficiently flexible for the purpose of this study.

2.2 General principles

2.2.1 Calcium carbonate precipitation

Calcium carbonate is precipitated according to the reaction:

$$Ca^{2+} + 2OH^{-} + CO_2 = CaCO_3 + H_2O$$

In soil, the rate of the reaction depends on:

1. the concentration of reactants in the soil solution,
2. the presence and concentration of potential inhibitors of precipitation,
3. the presence of suitable nucleation sites for precipitation,
4. the rate at which reactants Ca^{2+}, OH^- (or other soil base) and CO_2, as well as inhibitors, are delivered to such nucleation site by diffusion through the pore network.

Most studies of reactions between ions in soil have been made in shaken suspensions with a soil:solution ratio much smaller than those found in field conditions, e.g. for $CaCO_3$ precipitation (Inskeep and Bloom, 1986b). Such conditions disrupt soil structure, and rates of diffusion of reacting solutes through the pore network to reaction site are entirely different.

The present model was formulated for a simple idealised system to facilitate the experimental testing. The system is shown in Figure 2.1. It comprises a source of base - an anion exchange resin loaded with HCO_3^- - placed in contact with a block of moist soil loaded with exchangeable Ca^{2+} ions. The model allows for the following processes:

- At the soil-resin boundary, HCO_3^- is released in exchange for Cl^- in the soil solution
- As a result, Cl^- diffuses through the soil solution towards the resin and HCO_3^- diffuses in the opposite direction, simultaneously reacting with H^+ to form CO_2 which diffuses away rapidly in the soil air.
- The movements of Cl^- and HCO_3^- induce parallel movement of Ca^{2+} and H^+ to maintain electrical neutrality
- Reaction of HCO_3^- with Ca^{2+} to form $CaCO_3$ causes further acid-base changes and movement if Ca^{2+} towards the precipitation zone
- The rate of precipitation at any point in the soil is proportional to the $CaCO_3$ saturation index $SI = (Ca^{2+})(CO_3^{2-})/K_{SP}$, where K_{SP} is the solubility product of $CaCO_3$.

To test the model, experiments were made with blocks of soil placed in contact with HCO_3^--loaded anion-exchange resin as in Figure 2.1. After suitable periods, the soil was sectioned

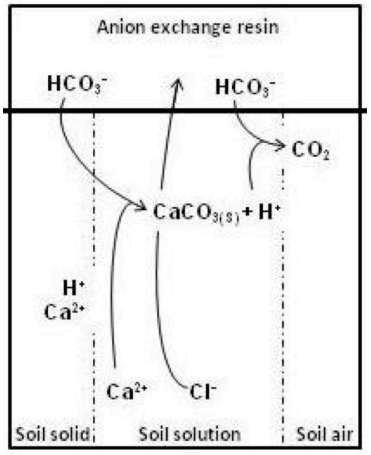

Figure 2.1: *Idealised system showing main ion movements and reactions near a source of HCO_3^- and associated zone of $CaCO_3$ precipitation.*

parallel to the resin layer and the concentration-distance profiles of the reactants determined. Thereby the soil structure was preserved so as to capture the effects of transport on $CaCO_3$ formation. Details are given in Chapters 3 and 4.

2.3 Mathematical model

2.3.1 Nomenclature

	Definition	Units
[ion]	Concentration of ion in soil solution. Ion is Ca^{2+}, $CaHCO_3^+$, HCO_3^-, CO_3^{2-}, Cl^-, H_3O^+	mol l^{-1} solution
[HS]	Total concentration of titratable acidity in the whole soil (excluding newly precipitated $CaCO_3$)	mol l^{-1} soil
b_{HS}	Soil pH buffer power: $-\frac{\mathrm{d[HS]}}{\mathrm{dpH}}$	mol l^{-1} (soil) pH^{-1}
b^*_{HS}	Soil pH buffer power: $-\rho\frac{\mathrm{d[HS]}}{\mathrm{dpH}}$ where ρ is the soil bulk density (kg l^{-1} soil)	mol kg^{-1} (soil) pH^{-1}
D_L	Diffusion coefficient of a given solute in free solution: subscripted Cl, H and B for Cl^-, H_3O^+, and HCO_3^- respectively	dm^2 s^{-1}
θ	Soil volumetric moisture content	l (solution) l^{-1} (soil)
f	Impedance factor for diffusion through the soil pore network	
R	Rate of $CaCO_3$ precipitation	
t	Time	s
x	Distance	dm

2.3.2 Theory of the method

In brief, the model allows for the diffusion of Ca^{2+}, Cl^- and soil base (i.e. HCO_3^- and other proton accepting species) to the zone of $CaCO_3$ precipitation, and for the kinetics of precipitation in the precipitation zone using an empirically-derived relationship based on the extent of super-saturation. In the model, diffusion equations are solved for the concentration-distance profiles of Cl^- and base, and then the profile of Ca^{2+} is found by balancing ionic charges for electrical neutrality. Thereby the problem of defining the correct equation for Ca^{2+} diffusion with simultaneous cation exchange is avoided. The details follow.

1. Chloride

   Chloride anions are not adsorbed on soil surfaces to a significant extent and are therefore free to diffuse in solution through the soil pore network. Inaccessible water fractions in very narrow pores do not have any role in the diffusion process, so need not be taken into account in defining the continuity equation for Cl^- diffusion (Pinner and Nye, 1982). The equation is

$$\frac{\partial \theta [Cl^-]}{\partial t} = \frac{\partial}{\partial x}\left(\theta f D_{LCl} \frac{\mathrm{d}[Cl^-]}{\mathrm{d}x}\right) \tag{2.1}$$

$$\text{i.e.} \qquad \frac{\partial [Cl^-]}{\partial t} = \frac{\partial}{\partial x}\left(f D_{LCl} \frac{\mathrm{d}[Cl^-]}{\mathrm{d}x}\right) \tag{2.1a}$$

2. Soil base

   Base is released from the anion-exchange resin at $x = 0$ and consumed in $CaCO_3$ precipitation in the precipitation zone as well as in buffering mechanisms in the soil. The consumption of base is equivalent to production of H^+. The conservation equation for

the propagation of the resulting pH changes through the soil by acid-base transfers with simultaneous production of H^+ is (after Nye, 1972):

$$\frac{\partial[\mathrm{HS}]}{\partial t} = \frac{\partial}{\partial x}\left(\theta f \sum D_{LHB_i}\frac{\mathrm{d}[\mathrm{HB}_i]}{\mathrm{d}x}\right) + 2R \tag{2.2}$$

where [HS] is the amount of titratable acidity in the soil (i.e. the amount of proton donating groups, as measured by the amount of strong base consumed per unit soil volume as a consequence of increasing the equilibrium soil solution to a standard pH), and $[\mathrm{HB}_i]$ is the concentration of a given acid in the soil solution, the sum being taken over all relevant acid-base pairs.

The most important acid-base pairs in the present system are H_3O^+/H_2O and H_2CO_3/HCO_3^-. The pair HCO_3^-/CO_3^{2-} will only be important at much higher pHs than arose in the experiments to test the model; but it would be straightforward to modify the model to allow for this and other acid-base pairs. Equation (2.2) hence becomes

$$\frac{\partial[\mathrm{HS}]}{\partial t} = \frac{\partial}{\partial x}\theta f\left(D_{LH}\frac{\mathrm{d}[\mathrm{H_3O^+}]}{\mathrm{d}x} - D_{LB}\frac{\mathrm{d}[\mathrm{HCO_3^-}]}{\mathrm{d}x}\right) + 2R \tag{2.3}$$

To solve Equation (2.3), concentrations have to be expressed in terms of a common variable. Because HCO_3^- is the dominant species over the relevant range of pH, it is used as the working concentration variable. The corresponding equation is derived as follows.

Considering the dissolution of carbon dioxide and the dissociation of H_2CO_3 in water:

$$\begin{array}{rcll} CO_2 + H_2O & = & H_2CO_3 & K_S \\ H_2CO_3 + H_2O & = & HCO_3^- + H_3O^+ & K_1 \end{array}$$

where K_1 is the apparent first dissociation constant of H_2CO_3 and K_S the solubility of CO_2 in water. This gives

$$[H_3O^+][HCO_3^-] = K_1 K_S P_{CO_2} \tag{2.4}$$

Taking logs on both sides of Equation (2.4) and differentiating gives

$$d\text{pH} = -d\text{p}[HCO_3^-] = \frac{d[HCO_3^-]}{2.303[HCO_3^-]} \tag{2.5}$$

From the soil pH buffer power, b_{HS}:

$$d[\text{HS}] = -b_{HS} d\text{pH} \tag{2.6}$$

where b_{HS} is expressed in moles of acid or base consumed per unit volume of soil per unit of pH change.

Combining Equation (2.5) and (2.6) gives

$$d[\text{HS}] = -b_{HS} \frac{d[HCO_3^-]}{2.303[HCO_3^-]} \tag{2.7}$$

Combining Equation (2.7) and (2.3) gives the final working continuity equation for soil

base:

$$\frac{\partial[\mathrm{HCO_3^-}]}{\partial t} = \frac{2.303[\mathrm{HCO_3^-}]}{b_{HS}}\left\{\theta f\frac{\partial}{\partial x}\left(D_{LB}\frac{\mathrm{d}[\mathrm{HCO_3^-}]}{\mathrm{d}x} - D_{LH}\frac{\mathrm{d}[\mathrm{H_3O^+}]}{\mathrm{d}x}\right) - 2R\right\} \quad (2.8)$$

3. Calcium

The electrical neutrality equation for the important ions in solution is:

$$2[\mathrm{Ca^{2+}}] + [\mathrm{CaCl^+}] + [\mathrm{CaHCO_3^+}] + [\mathrm{H_3O^+}] = [\mathrm{Cl^-}] + [\mathrm{HCO_3^-}] + 2[\mathrm{CO_3^{2-}}] \quad (2.9)$$

A simulation of the soil solution under the experimental conditions (Chapter 4) using the chemical speciation software Minteq version 2.61(http://www.lwr.kth.se/English/OurSoftware/vminteq/) indicates that these are the main species to consider.

Note that the concentration of Ca^{2+} in the soil solution must respect the electroneutrality equation above irrespective of cation exchange reactions on the soil solid.

4. Kinetics of $CaCO_3$ precipitation

The rate of precipitation R is some function of the degree of supersaturation of the soil solution with respect to the solubility product of $CaCO_3$, K_{sp}. For the purposes of this study, an empirical relation is used for this function, allowing for the effects of nucleation surfaces, the presence and rate of diffusion of inhibitors, and other factors (Chapter 3). The function is

$$\begin{aligned} \mathrm{R} &= 0 && \text{if SI} < 1 \\ \mathrm{R} &= \alpha \text{ x SI} && \text{if SI} \geq 1 \end{aligned} \tag{2.10}$$

where α is a rate coefficient determined by experiment when transport is not limiting, and SI is the $CaCO_3$ saturation index, given by

$$\mathrm{SI} = \frac{(\mathrm{Ca}^{2+})(\mathrm{CO}_3^{2-})}{K_{\mathrm{CaCO_3}}}$$

where K_{CaCO_3} is the solubility product of the $CaCO_3$ formed and (Ca^{2+}) and (CO_3^{2-}) are the activities of Ca^{2+} and CO_3^{2-} in soil solution.

5. Initial and boundary conditions

Equations 2.1 and 2.8 are solved subject to the following boundary conditions at the resin-soil interface (x = 0) and at the opposite end of the experimental soil block (x = L).

Equation 2.1

From the experimental results (Chapter 3), the balance between the flux of HCO_3^- from the resin into the soil and the flux of Cl^- in the opposite direction is such that a roughly constant concentration of Cl^- is maintained at the resin surface (x = 0), i.e. $[Cl^-] = [Cl^-]_0$. At the opposite end of the soil column (x = L), there is no transfer of Cl^- out of the soil, i.e. the flux of Cl^- ($F_{Cl} = -\theta f D_{LCl} \frac{\mathrm{d}[Cl^-]}{\mathrm{d}x}$) is zero.

Hence the initial and boundary conditions for Equation (2.1) are

$$
\begin{aligned}
[\mathrm{Cl}^-] &= [\mathrm{Cl}^-]_{initial} \qquad 0 \leq \mathrm{x} \leq \mathrm{L} \qquad \mathrm{t} = 0 \\
[\mathrm{Cl}^-] &= [\mathrm{Cl}^-]_0 \qquad \mathrm{x} = 0 \qquad \mathrm{t} > 0 \\
\theta f D_{LCl} \frac{\mathrm{d}[\mathrm{Cl}^-]}{\mathrm{d}x} &= 0 \qquad \mathrm{x} = \mathrm{L} \qquad \mathrm{t} > 0
\end{aligned}
$$

Equation 2.8

The flux of HCO_3^- across the resin surface is equal to the flux of Cl^- in the opposite direction: $-F_{Cl}$. The value of F_{Cl} can be found from the solution of Equation (2.1) with the boundary conditions above. There is no transfer of base across to the opposite end of the soil column. Hence the initial and boundary conditions for Equation (2.8):

$$\begin{aligned}
\mathrm{pH} &= \mathrm{pH}_{initial} && 0 \le \mathrm{x} \le \mathrm{L} && \mathrm{t} = 0 \\
\theta f\left(\mathrm{D_{LB}}\frac{\mathrm{d[HCO_3^-]}}{\mathrm{dx}} - \mathrm{D_{LH}}\frac{\mathrm{d[H_3O^+]}}{\mathrm{dx}}\right) &= \mathrm{-\ F}_{Cl} && \mathrm{x} = 0 && \mathrm{t} > 0 \\
\theta f\left(\mathrm{D_{LB}}\frac{\mathrm{d[HCO_3^-]}}{\mathrm{dx}} - \mathrm{D_{LH}}\frac{\mathrm{d[H_3O^+]}}{\mathrm{dx}}\right) &= 0 && \mathrm{x} = \mathrm{L} && \mathrm{t} > 0
\end{aligned}$$

In the model, Equations (2.1), (2.8) and (2.9) are solved simultaneously, subject to initial and boundary conditions, using standard numerical methods. The program for the model is written in FORTRAN (see complete transcript in Appendix A).

6. Parameter values

The model parameters are:

(a) the initial soil solution chloride concentration
(b) the initial soil pH
(c) the soil air concentration in CO_2
(d) the soil pH buffer power
(e) the soil initial moisture content
(f) bulk density
(g) the soil impedance factor
(h) the length of the soil section considered

All the parameters values are independently measured on the experimental soils used in this study to validate the model, as described in Chapters 3 and 4.

The values of the input variables for the experimental soils are presented in Table 2.1, equilibrium constants for the chemical reactions of the carbonate system in Table 2.2, and solute diffusion coefficients in Table 2.3.

The value of the diffusion impedance factor f was derived from fits to the experimental concentration-distance profile of Cl^- (Chapter 4). Note that for specified concentrations of Cl^- in the initial soil solution and at x = 0, the concentration-distance profile of Cl^- only depends on its diffusion coefficient ($f D_L$; Equation 2.1a) and not on $CaCO_3$ precipitation or the other reactants.

The values of the soil pH buffer power b_{HS} and precipitation rate constant α were obtained from shaken soil suspension experiments (Chapter 3).

The CO_2 pressure in the soil air was obtained from pH fits to the experimental distance profiles.

Table 2.1: *Values of model input variables for the experimental soils.*

	Soil		
	Ti	G	
$[Cl^-]_{initial}$	6.0×10^{-2}	6.0×10^{-2}	mol dm^{-3} (solution)
$pH_{initial}$	6.1	6.4	
P_{CO_2}	0.25×10^{-2}	0.75×10^{-2}	atm
b_{HS}	1.25×10^{-2}	2.10×10^{-2}	mol pH^{-1} dm^{-3} (soil)
θ	0.53	0.29	dm^3 (solution) dm^{-3} (soil)
f	0.35	0.60	
L	0.30	0.30	dm
α	5.0×10^{-10}	0.7×10^{-10}	mol dm^{-3} (soil) s^{-1}

Table 2.2: *Equilibrium constants for relevant acid-base equilibria at 25℃ and ionic strength = 0*[a].

Equilibrium	-log$K$
$H_2O = H^+ + OH^-$	14.00
$CO_{2(g)} + H_2O = H_2CO_3^*$	3.46[b]
$H_2CO_3^* = H^+ + HCO_3^-$	6.35
$HCO_3^- = H^+ + CO_3^{2-}$	10.33
$CaCl^+ = Ca^{2+} + Cl^-$	0.40
$CaHCO_3^+ = Ca^{2+} + HCO_3^-$	1.11
$Ca^{2+} + CO_3^{2-} = CaCO_3(s)$	8.48

[a] Values are taken from the MINTEQ version 2.61 chemical speciation software. Note the equilibrium constants refer to the ratios of ionic activities. In the model these are converted to a concentration basis (as in Equation (2.4)) using activity coefficients calculated with the Davies equation (Stumm and Morgan, 1996).
[b] P_{CO_2} in kPa.

Table 2.3: *Diffusion coefficients in free solution at 25℃ and ionic strength 0.*

Solute	D_L ($dm^2.s^{-1}$)
H_3O^+	9.55×10^{-7}
HCO_3^-	1.23×10^{-7}
Cl^-	2.00×10^{-7}

Example reactant concentration-distance profiles for the parameters in Table 2.1 are given in Figure 2.2. The model predictions are compared with the experimental results in Chapter 4. The methodologies for the experimental validation are given in Chapters 3 and 4.

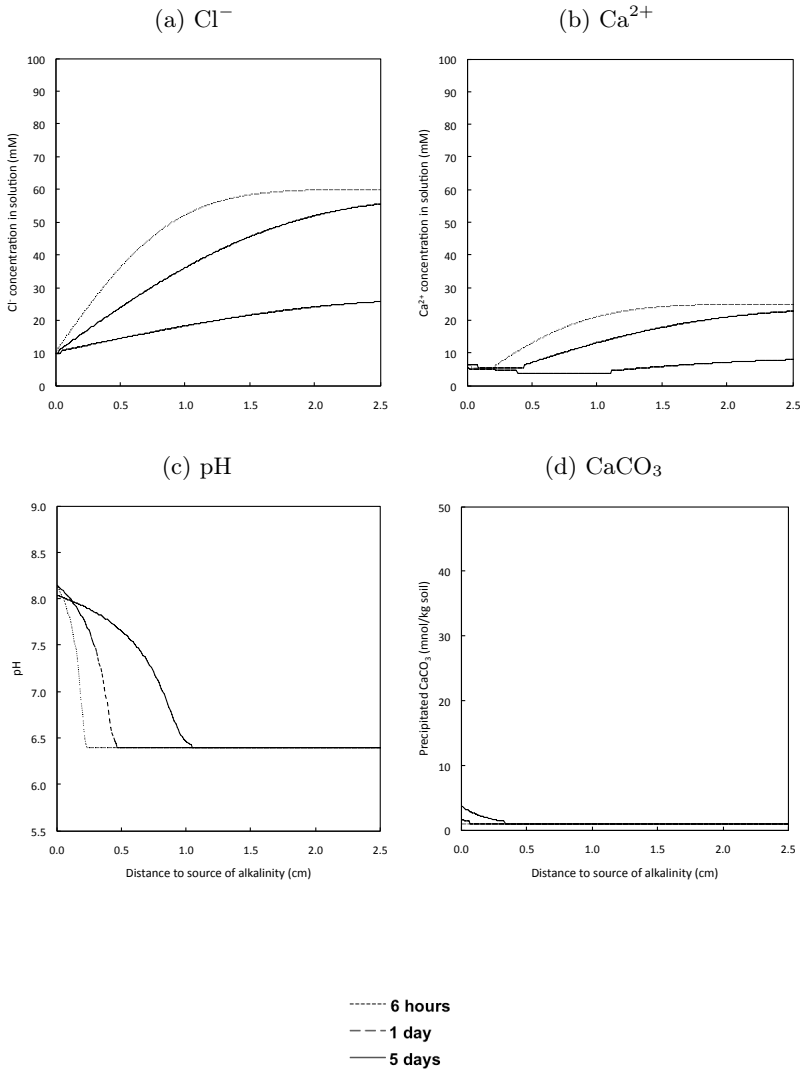

Figure 2.2: *Example simulated concentration-distance profiles using the parameters listed in Table 2.1 for soil G.*

Chapter 3

Calcium carbonate precipitation in the absence of transport limitations

3.1 Introduction

The characteristics of the $CaCO_3$ precipitation reaction in aqueous conditions have been extensively studied and described (Section 1.2 in Chapter 1). Variables influencing precipitation rates include the concentration of inhibitors such as P and dissolved organic carbon (DOC), as well as the reactant concentrations (Ca^{2+}, CO_2, pH).

When the reaction occurs in soils, the kinetics of precipitation and the interactions between these variables will be influenced by the particular biological and physicochemical properties of the soil, and the soil structure. These properties can vary immensely from soil to soil but also spatially within the same soil. Local concentrations of CO_2, phosphates and DOC will depend on, for example, distances from root surfaces or macropores, and the overall soil structure.

This chapter seeks to quantify how different concentrations of CO_2 in soil atmospheres, and P and DOC in soil solution affect the rate of $CaCO_3$ precipitation in soils with different initial properties, in the absence of limitations due to transport through the soil structure. The results will be used to derive the parameters for the model described in Chapter 2.

The basic experiment was to follow pH over time in shaken soil suspensions with a range of initial concentrations of NaOH and (a) different CO_2 pressures and (b) different P concentrations to match typical P fertiliser application rates. From the results, the parameter α was estimated in Equation 2.10 for the rate of precipitation as a function of the saturation index SI.

The results were also used to quantify the pH buffer power (b_{HS}) of the experimental soils from the pH changes for given additions of base (OH^-) to the soil, excluding the base consumed in $CaCO_3$ precipitation.

3.2 Materials and methods

3.2.1 Experimental soils

Four soils were used in this study. The initial experiment to study the effect of CO_2 on the precipitation of $CaCO_3$ was made with soils S and T. The main diffusion experiments (Chapter 4) and the experiments to quantify the inhibitory effect of P and DOC and the model parameters values were made with soils Ti and G.

Two of the soils were collected at the brickearth of Pegwell Bay, Kent, hereafter referred to as soils T (for topsoil) and S (for subsoil). Soil T, an organic-rich loamy-silt, was collected from the first 30 cm of the profile. Below 30 cm, the subsoil was divided into a "non-calcareous" brickearth (between 30 and 119 cm deep) and a "calcareous" brickearth (from 119 cm deep). Rootlet remains containing needle-fibre calcite were observed in the lower half of the upper, non-calcareous, part (Clarke et al., 2006). Soil S, was collected from the non-calcareous horizon. The soil samples were taken in October 2007, sieved to 5 mm to avoid excessive disturbance to the microbiology, and stored field-moist in cool dry conditions. The soil T and soil S had an initial pH in 10 mM $CaCl_2$ of 7.8 and 7.9, and a cation exchange capacity (CEC) of 0.15 and 0.10 $mol_c\ kg^{-1}$ soil respectively.

Additionally, two soils were selected from the National Soil Resource Institute (NSRI, Cranfield University) soil archive, hereafter referred to as soils Ti and G. Their initial pH in $CaCl_2$ 10 mM are 5.7 and 6.1, their CEC 0.23 and 0.05 $mol_c\ kg^{-1}$ soil respectively. The experimental soils were sampled two to three years before this experiment, as part of a project at Cranfield University entitled “Towards a general method to scale up process models in the arable landscape” (Corstanje et al., 2008). The sampling method, detailed in Corstanje et al. (2008), was to dig out 10 kg of soil at each site, discarding the top 10 cm. The soils were then air dried, sieved to 0.5 mm and stored air-dry. Table 3.1 below shows their initial physico-chemical properties.

Table 3.1: *Initial properties of experimental soils Ti and G.*

Soil		Ti	G
Cation Exchange Capacity (mol_c kg^{-1})		0.23	0.05
Initial pH (in 10mM $CaCl_2$)		5.7	6.1
Biomass (μg C g^{-1} soil)		462.7	49.8
Parent material		glacial till	greensand
Particle Size Distribution	0.6 - 2 mm (%)	4	13
	0.212 - 0.6 mm (%)	25	27
	0.063 - 0.212 mm (%)	16	26
	0.002 - 0.063 mm (%)	21	7
	$<$ 0.002 mm (%)	34	27

To simplify the composition of the soil exchange complex and soil solution, the soils were washed with a 10 mM $CaCl_2$ solution as follows. One kg of soil was mixed with 1.5 l of 10 mM $CaCl_2$ and left to settle. The supernatant was then poured off and the process repeated. Three washes were carried out with settling times of 5 hours for the first and last washes and overnight for the second one. After the third wash, the excess solution was removed and the soils were air-dried before being sieved to 0.5 mm and stored. The final experimental soils thus contained predominantly Ca^{2+} in their exchange complex and Ca^{2+} and Cl^- in solution.

3.2.2 Rates of $CaCO_3$ precipitation in shaken soil suspensions at different CO_2 pressures

Ambient CO_2 pressure

Portions (20 g) of air-dry soil were placed in 250 mL conical flasks and 50 mL of 10 mM $CaCl_2$ containing 0, 6, 12.5, 25 or 31 mmol kg^{-1} soil were added. Two set-ups of the atmospheric CO_2 concentration (0.038%) run were carried out, the first hermetically sealed between pH readings, the second open and allowed to re-equilibrate with the atmosphere continuously.

Triplicate flasks were made. The resulting suspensions were immediately shaken on a reciprocating shaker for 1 hour following standard operating procedure NR-SAS/SOP6/Version1 for pH measurement. After 1 h, the suspensions were left to settle for 30 minutes and the pH measured using a combination electrode. The electrode was thoroughly rinsed between measurements to minimise cross-contaminations. The exact time of each pH measurement was recorded. The suspensions were then returned to the shaker. Readings were then taken in the same order every 3 d for 18 days.

At the end of the pH runs, the soil suspensions were filtered into sealable tubes and the soil accurately weighed. Five ml of 1 M HCl was added through the seals with a syringe and the amount of CO_2 released measured by gas chromatography (GC). The amount of $CaCO_3$ present in the soil was calculated from the peak of CO_2 detected using a calibration curve drawn at the beginning of each session. The filtrates were then diluted and the concentration in Ca^{2+} remaining in solution measured by atomic absorption spectrophotometry (Perkin-Elmer AAnalyst 800).

Controlled CO_2 pressure

The concentrations of CO_2 in the headspace of the flasks was controlled by placing soil suspensions prepared as above in a Microprocessor Automatic Control (MAC) cabinet, previously set at the required CO_2 concentration, for an hour (+/- 10 minutes). Three CO_2 concentrations were tested: atmospheric (0.038%), 1% and 4%. The flasks were then sealed (stoppers with silicone grease) inside the cabinet and taken and shaken on an orbital shaker at 150 rev.min^{-1}.

After 1 h, the pH was measured, and the headspace CO_2 content was measured using gas chromatography. To avoid a negative pressure developing in the experimental system, 1 ml of carbon-free air was injected in the bottles to replace the amount of headspace sampled on each occasion. The flasks were then returned to the orbital shaker. Headspace concentrations of CO_2 and pH were then determined each day for one week.

3.2.3 Quantification of the inhibitory effect of P and dissolved organic carbon (DOC) on $CaCO_3$ precipitation

The two experimental soils Ti and G were amended with calcium hydrogen phosphate dihydrate ($CaHPO_4.2H_2O$) to contain 0, 0.25, 0.5 and 1.5 mol P kg^{-1} soil. These concentrations are equivalent to fertiliser P_2O_5 application ratesof 0, 35, 69 and 208 kg ha^{-1} (assuming 15 cm soil depth and 1.3 kg dm^{-3} bulk density).

The $CaHPO_4.2H_2O$ was added as dilute solution uniformly sprayed over the soil to give a moisture content of 50% v/v. The soils were then incubated for one month at 20°Cto allow equilibration.

The soil suspensions were prepared at the same 2.5:1 solution to soil ratio as before with 0, 5 and 12.5 mmol NaOH kg^{-1} soil, then shaken for an hour before the first pH measurement. The headspace above the soil suspensions was then brought to 5% CO_2 in the MAC cabinet, the flasks sealed and put to shake at 150 rev min^{-1} on an orbital shaker. After each subsequent sampling over an 18 day-period, the flasks were allowed to re-equilibrate in the MAC cabinet and re-sealed.

For each measurement, the pH was measured as detailed above, and a 10 ml sample of the soil suspension taken using a pipette with a widened cone tip to preserve the soil:solution ratio, and filtered through a glass fibre filter. Ion concentrations were measured in the filtrates, and the amount of $CaCO_3$ precipitated in the soil solid was measured as before. Concentrations of P and DOC were measured by chromatography on a segmented flow analyser (Burkard SFA2000), of Ca^{2+} by atomic absorption spectrophotometry, of Na^+ and K^+ by atomic emission spectrophotometry (Perkin Elmer AAnalyst 800), and of Cl^- by ion chromatography (Dionex).

3.2.4 Model parameters

To measure α and b_{HS} on soils Ti and G (which are used in the main experiment to test the model in Chapter 4), changes of pH over time were measured in shaken suspensions containing

a range of base additions at atmospheric CO_2 pressure as in Section 3.2.2. After 24 hours the amount of $CaCO_3$ precipitated in each flask was measured as before.

The rate of precipitation, α, was estimated by fitting an exponential regression curve to the $CaCO_3$-time profile for NaOH addition 31 mmol kg^{-1} soil. The regression line was of the form

$$\mathrm{CaCO_{3(s)}} = \mathrm{CaCO_{3(s)_0}} + \mathrm{a}e^{\mathrm{bt}} \tag{3.1}$$

where $\mathrm{CaCO_{3(s)_0}}$ is the initial amount of $CaCO_3$ in the experimental soil, a and b are coefficients. Thus the derivative

$$\frac{d\mathrm{CaCO_{3(s)}}}{dt} = \mathrm{ab}e^{\mathrm{bt}} = \alpha\mathrm{SI} \tag{3.2}$$

where SI is the saturation index.

The parameters were estimated using SigmaPlot 11.1, and SI was calculated by running a speciation programme (see Appendix A) for the pH and Ca^{2+} conditions in solution for each data point. The results of the speciation programme were double-checked against the speciation software Minteq (Version 2.16 http://www.lwr.kth.se/English/OurSoftware/vminteq/).

The soil buffer power b_{HS} (i.e. the amount of (OH^- neutralised in buffering reactions per unit increase in pH, excluding OH^- consumed in $CaCO_3$ precipitation) was measured by shaking 20 g portions of soil in 50 cm^3 of 10 mM $CaCl_2$ with different additions of NaOH at atmospheric CO_2 pressure and measuring the pH after 24 h, as in Section 3.2.2. The measured pH was plotted against OH^- added, less any OH^- precipitated in $CaCO_3$, and b_{HS} inferred from the relationship between pH versus OH^- reacting.

3.3 Results

3.3.1 Influence of CO_2

The five additions of NaOH increased the initial pH of soils T and S to give the range of values shown in Table 3.2.

Table 3.2: *Range of initial soil pH of the two soils from Pegwell Bay (soils T and S) shaken in 10 mM $CaCl_2$ containing the indicated additions of NaOH.*

	NaOH addition (mmol.kg^{-1} soil)	Range initial pH
Soil T	0	7.8 - 7.9
	6	8.3 - 8.6
	12.5	8.9 - 9.2
	25	9.4 - 9.8
	31	9.7 - 10.0
Soil S	0	7.8 - 8.0
	6	8.7 - 8.9
	12.5	9.3 - 9.5
	25	10.1 - 10.3
	31	10.4 - 10.6

All treatments then showed a slow decrease in pH over time (Figures 3.1 and 3.2, 3.4, 3.5).

Ambient CO_2 pressure

While the pH in $CaCl_2$ without addition of base for soils T and S was similar, the initial pH in suspensions with addition of base was consistently higher for soil S than for soil T by at least half a unit of pH. Under closed atmospheric conditions (Figure 3.1), the pH in suspensions of soil S was also found to be consistently higher than that in soil T over the duration of the experiment, and soil S suspensions did not revert to their initial pH of 7.9 after 19 days. In the absence of NaOH, the pH in soil S suspensions stayed constant, while the pH in soil T suspensions after 19

days was recorded lower than its initial pH by 0.5 unit (Figure 3.1 (a)). This difference between pH in soil S and T suspensions disappeared under open atmospheric conditions (Figures 3.2).

Under open atmospheric conditions (Figures 3.2), the pH in both soils T and S suspensions was constant in the absence of base addition (Figure 3.2 (a)), while the drop observed after 3 days under closed atmospheric conditions in the pH of soil T suspensions disappeared. In the case of an initial increase in pH, all suspensions settled and plateaued after 3 days. Suspensions of soils T and S dropped to a similar pH value at lower base additions (Figure 3.2 (b) and (c)), however in the presence of more OH^-, soil S suspensions plateaued at a pH a quarter of a unit lower than that of suspensions of soil T (Figures 3.2 (d) and (e)).

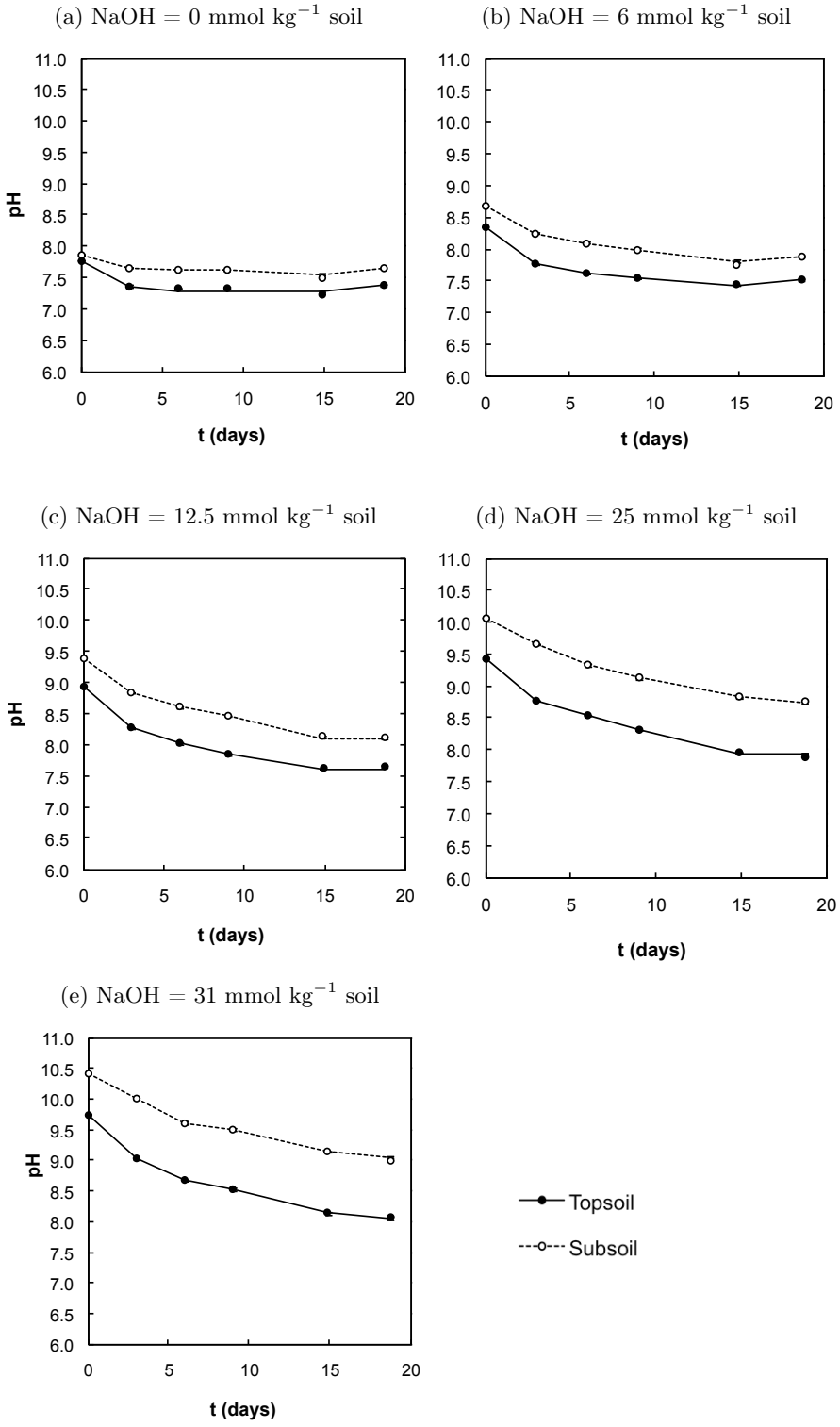

Figure 3.1: *Soil pH changes following addition of base under atmospheric carbon dioxide pressure (0.038%) in sealed flasks. Soils are topsoil (soil T) and subsoil (soil S) from Pegwell Bay, Kent (Points show means (n=3). Error bars are smaller than data points).*

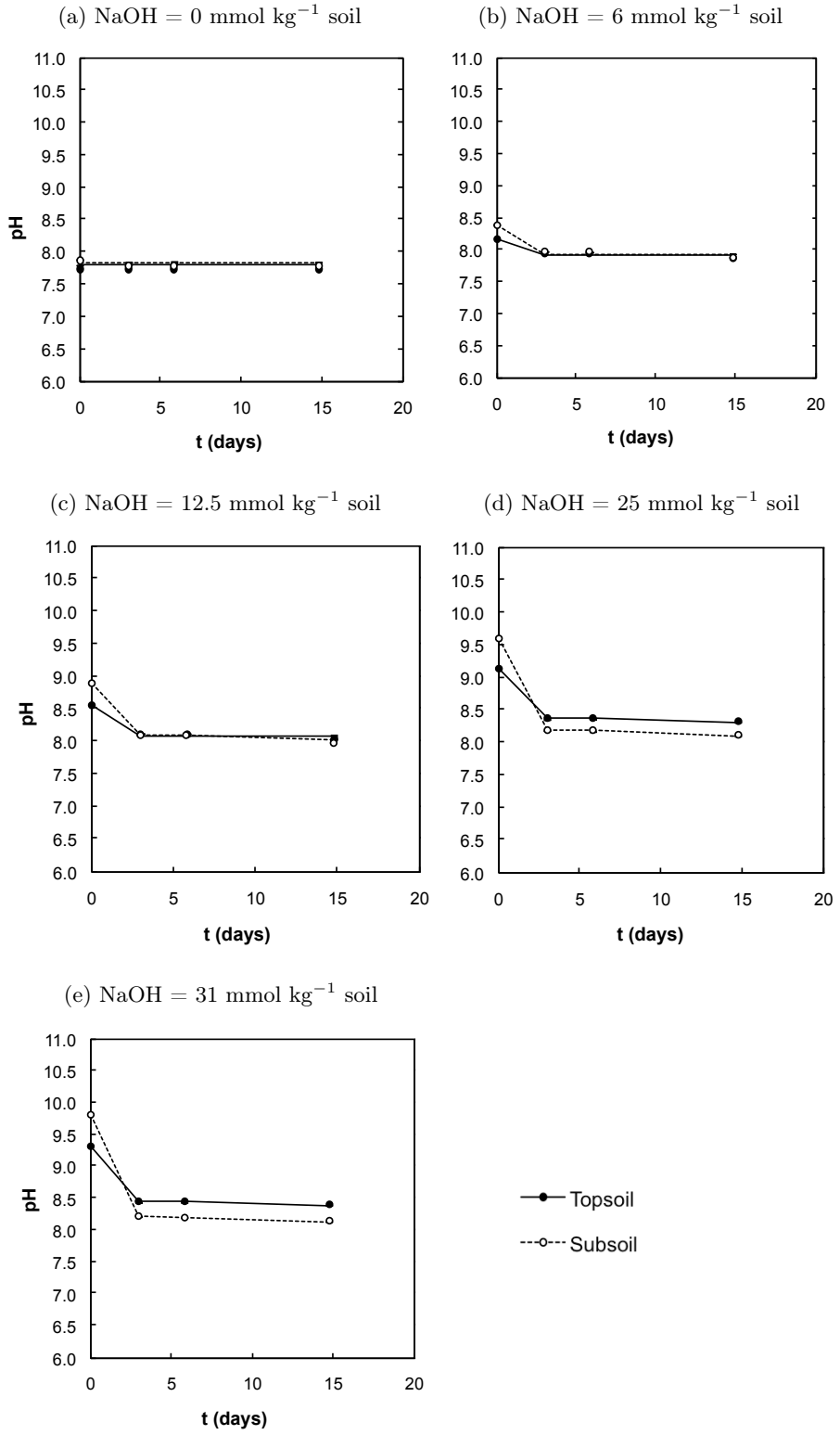

Figure 3.2: *Soil pH changes following addition of base initially under atmospheric carbon dioxide pressure (0.038%) in open flasks. Soils are topsoil (soil T) and subsoil (soil S) from Pegwell Bay, Kent (Points show means (n=3). Error bars are smaller than data points).*

The measurement of the CO_2 concentration in sealed flasks of both soils suspensions in the experiments Figure 3.1 showed that the soil T produced a significantly greater amount of CO_2 than soil S through the range of NaOH (Figure 3.3). After three days, the CO_2 concentration in soil T suspensions without NaOH reached 0.27% (Figure 3.3 (a)), 7 times the normal atmospheric content (0.039%). However, the CO_2 produced by soil S suspensions was not significant, and the CO_2 concentration in the flasks was found to remain at atmospheric level or below. The amount of CO_2 measured in both soils was found to consistently decrease with increasing NaOH concentration.

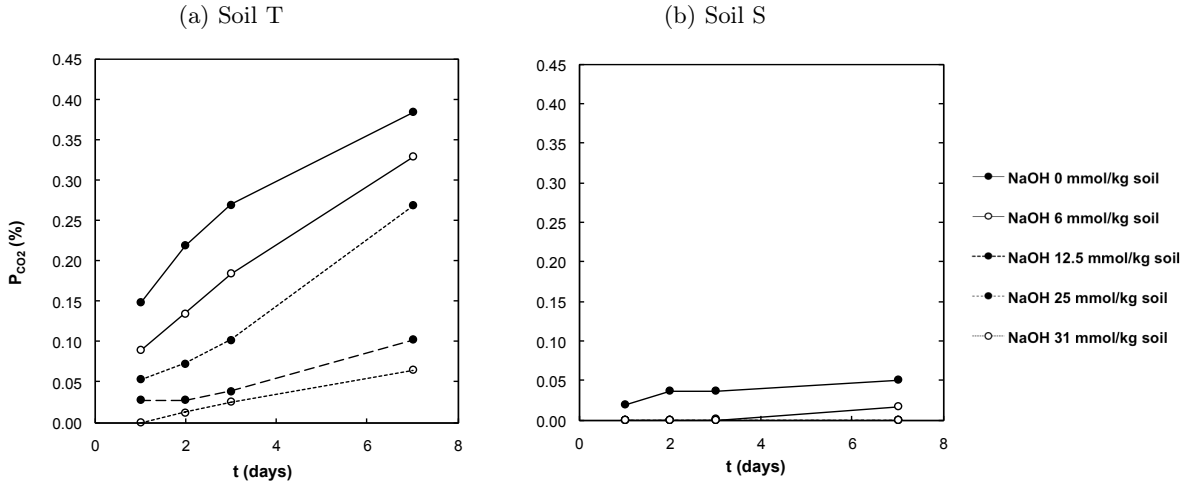

Figure 3.3: *Evolution of CO_2 in the headspace of the flasks in the experiments Figure 3.1. (Points are means (n = 3). Error bars are smaller than data points).*

Controlled CO_2 pressure

Under closed atmospheric conditions and increased CO_2 pressures, there was an increase in pH at t = 0 when there was no addition of NaOH (Figures 3.1, 3.4, 3.5), that was not observed under open atmospheric conditions (Figure 3.2 (a)).

Under increased CO_2 concentrations, a similar trend was observed, with soil S suspensions reaching an equilibrium pH equal or inferior to that at which soil T suspensions settled. However, under 1% and 4% CO_2 the plateau was recorded between 7.3 and 7.5 and 7.0 and 7.3 respectively, thus at lower values than under open atmospheric conditions. This equilibrium was reached between 7 and 16 days under 1% CO_2 and 4 and 10 days under 4% CO_2, the time to reach a pH plateau increasing with increasing NaOH addition.

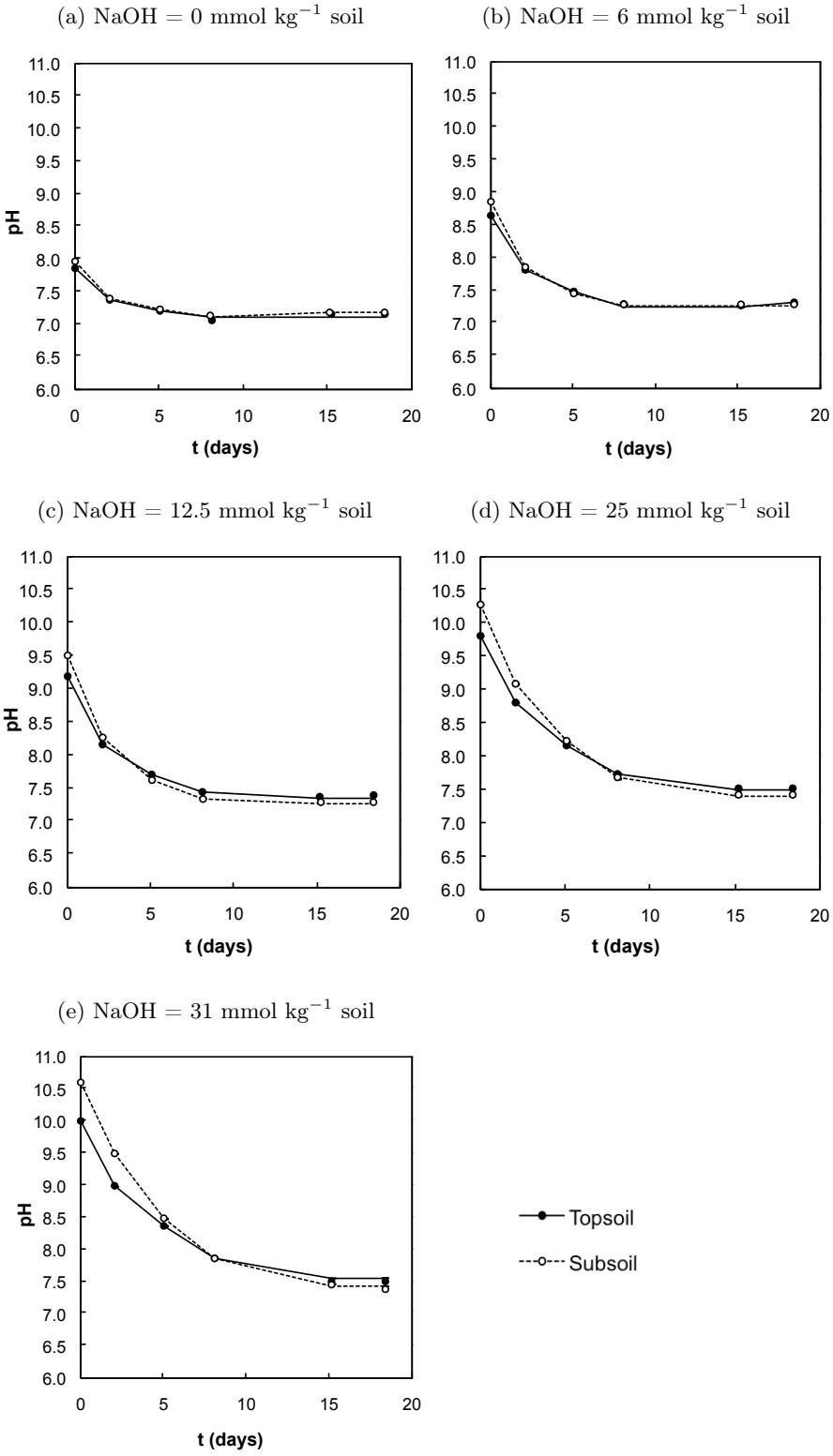

Figure 3.4: *Soil pH changes following addition of base under 1% carbon dioxide partial pressure. Soils are topsoil (soil T) and subsoil (soil S) from Pegwell Bay, Kent (Points show means (n=3). Error bars are smaller than data points).*

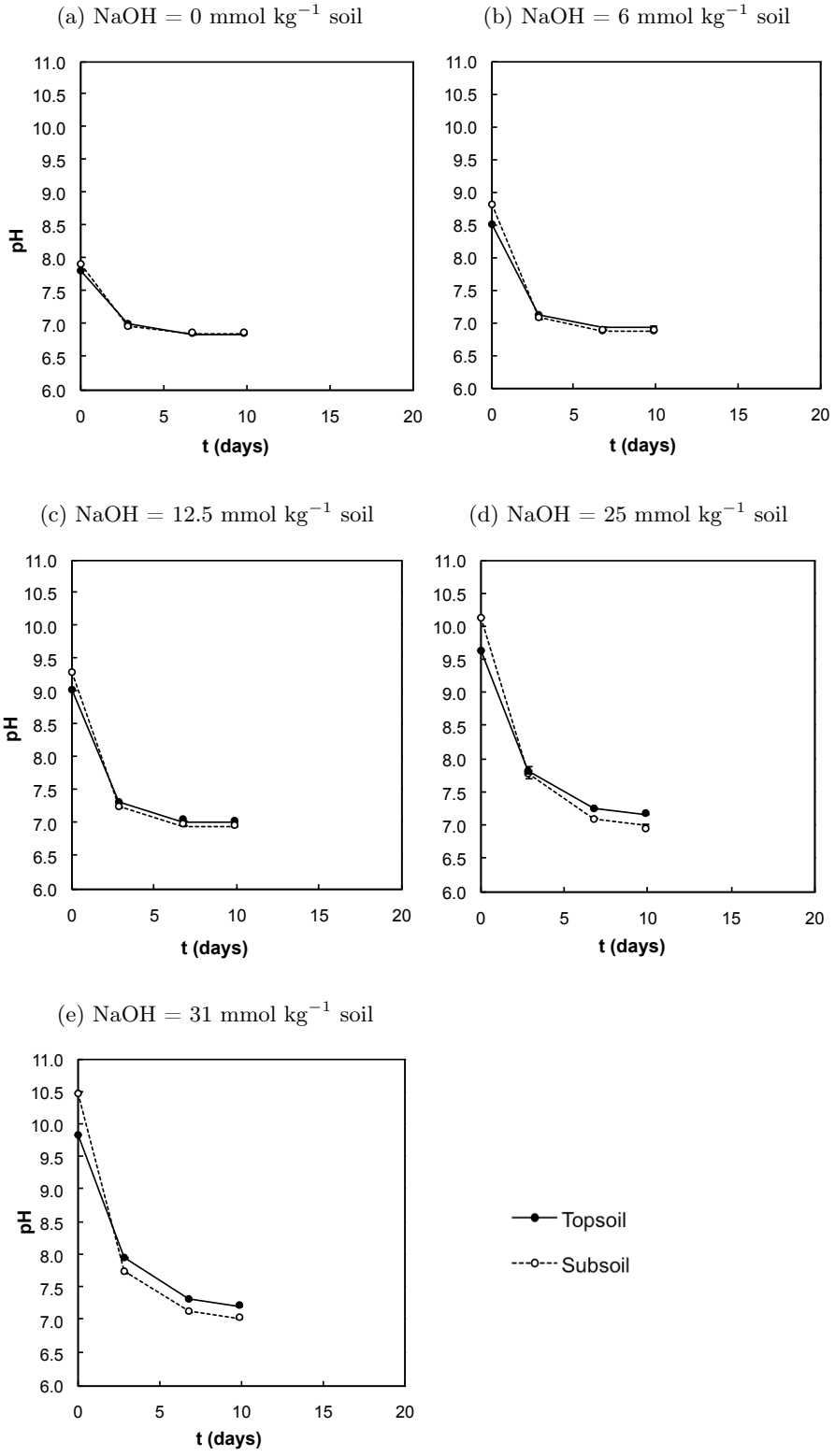

Figure 3.5: *Soil pH changes following addition of base under 4% carbon dioxide partial pressure. Soils are topsoil (soil T) and subsoil (soil S) from Pegwell Bay, Kent (Points show means (n=3). Error bars are smaller than data points).*

The concentration of Ca^{2+} left in solution after the recording of pH showed a steady decrease with increasing initial NaOH in the soil suspensions. The suspensions kept under 4% CO_2 showed the widest difference in final Ca^{2+} concentrations. In soil T suspensions, Ca^{2+} dropped from 10.44 mM (NaOH = 0) to 8.10 mM (NaOH = 31 mmol.kg^{-1} soil). Similar values were measured in corresponding S suspensions. Under lower CO_2 partial pressures, this trend in Ca^{2+} concentration was found to be similar although not as pronounced.

The amount of $CaCO_3$ precipitated measured in T and S soils at the end of the pH runs varied between 115 and 130, and 125 and 140 mmol kg^{-1} respectively. However this was found to be variable with treatments and not to follow a clear trend depending on either CO_2 or NaOH concentration in solution. The initial $CaCO_3$ in T and S was measured at 122 and 137 mmol kg^{-1} soil respectively.

3.3.2 Influence of P and DOC

Phosphorus was not detected in solution in any of the soil suspensions with or without P additions up to 1.5 mol kg^{-1}. The changes in pH with time were not found significantly different in any of P treatments. However, DOC content was found to increase with increasing NaOH concentration in suspensions of both soils Ti and G. To study the influence of DOC, the profiles in soils without P addition were used and referred to (Figures 3.6 and 3.7). The corresponding figures at higher P concentrations are given for reference (Appendix B.3).

The DOC concentration in suspensions of soils Ti and G without addition of NaOH were 15 and 2.5 mM respectively, and remained constant over time. With increasing NaOH concentrations, the amount of DOC in solution increased. For NaOH 31 mmol kg^{-1}, DOC reached 20 and 5 mM at t = 0 in suspensions of soils Ti and G respectively. In soil G suspensions at higher NaOH concentrations, DOC remained constant over time (Figure 3.7 (c)). However, in suspensions of soil Ti, for NaOH 12.5 and 31 mmol kg^{-1}, DOC steadily increased over time from

16 to 20 and 20 to 27 mM respectively (Figure 3.6 (c)).

The results found from the observation of pH over time in suspensions of soils Ti and G were similar to the observations made on suspensions of soils T and S in Section 3.3.1. Following addition of NaOH to the soil suspensions, an initial increase in pH was observed in both soils Ti and G. The initial value of pH increased with increasing initial NaOH concentration. In the suspensions with NaOH = 0, the pH was found to remain constant over time in Ti suspensions, but decreased slightly in G suspensions.

In both soils, pH reached a plateau after 4 days, and remained constant at that value until the last recording. The values at the plateau were also found to increase with increasing NaOH concentration, and neither soil settled back to its initial pH value. The pH in soil G suspensions was found to settle at 6.7 for NaOH 31 mmol kg^{-1}, half a unit higher than the corresponding suspensions at NaOH 12.5 mmol kg^{-1}, and over a unit higher than in the control suspension (Figure 3.7 (a)). The difference in final pH values was not found to be as significant in soil Ti (Figure 3.6 (a)).

In parallel to the decrease in pH, detectable amounts of $CaCO_3$ were precipitated over time in both soil suspensions, including in the controls (NaOH = 0). The amount of $CaCO_3$ increased with increasing NaOH concentration in suspension. At lower NaOH concentrations, $CaCO_3$ was precipitated after the thirteenth day of the experiment, while at NaOH 31 mmol kg^{-1} the precipitation of $CaCO_3$ appeared to start from t = 0 for both soils. Double the amount of $CaCO_3$ was precipitated in soil G suspensions (Figure 3.7 (b)) as in soil Ti (Figure 3.6 (b)).

The initial concentration of Ca^{2+} in solution was 14 mM for both soils without NaOH, and found to consistently decrease with increasing NaOH concentrations. For NaOH additions of 0 and 12.5 mmol kg^{-1}, the concentration of Ca^{2+} was found to be lower in soil G than soil Ti. In both control suspensions (NaOH = 0), the Ca^{2+} concentration appeared constant until the fourth day of the experiment, when it started decreasing. The same decrease was observed at the same moment in suspensions with higher NaOH concentrations. However between the initial

measurement and the fourth day, an increase in Ca^{2+} in solution was recorded in both soils, for both addition of base (Figures 3.6 and 3.7 (d)).

Likewise, the concentration of Na^{+} in solution decreased over time for both soils and all NaOH concentrations. However, in soil Ti suspensions, Na^{+} in solution started to drop after 4 days (Figure 3.6 (e)), while it appeared to stay constant until 13 days in soil G (Figure 3.7 (e)). The initial concentration of Na^{+} increased with increasing NaOH additions, and was found to be consistently lower in soil G suspensions than in soil Ti. The concentration of K^{+} was negligible compared to other ions in both soils.

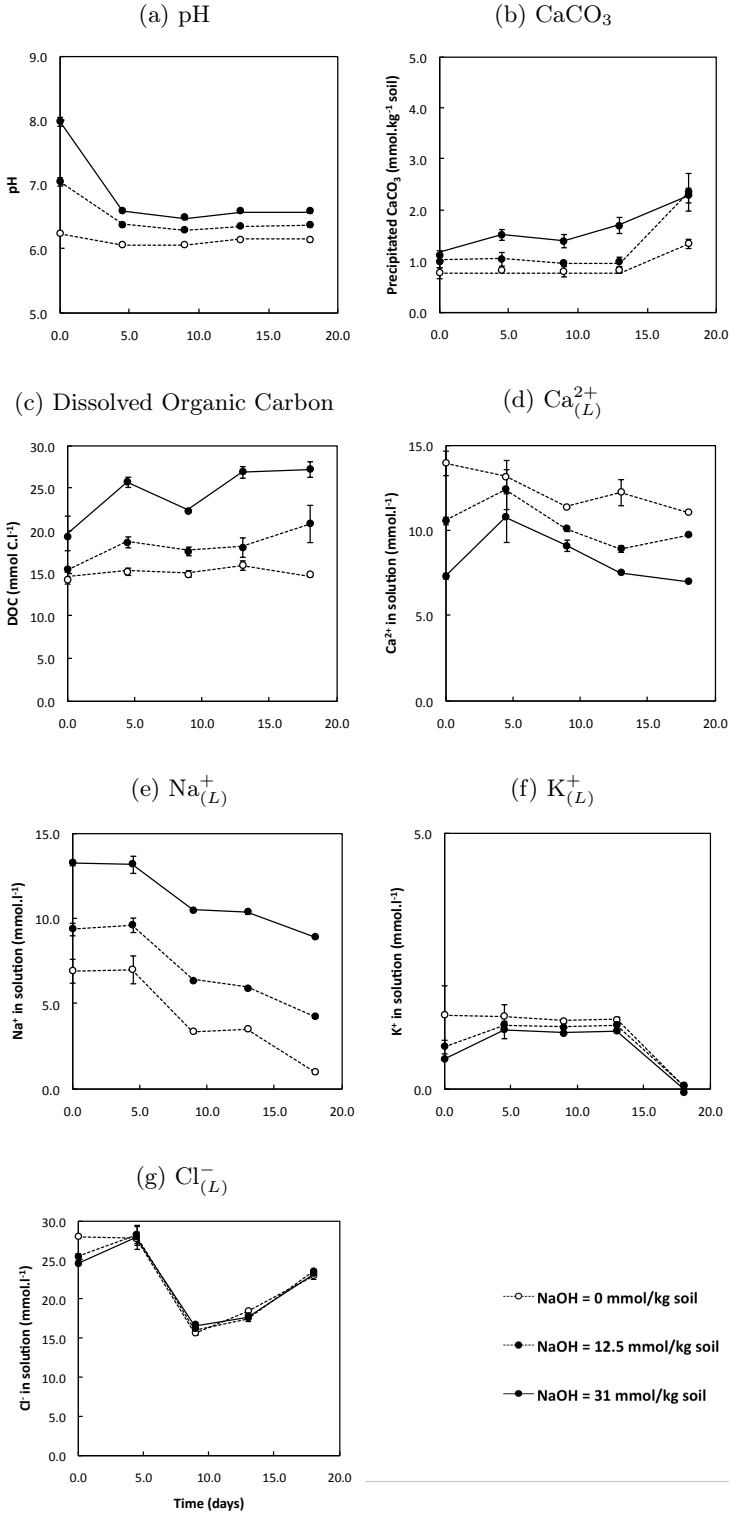

Figure 3.6: *Changes over time in experimental soil Ti suspensions without addition of P after different additions of base (see legend), under 4% carbon dioxide partial pressure. (Points show means (n = 3). When error bars are not visible they are smaller than the data points.)*

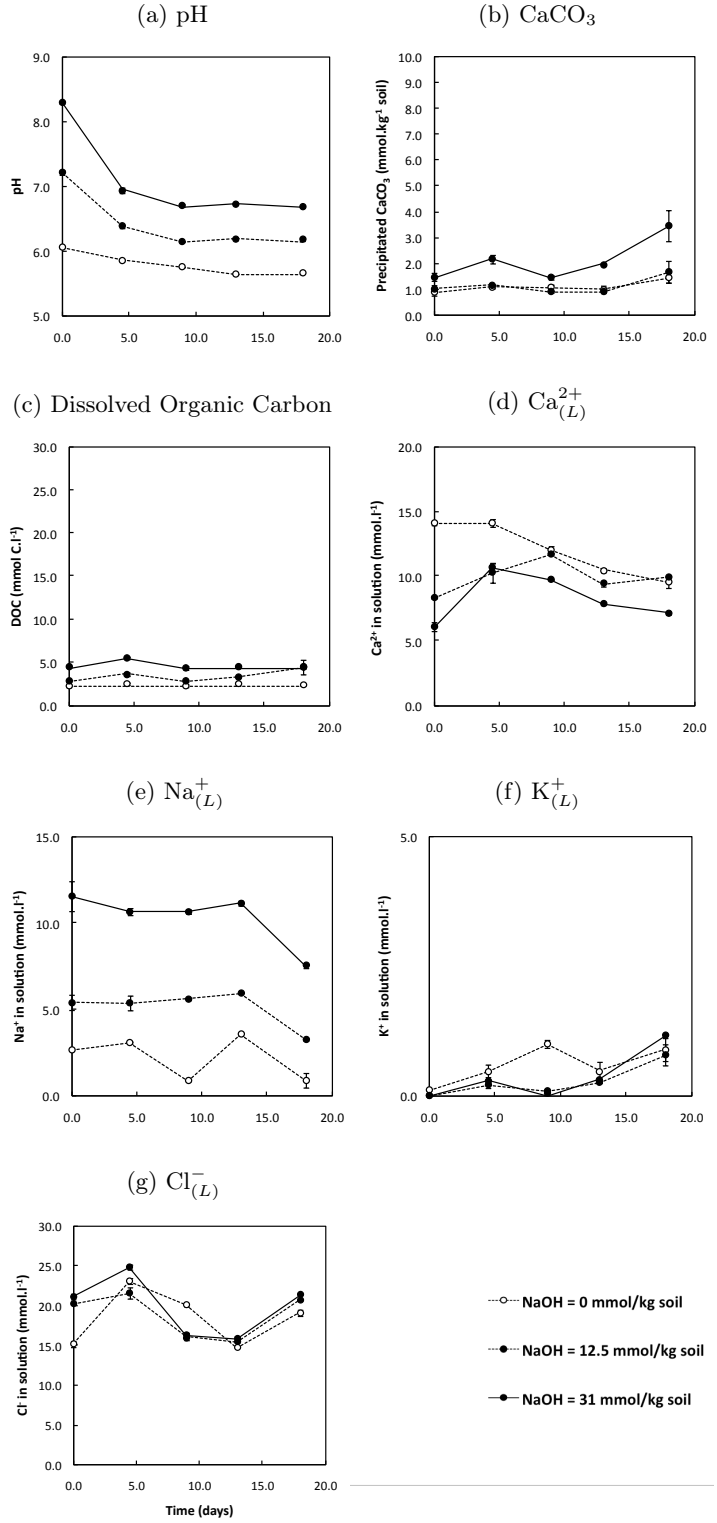

Figure 3.7: *Changes over time in experimental soil G suspensions without addition of P after different additions of base (see legend), under 4% carbon dioxide partial pressure. (Points show means (n = 3). When error bars are not visible they are smaller than the data points.)*

3.3.3 Model parameters

Rates of $CaCO_3$ precipitation at different times were derived from fitting Equation 3.2 to the data for soils Ti and G with NaOH 31mmol kg^{-1} (Figure 3.8). The fitted equations were

$$\text{Soil Ti} \qquad \frac{\mathrm{dCaCO_3}}{\mathrm{dt}} = 0.064 \times 1.81 \times 10^{-6} e^{(1.81 \times 10^{-6} t)} \qquad (3.3)$$

$$\text{Soil G} \qquad \frac{\mathrm{dCaCO_3}}{\mathrm{dt}} = 0.001 \times 5.05 \times 10^{-6} e^{(5.05 \times 10^{-6} t)} \qquad (3.4)$$

The saturation index in the soil suspensions over time were calculated with the speciation routine detailed in Appendix A. After addition of NaOH to the soil, SI was 156 and 303 in soils Ti and G respectively (Table 3.3).

Thus values of the parameter α were calculated to be 0.28×10^{-10} and 0.07×10^{-10} mol kg^{-1} s^{-1} for soils Ti and G respectively.

Table 3.3: *Saturation index (SI) in soils Ti and G suspensions kept under 4% CO_2, with NaOH = 31 mmol kg^{-1} soil and Cl^- = 20 mM calculated with the speciation FORTRAN routine detailed in Appendix A. ($Ca^{2+}_{(L)}$ in mM).*

	Soil Ti			Soil G		
Time (days)	pH	$Ca^{2+}_{(L)}$	**SI**	pH	$Ca^{2+}_{(L)}$	**SI**
0	8.0	7.33	**156.1**	8.3	6.09	**302.9**
4	6.6	10.79	**0.8**	6.9	10.67	**3.8**
9	6.5	9.12	**0.4**	6.7	9.71	**1.2**
13	6.6	7.50	**0.6**	6.7	7.84	**1.1**
18	6.6	7.00	**0.5**	6.7	7.10	**0.9**

(a) Soil Ti

$$CaCO_3 = 1.22 + 0.064e^{(1.81\times10^{-6}t)}$$
$$R^2 = 0.935$$

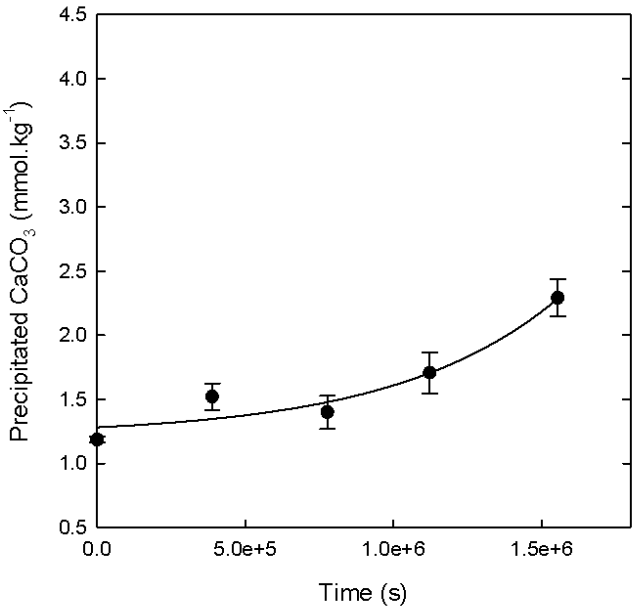

(b) Soil G

$$CaCO_3 = 1.69 + 0.001e^{(5.05\times10^{-6}t)}$$
$$R^2 = 0.934$$

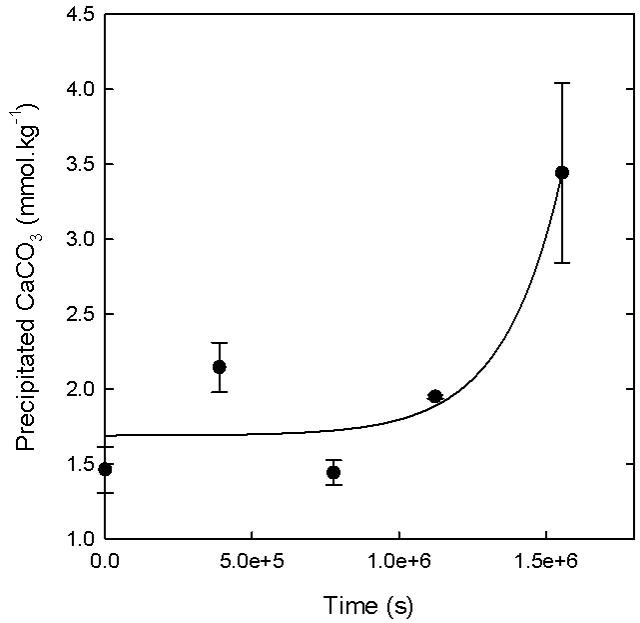

Figure 3.8: *Three parameter exponential functions fitted to the $CaCO_3$ concentration-time profiles for soils in $CaCl_2$ 10 mM and NaOH 31mmol kg^{-1} suspensions. The subcaptions give the equations of the regression lines for soil Ti (a) and G (b) and an estimation of the goodness of fit to the experimental data R^2. (Points show means (n = 3). Bars show standard error.)*

Based on the shaken suspension experiments equilibrated for 24 h at atmospheric CO_2 pressure, and the pH change per unit base reacting, allowing for base consumed in $CaCO_3$ precipitation (Figure 3.9), the pH buffer power b_{HS} (= d[OH^-]/dpH) was calculated to be 31.3 and 25.0 mmol kg^{-1} pH^{-1} for soils Ti and G respectively.

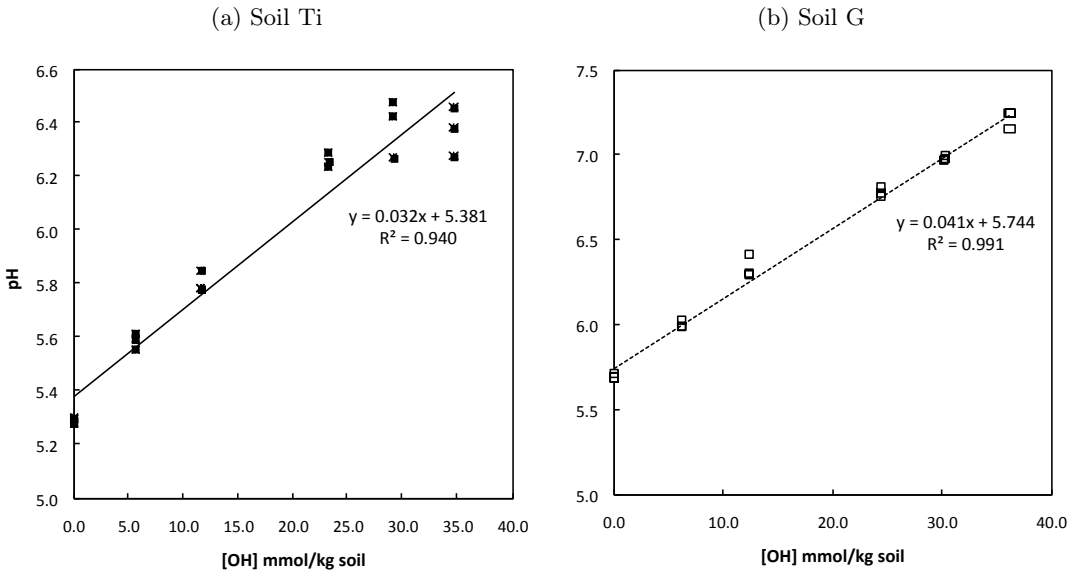

Figure 3.9: *pH as a function of changes in soil base for soils Ti and G.*

3.4 Discussion

The topsoil and subsoil sampled from the brickearth in Pegwell Bay had similar initial pH, but the initial pH increase after NaOH addition differed between them. This indicates that the pH buffer powers (b_{HS}) of the two soils were different, with b_{HS} of the topsoil greater than that of the subsoil. In calculating b_{HS}, processes responsible for buffering pH other than $CaCO_3$ precipitation were assumed to be complete within a few hours of the experimentally-induced increase in pH. The subsequently observed decrease in pH was therefore solely due to $CaCO_3$ precipitation. In practice, there may be other slow reactions of base with the soil such as diffusive penetration of base through narrow-access pores to reaction sites (Nye and Ramzan, 1979). But as a first approximation the assumption is realistic (Nye and Ameloko, 1986).

In both soils, significant $CaCO_3$ precipitated by the end of the pH runs. The concentration of Ca^{2+} in the solution equilibrated with the soils decreased by approximately 2 mM. Assuming all this Ca^{2+} was used in the formation of $CaCO_3$, the amount precipitated was approximately 5 mmol kg^{-1}. This would not have been detected against the high background $CaCO_3$, which was greater than 120 mmol $CaCO_3$ kg^{-1} in both soils. A similar experiment conducted on non-calcareous soils Ti and G, with a background between 1 and 1.5 mmol $CaCO_3$ kg^{-1} soil, and kept at 4% CO_2, did show a two-fold increase in $CaCO_3$ content.

Precipitation of $CaCO_3$ requires sources of Ca^{2+}, OH^- and CO_2, and it is commonly found that the rate of precipitation is proportional to the extent of super-saturation, according to a rate law of the type in Equation 3.2. Increasing the CO_2 pressure in solutions supersaturated with Ca^{2+} and carbonate ions accelerated $CaCO_3$ precipitation through at least two mechanisms (Lebron and Suarez, 1998): through increases in the activity of $CaHCO_3^+$ which may be an intermediary in the precipitation reaction; and through increases in the density of negative charges on the surface of existing $CaCO_3$ crystals as a result of CO_3^{2-} adsorption, thus promoting crystal growth (Charlet et al, 1990).

The effect of high CO_2 pressure on $CaCO_3$ precipitation was shown in the experiments in this chapter by a sharper decrease in pH observed in suspensions kept under high CO_2 pressures and in open atmospheric conditions where CO_2 was not limiting.

The evolution of CO_2 from the suspensions of soils T and S caused different pH changes depending on whether the flasks were sealed or open. The two soils were sampled from different depths of the same soil profile, and the organic C content of the topsoil was three times higher than that of the subsoil. The biotic activity and respiratory production of CO_2 differed correspondingly.

The pH of the topsoil suspensions open to the atmosphere reached equilibrium value after 2 days, while those under sealed atmospheres equilibrated more slowly, and their final pHs were 0.5 units higher. This was presumably due to the time necessary for CO_2 to build up in the headspace of the sealed flasks. This was also observed in the suspensions with high NaOH additions despite a sharp decrease in CO_2 availability compared with the control (NaOH = 0). While the presence of base at higher concentrations could be expected to inhibit microbial respiration, CO_2 was still produced in measurable quantities over time (Figure 3.3), and thus would not be a limiting factor in the $CaCO_3$ precipitation reaction.

In the subsoil suspensions kept under open atmospheric conditions, the observed decrease in pH was sharper than in the topsoil, indicating more rapid $CaCO_3$ precipitation. A possible explanation is that precipitation in the subsoil was less inhibited by DOC, it having a much smaller organic content. Possibly also, the greater $CaCO_3$ content of the subsoil enhanced precipitation by providing nucleation surfaces.

Likewise, the differences in rates of precipitation in soils Ti and G could be explained by the difference in DOC concentrations. The DOC concentration was found to increase with increasing NaOH concentration, consistent with increased organic matter solubility at higher pH. The absence of detectable P concentrations in the soil solutions and no differences in precipitation rates between the P treatments suggest P did not influence the $CaCO_3$ precipitation reaction.

Visconti et al. (2010) found that concentrations of DOC between 7 and 12 mM were sufficient

to inhibit $CaCO_3$ precipitation in water-saturated soils. The DOC concentrations were greater than 12 mM in soil Ti suspensions with 31 mmol NaOH kg^{-1} and increased over time. Whereas in soil G they were below 7 mM and tended to decrease over time.

Further, soil G was found to have a lower buffer power b_{HS}. After addition of NaOH this would lead to a higher pH in soil G suspensions, and therefore a higher saturation index SI. This combined with a lower DOC content led to higher $CaCO_3$ precipitation rates in soil G than soil Ti.

Lebron and Suarez (1998) reported that DOC inhibits $CaCO_3$ precipitation by coating existing $CaCO_3$ crystal surfaces, thus blocking their nucleation sites and stopping homogeneous crystal growth. They also noted that the concentration of DOC necessary to inhibit $CaCO_3$ formation by such a mechanism increased with increasing CO_2. The soils G and Ti suspensions being kept under 4% CO_2, this could partly explain the apparent absence of inhibition as DOC increased over time in soil Ti. However the fact that $CaCO_3$ precipitated despite increasing DOC concentrations in soil suspensions could also indicate that in this experimental setting, the rate of $CaCO_3$ precipitation was controlled by heterogeneous nucleation rather than homogeneous crystal growth. Soil microbes have been proposed as "seeds" for $CaCO_3$ nucleation (Lebron and Suarez, 1996). This would be corroborated by higher soil biomass content relating to the higher precipitation rate measured in soil Ti than in soil G.

The change in pH over time matched the $CaCO_3$ concentration-time profiles. The differences between the soils in equilibrium pH with increasing NaOH concentrations matched the differences in b_{HS}. Although more $CaCO_3$ precipitated in soil G suspensions, the final pH values were consistently higher than in soil Ti suspensions because b_{HS} is smaller in soil G.

The profiles of Ca^{2+} also matched the changes in pH and $CaCO_3$ over time. Except in the controls (NaOH = 0), an initial increase in Ca^{2+} in solution following NaOH addition was followed by a steady decrease over time. Presumably the initial increase in Ca^{2+} in solution was due to displacement from the soil exchange complex by Na^{+}. Further, as exchangeable Ca^{2+}

is removed in $CaCO_3$ precipitation, more Na^+ is sorbed on the exchange complex. This was confirmed by the steady decrease in Na^+ concentration in solution over time, in parallel with $CaCO_3$ increasing. The decrease in solution Na^+ was sharper in soil Ti than soil G, consistent with the greater CEC of soil Ti.

3.5 Conclusions

Highly calcareous soils sampled from sites where $CaCO_3$ was known to form proved poorly suited to laboratory study of $CaCO_3$ precipitation. The amounts precipitated under the experimental conditions used were not detectable against high backgrounds. The two non-calcareous soils proved more suitable and had sufficiently different physicochemical properties to provide contrasting behaviours. These soils were therefore selected for the experiments to test the $CaCO_3$ model developed in Chapter 2. Two parameters for the model - the precipitation rate coefficient α and the soil pH buffer power b_{HS} - were then estimated for these soils.

The experiments looking at the influence of P on $CaCO_3$ precipitation indicated little effect of P in the soils considered. For additions of P up to four times the UK standard recommended application rate for P fertilisers, no soluble P could be measured in the soil solution for the duration of the experiment, and there were no differences in $CaCO_3$ precipitation between the P treatments. However, DOC concentrations were found to affect on the precipitation rates in all the soils studied.

The partial pressure of CO_2 strongly affected $CaCO_3$ precipitation rates in the soils. At CO_2 partial pressures higher than atmospheric, the rate at which pH equilibrated following addition of NaOH increased and the equilibrium pH was lower. Additionally, the production of CO_2 by soil microbes was shown to be potentially significant in influencing the rate of $CaCO_3$ precipitation in soils.

An inhibitory effect of DOC on $CaCO_3$ precipitation was also found in soils Ti and G. Because soil microbes regulate DOC concentrations, this suggests a further way in which soil microbes may influence precipitation. In addition, microbes may provide surfaces for heterogeneous nucleation.

The above microbial effects on precipitation have been considered in previous studies of

$CaCO_3$ precipitation in idealised laboratory conditions, removed from natural circumstances. But the effects of whole microbial communities in structured soil systems have received little attention. The results in this chapter indicate the need for further investigation into the role of soil microbial communities. The ways in which bacterial and fungal communities present in soils affect precipitation, together with transport limitations in structured soils are considered in Chapter 5.

Chapter 4

Reactant concentration-distance profiles near a calcium carbonate precipitation zone

4.1 Introduction

Most studies relating to $CaCO_3$ precipitation in soils have have been made in idealised aqueous systems or in shaken soil suspensions of the type in Chapter 3 (see Introduction). In real, structured soils, surface-mediated reactions are likely to be different, and the influence of transport on reaction rates is likely to be greater. In structured soils, transport of gases and solutes to reaction sites is influenced by the shape and complexity of the soil pore network, by differential sorption in surfaces, and potentially also by biological processes. Transport properties can thus vary greatly from one soil to the other but also spatially within the same soil.

The model described in Chapter 2 allows for these potential transport limitations. In this chapter an experimental system is developed to measure the effects of transport and reactants concentration-distance profiles near a zone of $CaCO_3$ precipitation in a structured soil so as to test the model.

The experimental system is based on the scheme in Figure 2.1. It allows measurement of the profiles of pH, Ca_L^{2+}, Cl_L^- and precipitated $CaCO_3$ with distance away from a source of alkalinity, with which to assess the model outputs. In the system, HCO_3^- ions from the resin will diffuse into the soil profile in exchange for Cl^-, and react with Ca^{2+} in solution and from the soil exchange complex to precipitate $CaCO_3$. The experiments were made with this system using the two soils identified in Chapter 3.

4.2 Materials and methods

4.2.1 Experimental soils

The two experimental soils (labelled Ti and G) were chosen for their contrasting parent material, CEC, pH and texture (Table 3.1). As described in Chapter 3, the soils were washed

with a 10 mM $CaCl_2$ solution, air-dried and sieved to 0.5 mm.

4.2.2 Experimental system

Figure 4.1 shows the experimental system. Diffusion cells were prepared from 4 cm internal diameter plastic piping cut in 3 cm lengths. Enough cells were made for three replicates of each soil, for three diffusion times (6 hours, 1 day and 5 days) and a control. The controls consisted of packed soil columns at the same moisture content and bulk density as in the treatments, but without a layer of anion exchange resin.

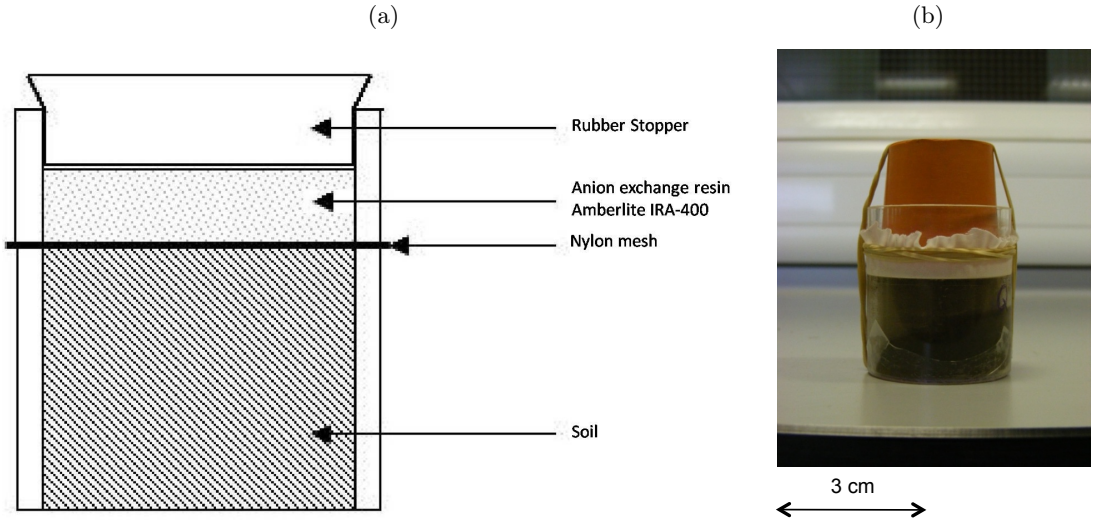

Figure 4.1: *Diffusion system (a) and photo of the experimental setup (b).*

The bottom of each cell was closed with nylon mesh to facilitate soil packing. The required weight of air-dry soil was placed in layers into the cells and compacted. Before adding the next layer, the surface of the previous compacted layer was roughened using a blade to get better packing uniformity. The soil columns were then placed on watch glasses and a measured volume of 10 mM $CaCl_2$ solution was added to the watch glass to bring them to the appropriate moisture

content by capillary rise, overnight. The target volumetric moisture contents (cm cm^{-3}) and bulk densities (g cm^{-3}) were 0.50 and 1.0 for soil Ti and 0.30 and 1.4 for soil G, respectively.

The addition of solution made the soils swell by a few millimetres. The excess soil was removed to produce a flat surface for optimum contact between the soil and ion exchange resin. The final bulk density of the soil was determined from the final weight of dry soil in the cell and its volume.

Because the soils had been stored air dried, the rewetting process will have provoked a boost in microbial activity lasting up to a week. The soils were therefore allowed to equilibrate for a week before bringing them into contact with the anion exchange resin. During equilibration the soils were placed in sealed incubation chambers with water saturated atmosphere and connected to the outside atmosphere via a HEPA filter to allow gaseous exchange.

After equilibration, a 1 cm thick layer of HCO_3^- anion exchange resin (Amberlite IRA-400 - ion exchange capacity >1.40 mol_c l^{-1} wetted bed volume) was made in the bottom of a second diffusion cell. The resin had been shaken overnight with five times its exchange capacity equivalent of $NaHCO_3$ to saturate it with HCO_3^-, following manufacturer's guidelines, . The base of the resin was covered with a layer of 24 μm pore-diameter nylon mesh. The resin moisture content was adjusted on sand tables so that the water potential matched that of the soil so that there was no mass flow of water between soil and resin. The two cells were then brought into contact. To ensure good soil-mesh-resin contact, a rubber bung was placed in the upper cell and pushed down. Silicone grease was then spread over the join between the two cells to reduce water loss. The system was incubated at constant temperature (20°C) in the same water-saturated environment as described above. The HEPA filters allow for constant equilibration between the inside of the incubation chamber and the external atmosphere to prevent a build up of CO_2 around the cells and in the soils.

4.2.3 Analytical methods

At the end of the diffusion period, the two cells were separated and the soil sectioned parallel to the soil-resin boundary using a microtome and a stainless steel blade (Figure 4.2). Twenty slices were taken, between 0.5 and 1 mm thick.

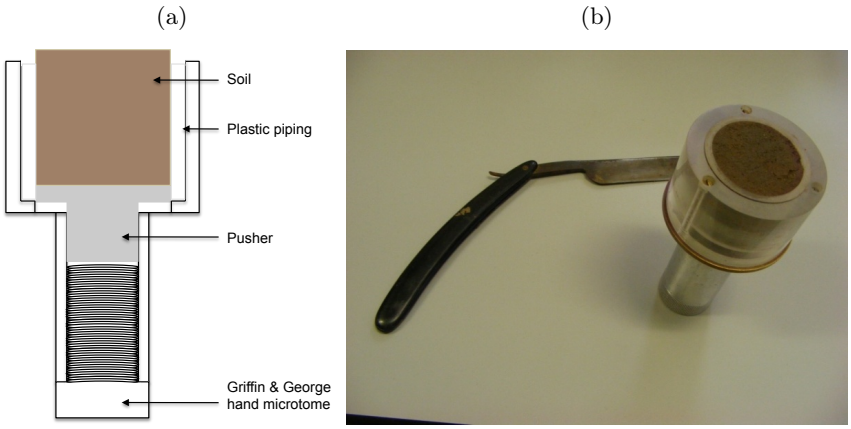

Figure 4.2: *(a) Schematics and (b) photo of the soil slicing apparatus.*

Each soil slice was weighed and then centrifuged (10 minutes, 2835 g-units) in a Durapore® centrifugal filter unit to extract the soil solution. The volume of soil solution extracted was determined by weight, and its pH measured immediately using a combination microelectrode. The soil solution was then diluted with deionised water and analysed for Ca^{2+} by atomic adsorption spectrophotometry (Perkin-Elmer AAnalyst 800), and Cl^- by ion exchange chromatography (Dionex). The amount of calcium carbonate in each slice was measured after centrifugation by adding 5 cm^3 of 1 M HCl to the residual soil and measuring the amount of CO_2 produced by gas chromatography.

It was also originally intended that exchangeable calcium would be measured in the soil sections. However preliminary experiments (see Appendix C.5) failed to produce a satisfactory method for this in the presence of a high content of precipitated $CaCO_3$. This was therefore not

included in the analytical protocol.

The processing sequence for each slice is summarised in Figure 4.3.

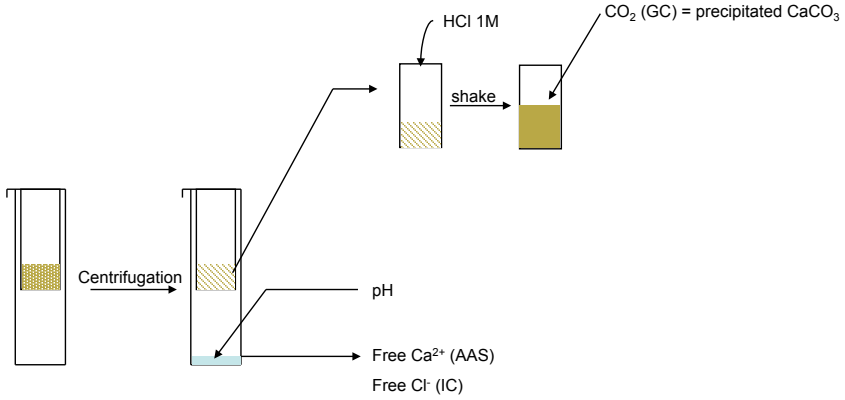

Figure 4.3: *Processing sequence for each slice of soil after diffusion. AAS = Atomic Adsorption Spectrophotometry, GC = Gas Chromatography, IC = Ion exchange Chromatograhy.*

The distance from the source of base (x axis) was calculated from the dry weight of individual slices and the packed soil bulk density over the whole collar. These values were thus not measured but calculated making the assumption that the soil was uniformly packed in the collars.

4.2.4 Determination of the impedance factor f_L and CO_2 pressure

The diffusion impedance factors of the soils under the conditions of the above experiments were obtained by fitting the experimental data for Cl^- concentration with distance away from the source of alkalinity to the solution of Equation 2.1. Note that with the boundary conditions for Equation 2.1 defined for the model, the concentration-distance profile of Cl^- at a particular time solely depends on the Cl^- diffusion coefficient $f_L D_{LCl}$. Hence f_L can be obtained directly from the concentration-distance profiles.

The CO_2 concentration in soil air in the experimental soil columns was estimated by fitting the experimental data for pH to the model outputs. It is assumed that the effect of the rate of precipitation coefficient α is negligible compared to the influence of P_{CO_2} on soil pH.

4.3 Results

Figures 4.4 to 4.11 show the observed and predicted concentration-distance profiles for Cl^-, Ca^{2+}, pH and $CaCO_3$ in the two soils at three times. The fitted and measured model parameter values are shown in Table 4.1.

Table 4.1: *Summary of the model parameters for each soil.*

	Soil Ti	Soil G
b_{HS} (mol OH^- kg^{-1} soil pH^{-1})	1.25×10^{-2}	2.1×10^{-2}
pH_0	6.1	6.4
P_{CO_2} (atm)	0.25×10^{-2}	0.75×10^{-2}
Cl_a (M)	3.0×10^{-2}	1.0×10^{-2}
Cl_0 (M)	6.0×10^{-2}	6.0×10^{-2}
Cat (M)	1.5×10^{-2}	0.5×10^{-2}
ρ ($kg.dm^{-3}$)	0.95	1.44
θ (v/v)	0.53	0.29
f_L	0.35	0.60
α (mol kg^{-1} soil s^{-1})	0.50×10^{-9}	0.07×10^{-9}
$CaCO_{3_0}$ (mol kg^{-1})	2.0×10^{-3}	1.0×10^{-3}

4.3.1 Chloride

Both soils showed a decrease in Cl^- concentration in solution near the soil-resin interface (Figures 4.4 and 4.5). Over time the zone of Cl^- depletion in solution spread further away from

the interface through the soil. After five days, Cl^- was nearly exhausted from the soil solution in soil G, but not in soil Ti (Figure 4.4 and 4.5 (c)). In both soils, the concentration of Cl^- in solution at the soil-resin interface was approximately constant over time at approximately 10 mM in soil G and 30 mM in soil Ti. The concentrations of Cl^- in solution in the soil bulk beyond the depletion zones differed between replicated end times in each soil. This made it difficult to fit the model to the data for each soil with single values of $[Cl^-]_{initial}$. Nonetheless, the simulated profiles for Cl^- correctly captured the main trends and spread of depletion over time.

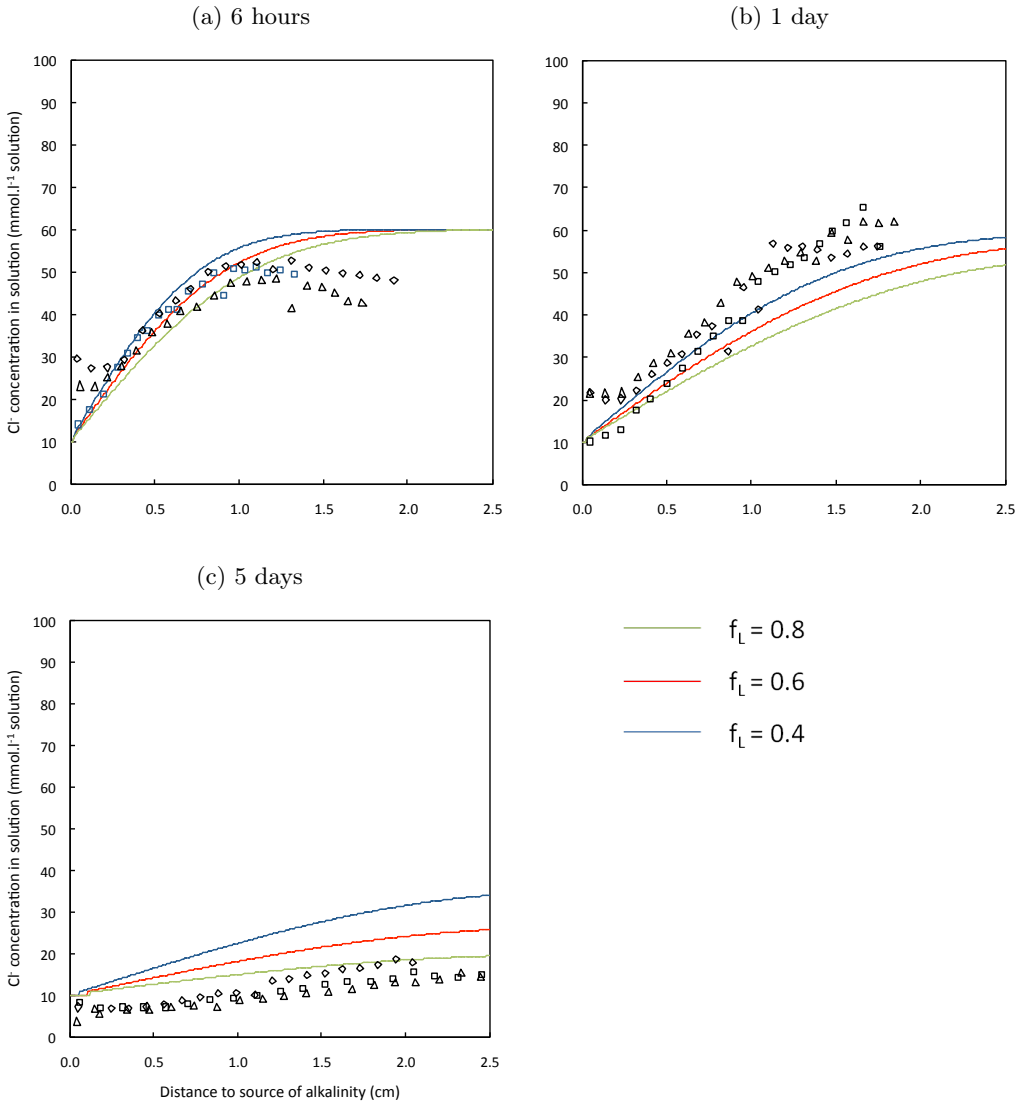

Figure 4.4: *Chloride experimental concentration-distance profiles for soil G in contact with HCO_3^- loaded anion-exchange resin for increasing lengths of time, and corresponding simulated profiles for 3 values of impedance factor f_L. Different symbols represent different replicates.*

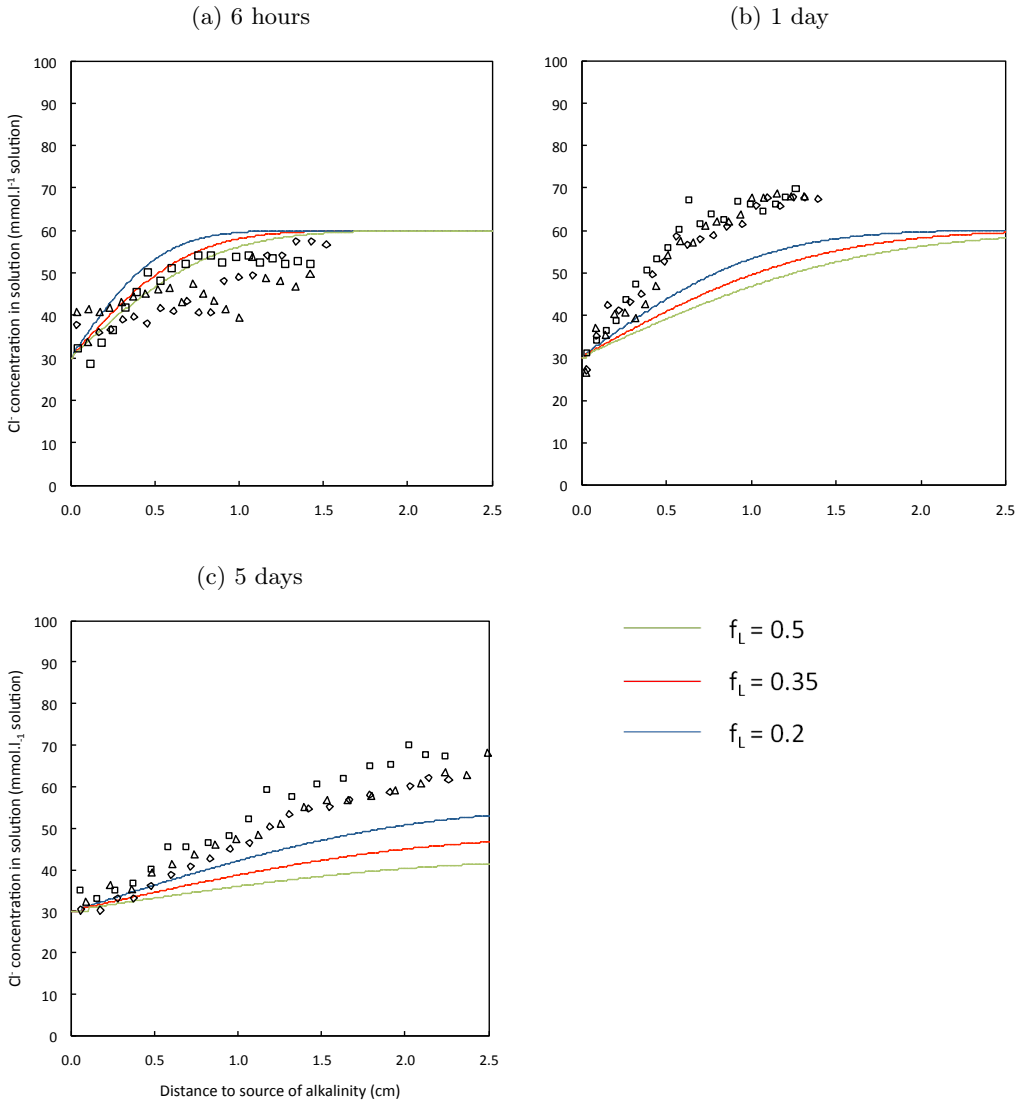

Figure 4.5: *Chloride experimental concentration-distance profiles for soil Ti in contact with HCO_3^- loaded anion-exchange resin for increasing lengths of time, and corresponding simulated profiles for 3 values of impedance factor f_L. Different symbols represent different replicates.*

4.3.2 Calcium

The simulated profiles of Ca^{2+} in solution agreed with the experimental data quite well for soil G, but less so for soil Ti. In both soils the concentrations of Ca^{2+} in solution were less than expected for electrical neutrality based on Equation 2.9, the measured concentrations of Cl^- and the inferred concentrations of HCO_3^- (which were at least an order of magnitude smaller than the concentrations of Cl^-). It was therefore apparent that there were some unaccounted for cations in solution with a total concentration of approximately 5 mM for soil G and 15 mM for soil Ti. Based on analyses of the solution, the unaccounted for cations were probably Na^+ in soil G and Na^+ and Mg^{2+} in soil Ti. Equation 2.9 was therefore modified in the model with a term for this.

Nonetheless, in soil Ti the model underestimated the drop in Ca^{2+} concentration at the soil-resin interface, and overestimated its spread through the soil column.

Since little $CaCO_3$ was precipitated in soil G (Figure 4.10), the precipitation coefficient α had a negligible effect on the concentration profiles of Ca^{2+} for any diffusion time. However, a lower concentration of CO_2 was predicted to lower Ca^{2+} in solution near the source of alkalinity. The response of the Ca^{2+} profile to P_{CO_2} matched that of pH in soil G (Figure 4.8). By contrast in soil Ti, the concentration of Ca^{2+} was affected both by the CO_2 partial pressure and the rate coefficient α, with an increase in P_{CO_2} having the same effect as in soil G, and a decrease in α leading to an increase in Ca^{2+} in solution. A two-fold increase in P_{CO_2} decreased Ca^{2+} in solution to the same extent as a six-fold increase in α decreased it.

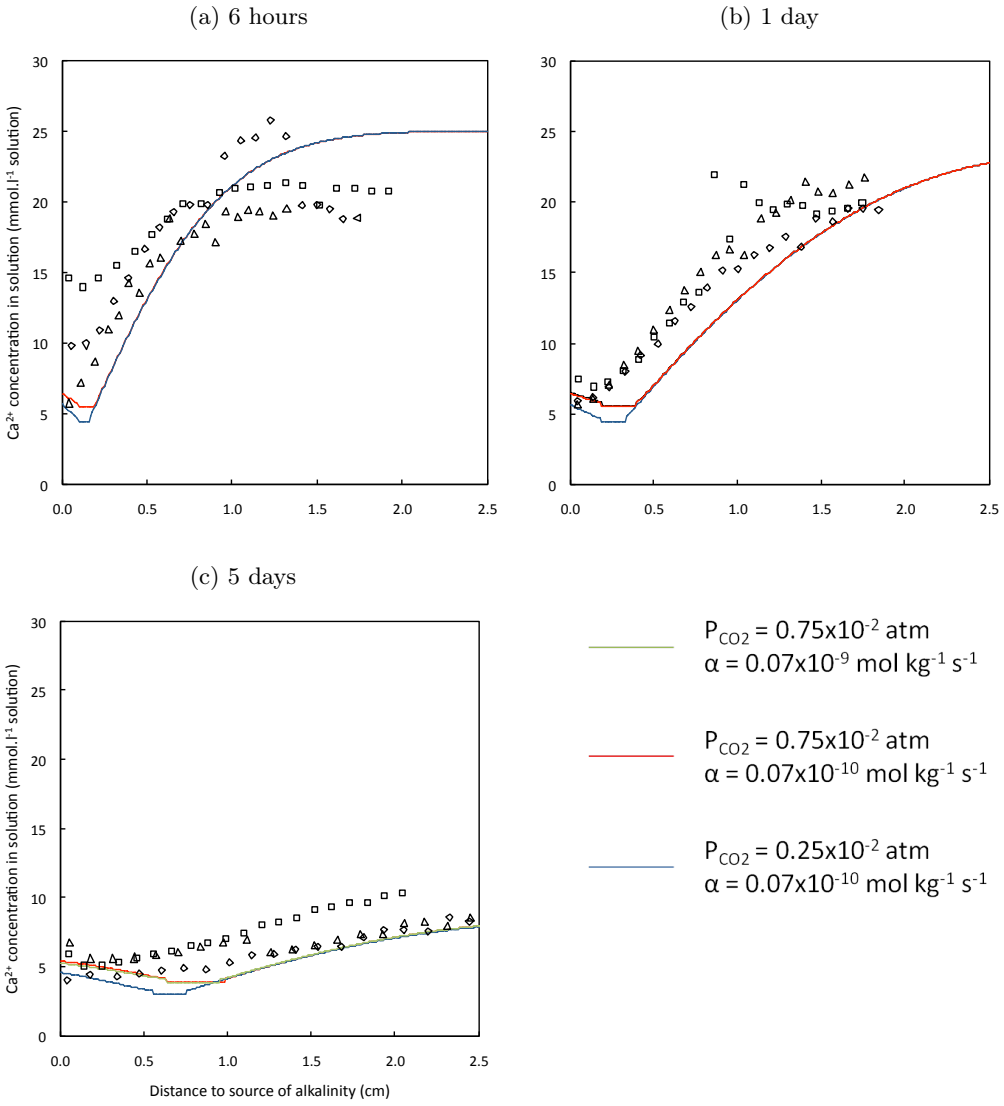

Figure 4.6: *Calcium experimental concentration-distance profiles for soil G in contact with HCO_3^- loaded anion-exchange resin for increasing lengths of time, and corresponding simulated profiles for 3 sets of parameters. Different symbols represent different replicates.*

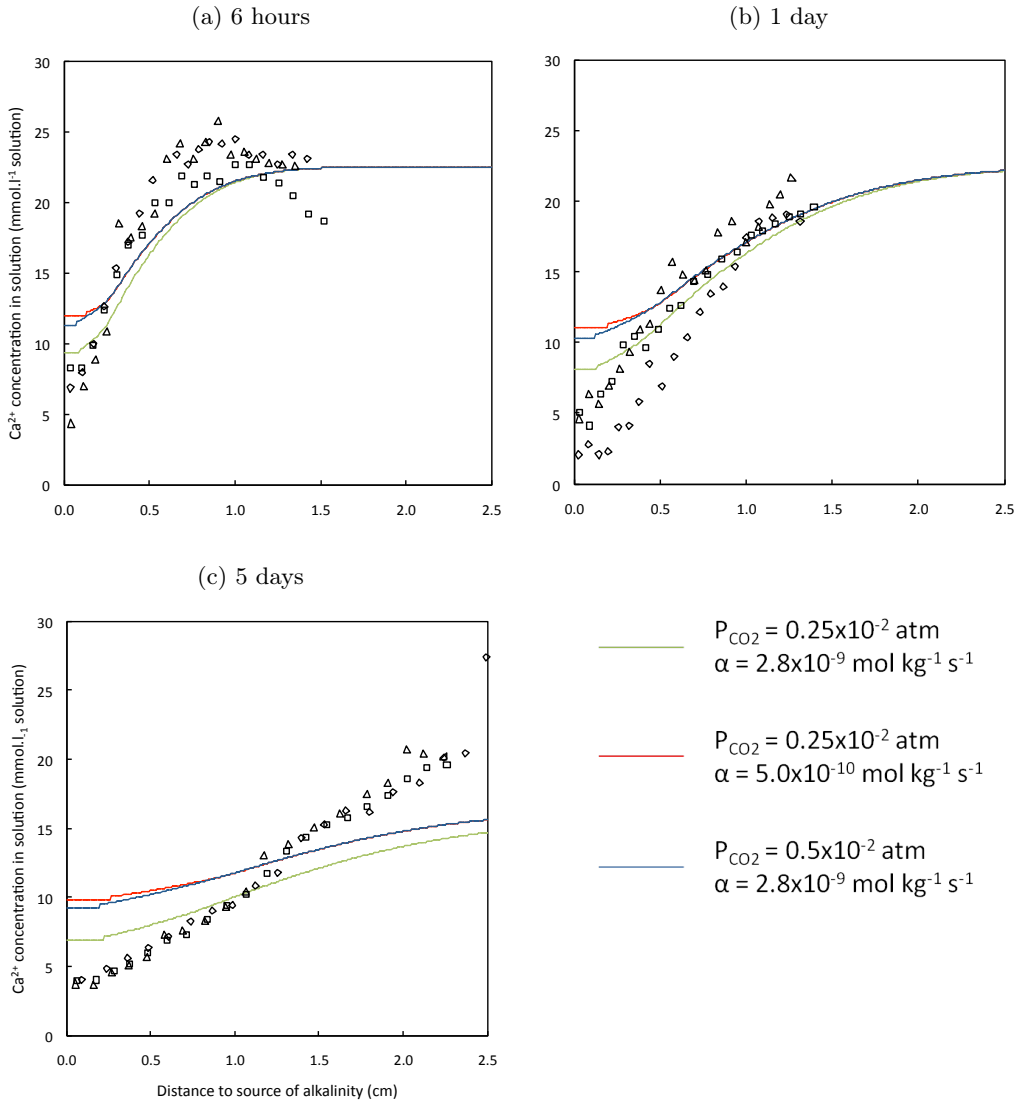

Figure 4.7: *Calcium experimental concentration-distance profiles for soil Ti in contact with HCO_3^- loaded anion-exchange resin for increasing lengths of time, and corresponding simulated profiles for 3 sets of parameters. Different symbols represent different replicates.*

4.3.3 pH

Both soils also showed an increase in pH near the soil-resin interface (Figures 4.8 and 4.9). These changes were not observed in the control soil systems (Figures 4.12 and 4.13), the control values for pH for soils Ti and G were 6.1 and 6.4 respectively.

The increase in pH in the vicinity of the soil-resin interface spread into the soil profile over time. At corresponding diffusion times, the increase in pH spread further in soil G than Ti. After 5 days, the spreads of the pH disturbances were 2.5 cm and 1.2 cm in soils G and Ti respectively.

The model described the pH profiles in both soils quite well. The simulated pH profiles in soil G were not affected by changes in precipitation coefficient α, as expected from the results for Ca^{2+}. An increase in P_{CO_2} decreased pH at the soil-resin interface but increased the distance the pH change spread through the soil. The same effect of CO_2 pressure was observed for soil Ti, but pH was also affected by the precipitation rate coefficient α. From fitting the experimental data with the solution of the model, P_{CO_2} values were 0.0075 and 0.0025 in soils G and Ti respectively.

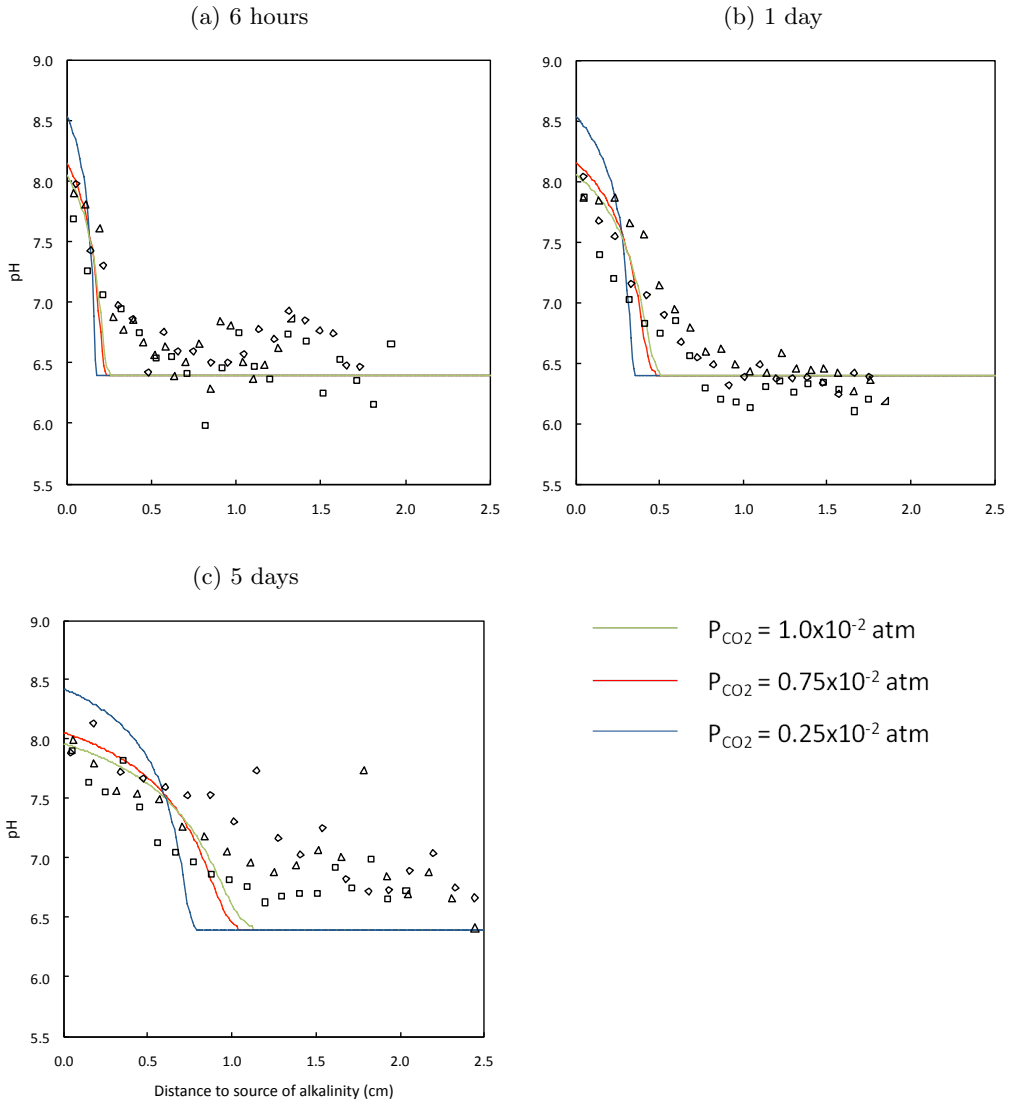

Figure 4.8: *Experimental pH-distance profiles for soil G in contact with HCO_3^- loaded anion-exchange resin for increasing lengths of time, and corresponding simulated profiles for 3 sets of parameters. Different symbols represent different replicates.*

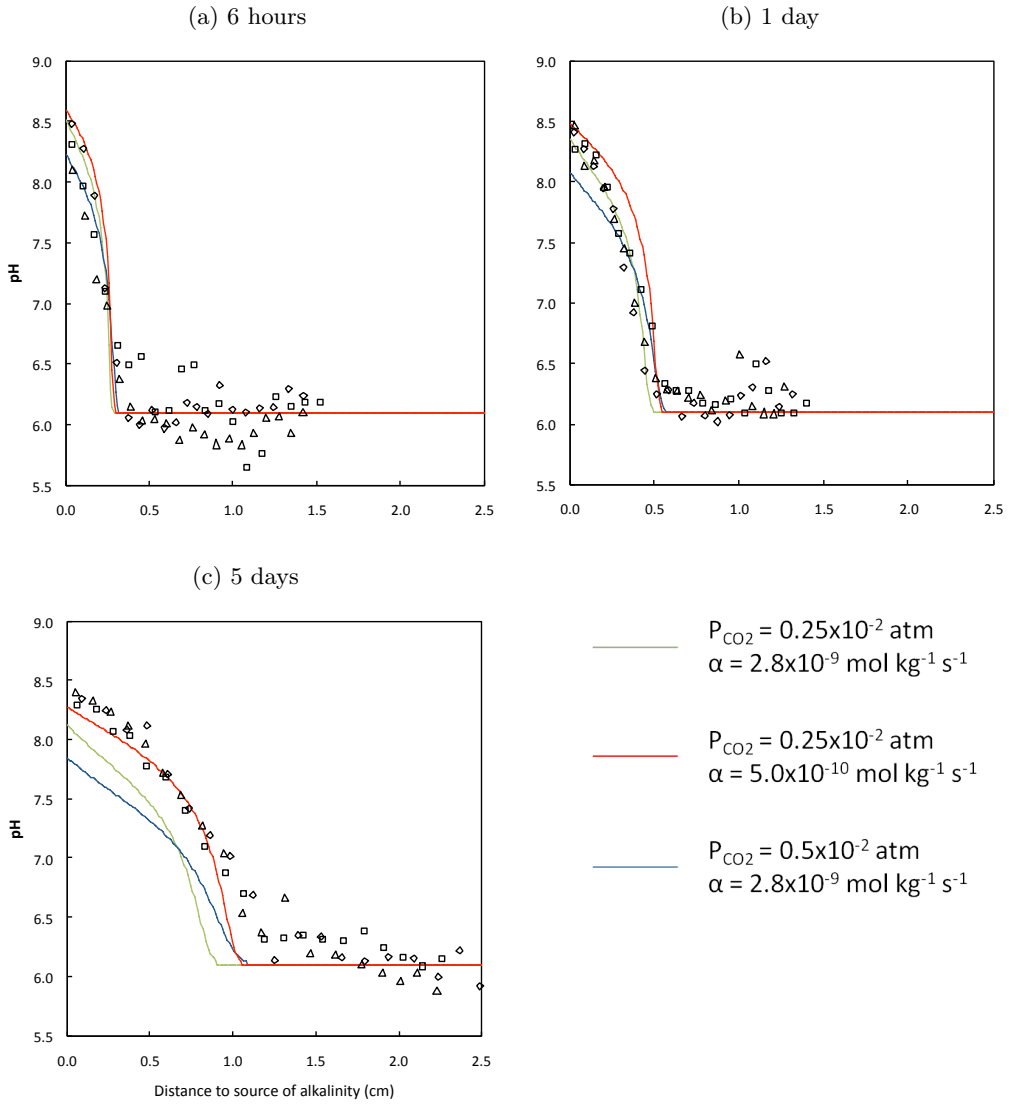

Figure 4.9: *Experimental pH-distance profiles for soil Ti in contact with HCO_3^- loaded anion-exchange resin for increasing lengths of time, and corresponding simulated profiles for 3 sets of parameters. Different symbols represent different replicates.*

4.3.4 Calcium carbonate

The initial $CaCO_3$ contents were approximately 1.0 and 2.0 mmol kg^{-1} in soils G and Ti respectively, and they remained constant through the control soil columns (Figures 4.12 and 4.13). In the columns exposed to HCO_3^-, little $CaCO_3$ precipitated in soil G throughout the experiment (Figure 4.10) but significant amounts formed in soil Ti and at least an order of magnitude more $CaCO_3$ was precipitated by the end of the experiment (Figure 4.11).

In soil Ti, after 6 hours of HCO_3^- resin/soil contact, the $CaCO_3$ concentration at the interface increased from 1.3 to 5 mmol kg^{-1} soil (Figure 4.11 (a)). The presence of precipitated $CaCO_3$ was detected over the first 2 mm of the soil column. This spread to 0.5 mm after one day, with the amount at the interface remaining at 5 mmol kg^{-1} soil (Figure 4.11 (b)). After 5 days, the concentration of $CaCO_3$ at the soil-resin interface was 40 mmol kg^{-1} soil, and changes reached 1 cm into the soil columns (Figure 4.11 (c)). The baseline amount of $CaCO_3$ was also slightly raised through the sliced soil distance, with a plateau measured at 3 mmol kg^{-1} soil beyond 1 cm from the soil-resin interface.

The best-fitted $CaCO_3$ precipitation rate coefficients α were 0.07 and 0.5 $\times 10^{-9}$ mol kg^{-1} s^{-1} for soils G and Ti respectively.

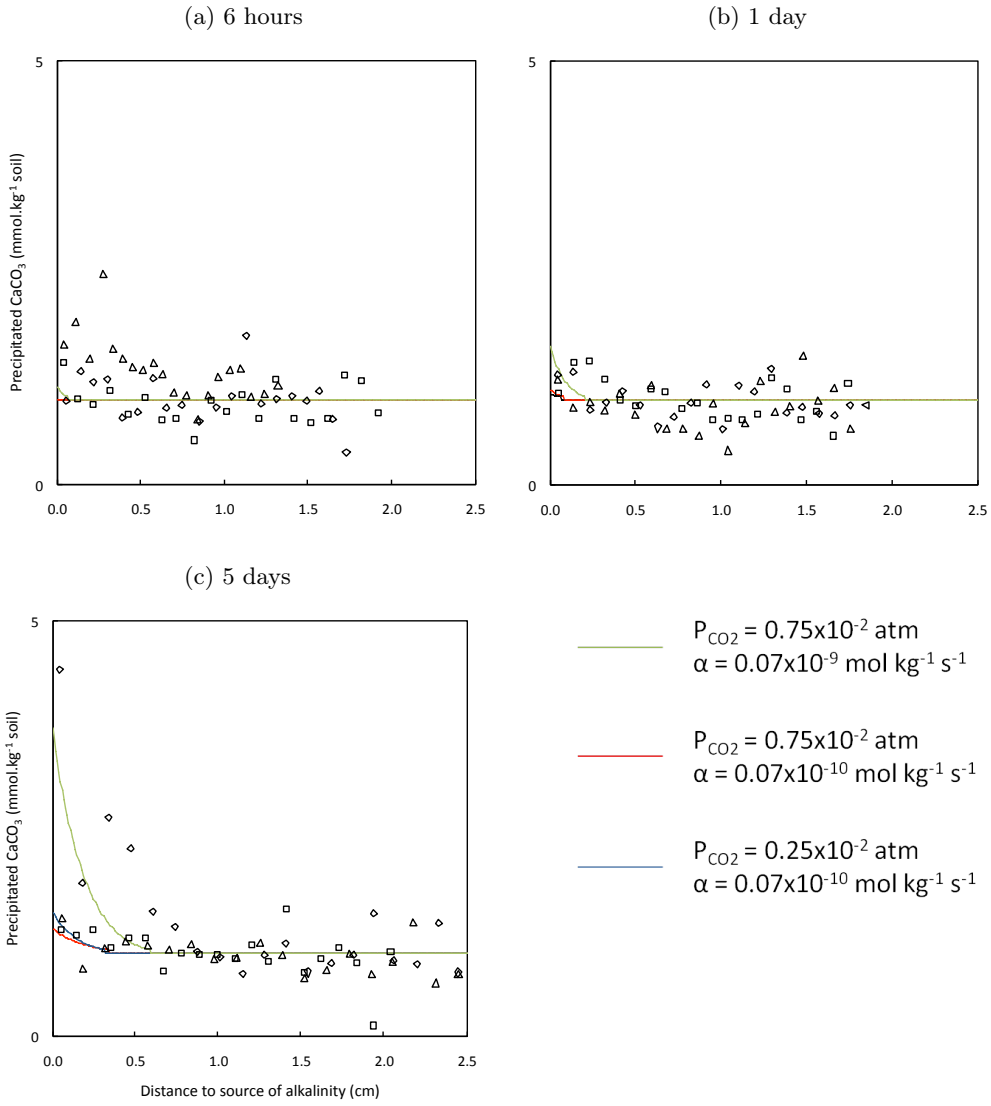

Figure 4.10: *Calcium carbonate experimental concentration-distance profiles for soil G in contact with HCO_3^- loaded anion-exchange resin for increasing lengths of time, and corresponding simulated profiles for 3 sets of parameters. Different symbols represent different replicates.*

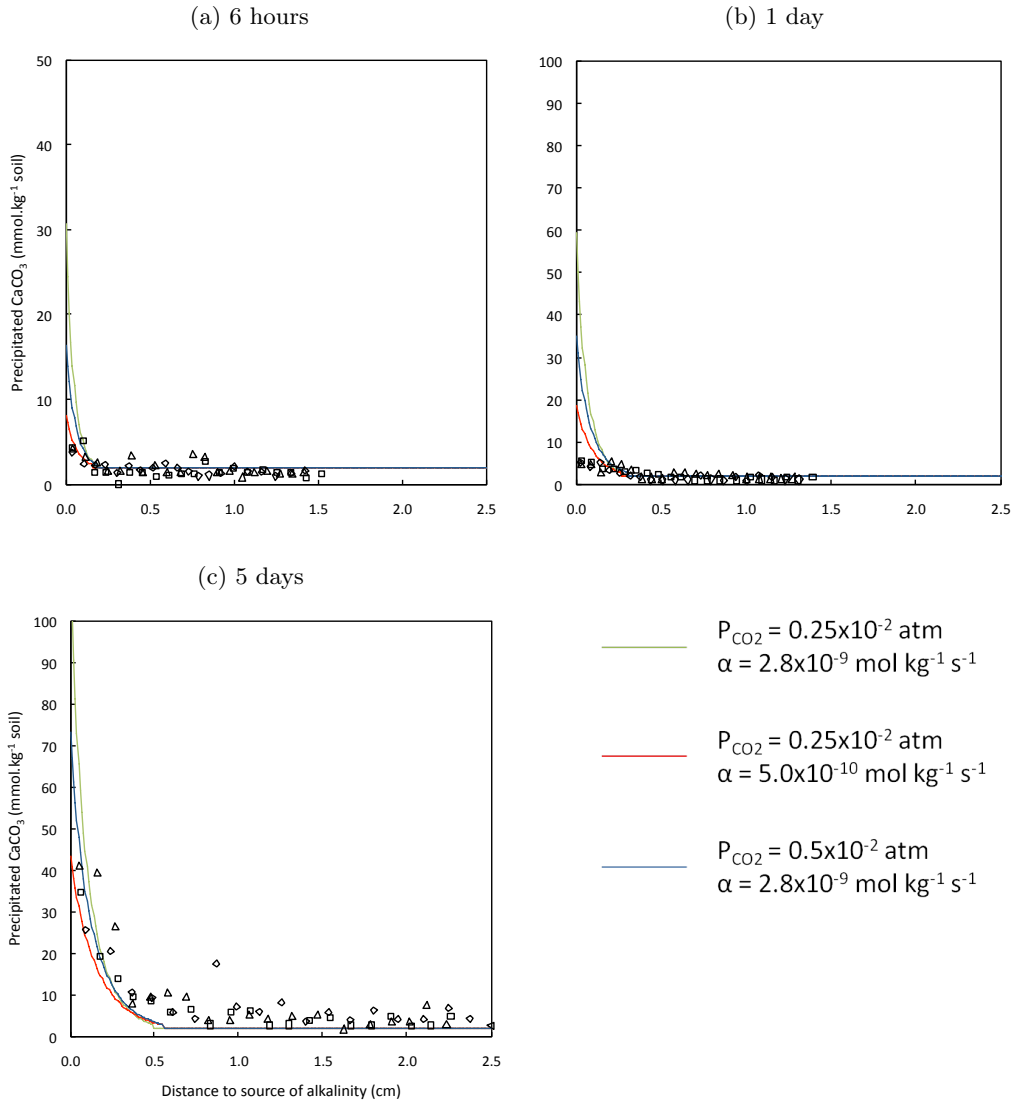

Figure 4.11: *Calcium carbonate experimental concentration-distance profiles for soil Ti in contact with HCO_3^- loaded anion-exchange resin for increasing lengths of time, and corresponding simulated profiles for 3 sets of parameters. Different symbols represent different replicates. (Note the difference in scales)*

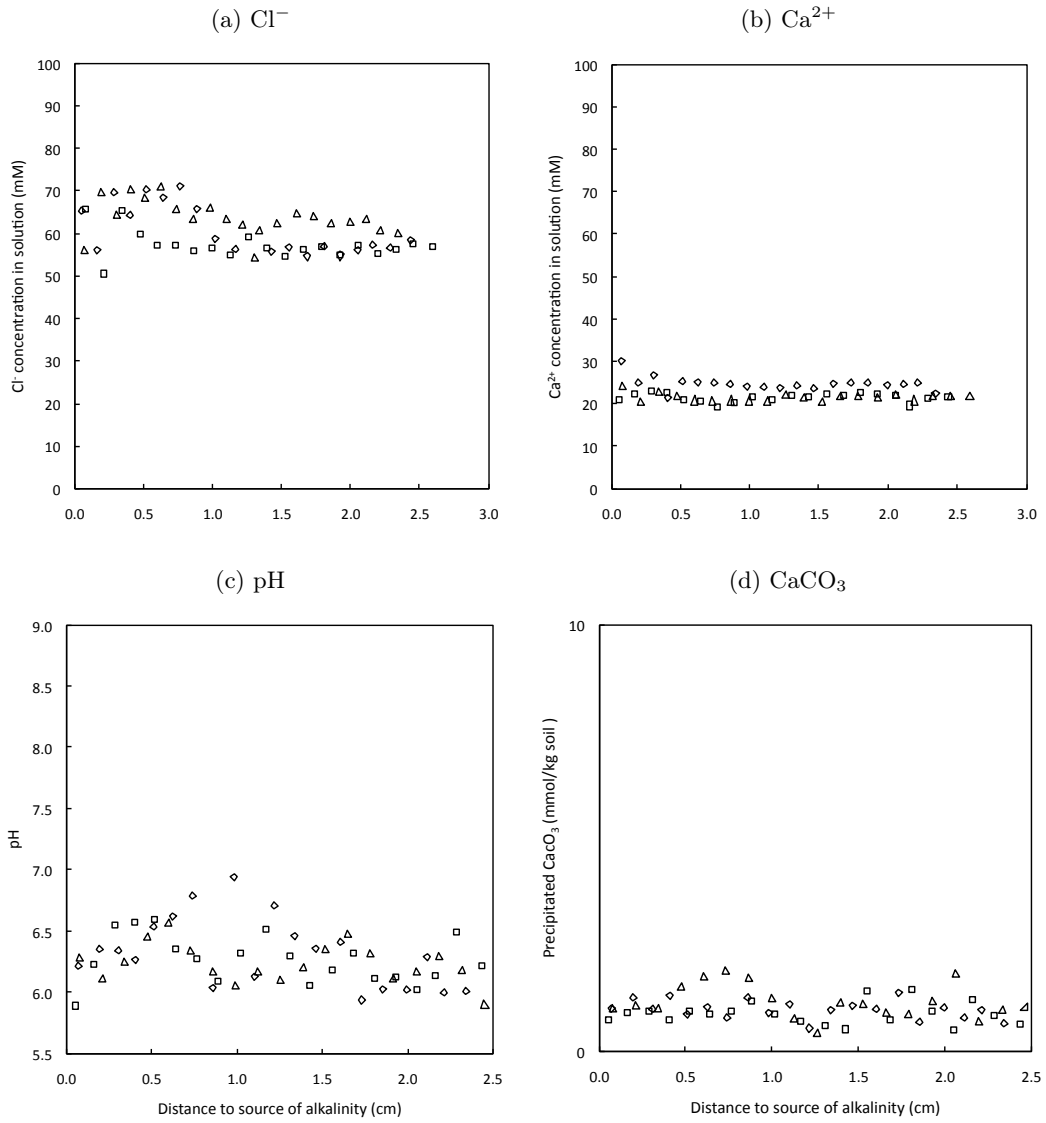

Figure 4.12: *Control concentration-distance profiles for experimental soil G. The control involved the experimental system left for 5 days in contact with a collar empty of resin. Different symbols represent different replicates.*

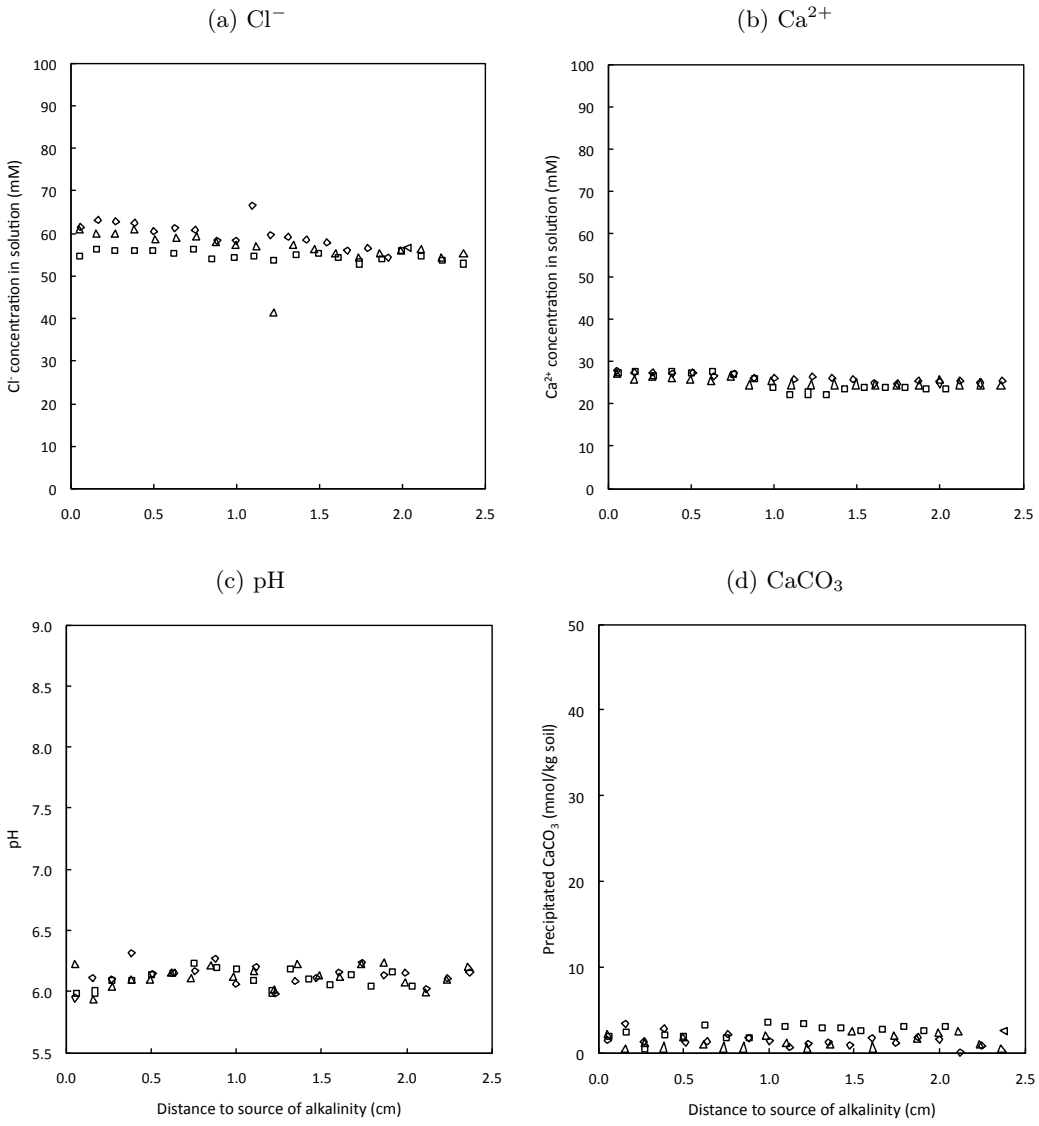

Figure 4.13: *Control concentration-distance profiles for experimental soil Ti. The control involved the experimental system left for 5 days in contact with a collar empty of resin. Different symbols represent different replicates.*

Figures 4.14 and 4.15 give the simulations combined together.

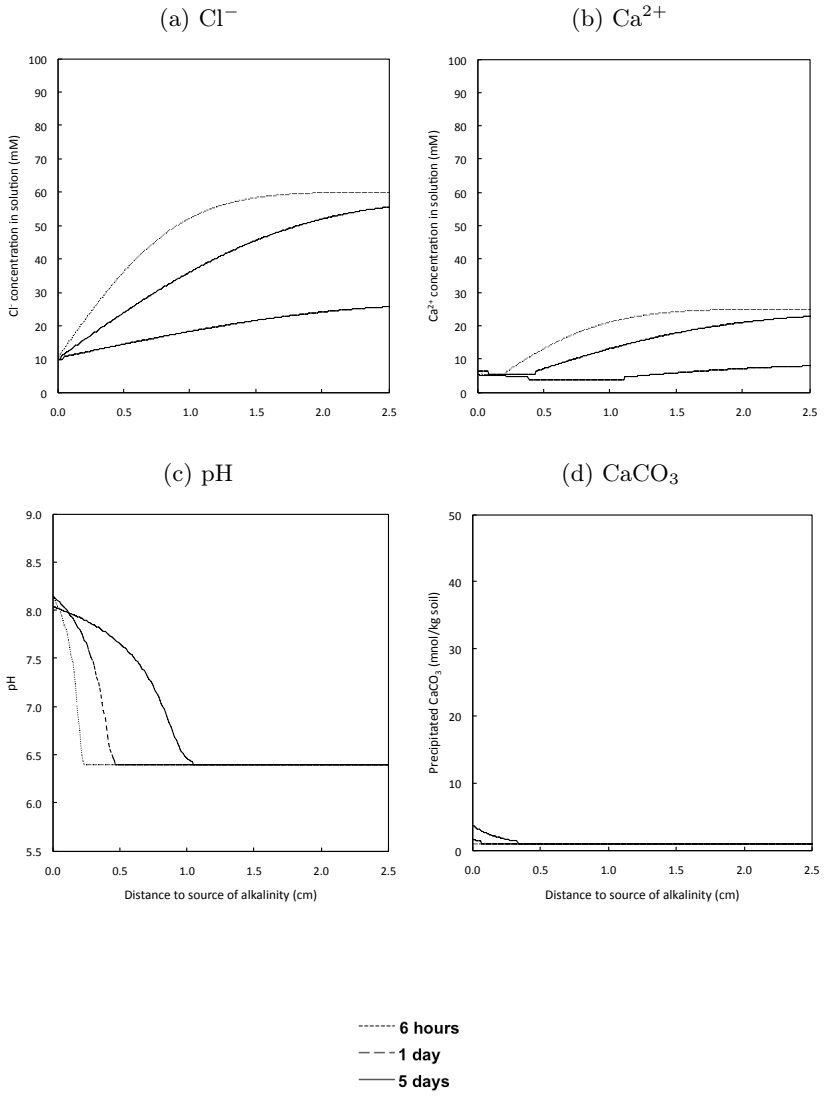

Figure 4.14: *Simulated concentration-distance profiles using the parameters listed in Table 4.1 for soil G.*

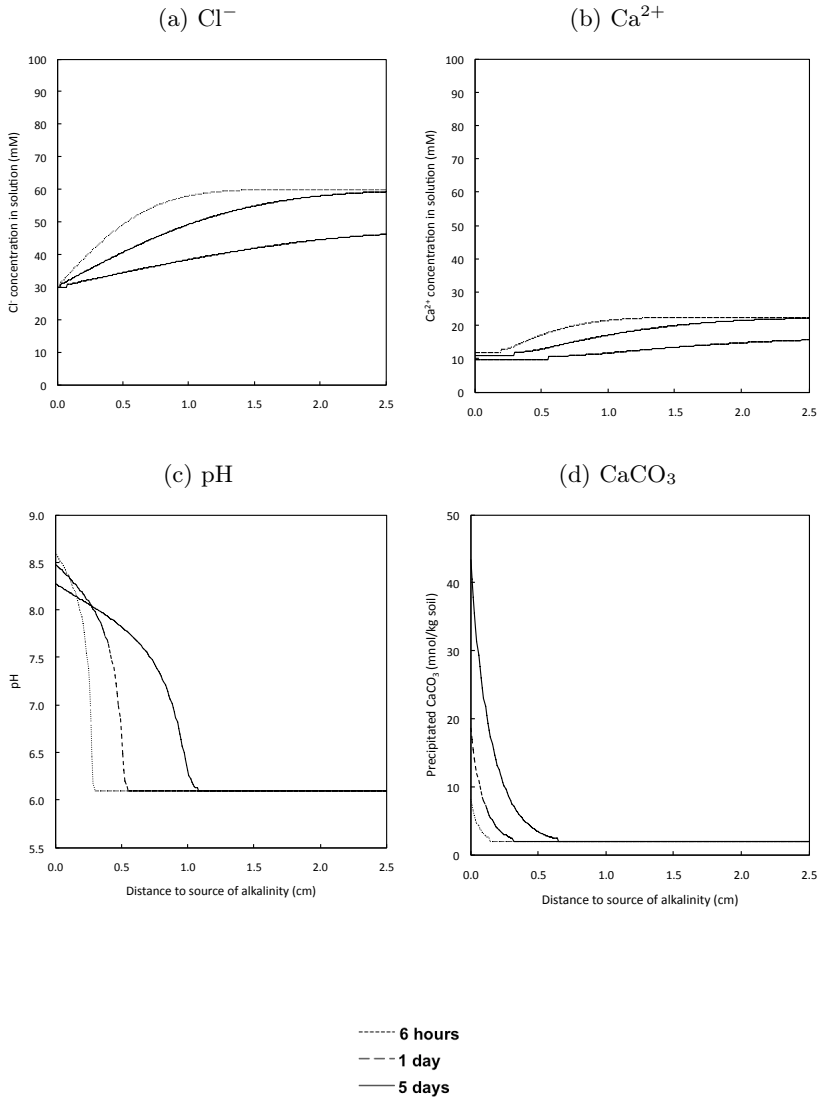

Figure 4.15: *Simulated concentration-distance profiles using the parameters listed in Table 4.1 for soil Ti.*

4.4 Discussion

The two soils behaved differently. In soil G, exchange of HCO_3^- from the resin with Cl^- in the soil resulted in (i) depletion of Cl^- from the soil solution; (ii) depletion of Ca^{2+} from the soil solution, matching the decrease in anion concentration in solution as Cl^- decreased; (iii) increase in pH where HCO_3^- reacted with the soil; but (iv) little precipitation of $CaCO_3$. Whereas in soil Ti, while there were also depletions of Cl^- and Ca^{2+} from the soil solution and increases in soil pH, there was a substantial accumulation of newly precipitated $CaCO_3$ in the region of the resin-soil boundary.

The initial concentrations of Ca^{2+} in solution in the two soils were comparable (approx. 25 mM) and the initial pH of soil G was slightly greater than that of soil Ti (pH 6.4 versus 6.1). However the initial CEC of soil G was five times smaller than that of Ti (5 versus 23 $cmol_c$ kg^{-1}), and hence the concentration of exchangeable Ca^{2+} available for $CaCO_3$ precipitation was far smaller. Evidently depletion of Ca^{2+} from the soil solution in soil G was the result of increased sorption of Ca^{2+} on the soil solid as HCO_3^- reacted with it, i.e. the reaction was of the form

$$\text{Soil–H} + 0.5\text{Ca}^{2+} + \text{HCO}_3^- = \text{Soil–Ca}_{0.5} + \text{CO}_2 + \text{H}_2\text{O} \qquad 4.a$$

where Soil–H represents base-neutralising groups in the soil solid. So the smaller CEC of soil G was probably the main reason that much less $CaCO_3$ formed.

The increase in soil pH at the soil-resin interface was approx. 0.8 units greater in soil Ti than soil G (approx. from pH 6.1 to 8.5 in Ti versus pH 6.4 to 8.0 in G). This was in spite of the greater rate of $CaCO_3$ precipitation in soil Ti – and corresponding consumption of HCO_3^- – and the smaller net flux of HCO_3^- from the resin into the soil, indicated by the smaller net depletion of Cl^-. According to the model parameterisation, the greater pH increase in soil Ti was in part due to a smaller soil pH buffer power (b_{HS} = 12.5 and 21 mmol kg-1 pH-1 in soils Ti and G,

respectively) and in part due to a smaller CO_2 pressure (= 0.025 and 0.075 atm in soils Ti and G, respectively) and resulting smaller flux of H_2CO_3-HCO_3^- through the soil.

The modelled values of b_{HS} in the diffusion system did not match the values estimated from the shaken suspension experiments. The ranges of shaken suspension values were from 25 and 33 mmol kg^{-1} pH^{-1} for soils Ti and G with the 24 h equilibration at atmospheric CO_2 pressure (Fig 3.9), to 16 mmol kg^{-1} pH^{-1} for both soils with 1 h equilibration at 4% CO2 (initial pH changes after NaOH addition in Figs 3.6 and 3.7). Ramzan and Nye (1979) also found a continuing slow reaction of base with soils in shaken suspensions after an initial fast reaction, and the apparent pH buffer powers for HCO_3^- diffusion through soil columns were several-fold smaller than those found in shaken suspensions. A possible explanation is that reaction rates are limited by slow acid-base equilibration at sites within soil particles, and, in shaken suspensions, access to such sites is increased as a result of disaggregation and increased convection. Ptashnyk et al. (2010) showed that slow diffusive movement of reactants to or from sites within soil particles can explain slow reactions at this sort of time scale. Intra-particle diffusion is likely to be slower in fine-textured soil Ti than in coarse-textured soil G because of the greater proportion of fine pores. This may explain the greater disparity between the b_{HS} values in the diffusion systems and the shaken suspensions in soil Ti.

According to the model fits to the data, the CO_2 partial pressure in soil G was approx. three times that in soil Ti. As shown by the model sensitivity analysis in Figures 4.8 and 4.9, a greater CO_2 pressure results in more rapid movement of soil base (i.e. HCO_3^-) away from the resin into the soil, and hence a smaller pH rise at the interface. The distance over which the change in pH spread in the soil column was correspondingly increased in soil G. Greater CO_2 partial pressure may develop in soil G because the flux of HCO_3^- from the resin was greater and it was apparently mainly converted to CO_2 in Reaction 4.a, whereas in soil Ti it was consumed in $CaCO_3$ precipitation. Hence, the rate of abiotic CO_2 generation in soil G was greater. Further, the bulk density of soil G in the soil columns was substantially greater (1.44 versus 0.95 kg dm^{-3}) and the total porosity was correspondingly smaller (though with a greater proportion of

coarse pores as discussed in the previous paragraph). Hence, at the high moisture contents of the experiments, the air-filled porosity was smaller and the rate of equilibration of the soil air with the external atmosphere correspondingly slower.

The diffusion impedance factors estimated for the two soils were consistent with values in the literature for soils with clay contents, bulk densities and moisture contents (Tinker and Nye, 2000).

From electrical neutrality, it was expected that the concentration of Cl^- in the soil solution would be approximately twice that of Ca^{2+}, they being the main anion and cation expected in solution given that the soils had been washed repeatedly in $CaCl_2$ solution prior to the experiments. However, in both soils there was an apparent discrepancy in the cation-anion balance, indicating the presence in solution of other cations. To correct for this, an additional term (Cat) was added to the equation for electrical neutrality in the model. The fitted values of Cat were 15 and 5 mM in soils Ti and G, respectively. Consistent with this, concentrations of Na^+ of 8 and 5 mM in soils Ti and G (respectively) were detected in solution in the shaken soil suspension experiments without added NaOH (Figs 3.7 and 3.6). Thus Na^+ remaining in the soils could account for some of the error in soil Ti and all of it in soil G.

The sensitivity of precipitation to the value of α indicated in Figures 4.10 and 4.11 shows that both transport rates and the kinetics of the precipitation reaction are important determinants of overall rates of precipitation in soils. The fitted values of the $CaCO_3$ precipitation rate coefficient α (0.50×10^{-9} and 0.07×10^{-9} mol kg^{-1} s^{-1} in soils Ti and G respectively) were an order of magnitude greater than the values estimated in the shaken soil suspensions (3×10^{-11} and 7×10^{-12} mol kg^{-1} s^{-1}). This is perhaps not surprising given the sensitivity of precipitation rates to nucleation conditions, and probably also to differences in the concentrations of inhibitors. Enhanced dissolution of soil organic matter in the shaken suspensions may have led to increased DOC concentrations. It is also likely that biological activity differed between the shaken suspensions, where fungal growth is not possible, and the soil columns.

4.5 Conclusions

The agreement between the observed and predicted results using model parameter values measured independently in the experiments in Chapter 3, or estimated from the properties of the experimental soils, was not perfect. However, the overall behaviour of the system was satisfactorily described. Given the complexity of the system, the complexity of the changes in pH, Ca^{2+}, Cl^{-} and $CaCO_3$ with distance away from the soil-resin boundary, the large difference between the two experimental soils, and the large number of model parameters to be characterised, the satisfactory agreement between the observed and predicted results indicates that the model correctly describes the system and that no important processes have been left out.

The sensitivity of the model to its input parameters demonstrates the importance of the kinetics of the precipitation reaction as well as the transport of reactants and products through the soil to and away from the precipitation zone. The particular importance of CO_2 was clear, both as a reactant and as it governs the rate of propagation of pH changes through the soil by the movement of the H_2CO_3-HCO_3^- acid-base pair. The results showed that the CO_2 pressure is determined by both biotic and abiotic processes, but so far the model does not allow explicitly for biotic processes. How to do this is considered in the next chapter.

Chapter 5

Effects of community-scale manipulation of soil biota on calcium carbonate precipitation

5.1 Introduction

It is well established that microbes can contribute to a great extent to the precipitation of carbonates (Buczynski and Chafetz, 1991; Stocks-Fischer et al., 1999; Warren et al., 2001; Bachmeier et al., 2002; Mitchell and Ferris, 2006; Rivadeneyra et al., 2006; Rogerson et al., 2008; Masaphy et al., 2009). Microbially-induced precipitation raises scientific interest because of the wide range of its potential applications, from carbon cycling and sequestering (Renforth et al., 2009), to soil improvement techniques (DeJong et al., 2006; Whiffin et al., 2007) and encompassing such fields as petrology (Rodriguez-Navarro et al., 2007), the study of past environmental conditions (Rogerson et al., 2008), bioremediation of heavy metal contaminants (Warren et al., 2001; Mitchell and Ferris, 2006), and the remediation of cracks in buildings or subsurface reservoirs (Stocks-Fischer et al., 1999; Dupraz et al., 2009).

Most studies into microbially-induced precipitation to date have been laboratory-based and have focused on bacteria. One well documented mechanism is the use of ureolytic microbes, generally bacteria such as *Bacillus pasteurii*. The hydrolysis of urea into ammonia and CO_2 directly results in a pH increase in the surrounding environment, leading to the precipitation of Ca^{2+} and CO_3^{2-} into $CaCO_3$ as a buffering mechanism (Warren et al., 2001; Bachmeier et al., 2002; Mitchell and Ferris, 2006; Achal et al., 2009); see also Section 1.3.3.

This is a common mechanism of carbonate precipitation in soils, however mounting evidence is accumulating on the role played by soil fungi in the facilitation of calcification (Masaphy et al., 2009; Gadd, 2007). Samples of soil taken from Midlands and South East England show microfine structures of secondary calcium carbonate of distinct morphology (Figure 5.1). These structures are characterised by a network-like underlying arrangement that suggests some association with fungal mycelia, which often show a notably similar morphology when present in soils (Ritz and Young, 2004).

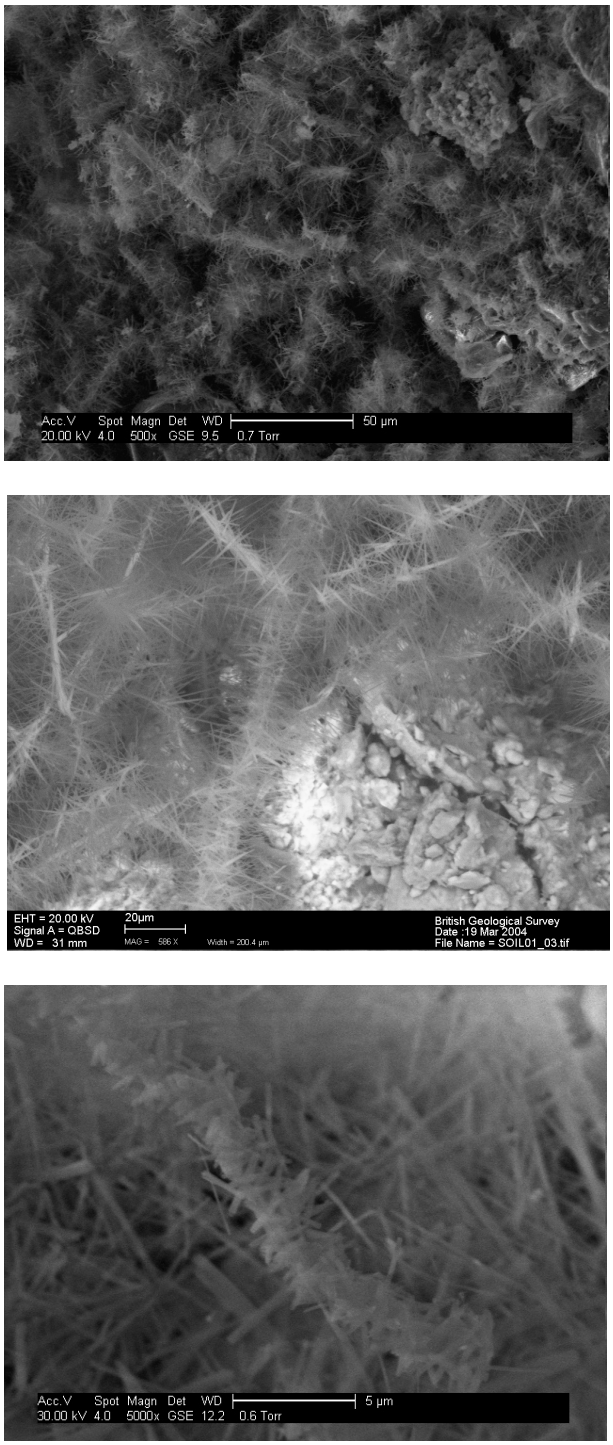

Figure 5.1: *Microfine structure of $CaCO_3$ deposits sampled in Nottinghamshire, UK. Courtesy of Dr. Antoni Milodowski, British Geological Survey.*

Fungal hyphae can act as potential nucleation sites for the formation of secondary crystals (Manoli et al., 1997; Gadd, 2007). Indeed, fungal cell walls contain chitin, which typically complexes with soluble proteins. The adsorbed proteins then bind to metal ions in solution, such as Ca^{2+}, and thus serve as nucleation sites which induce $CaCO_3$ precipitation. Microbes can also have an indirect role by modifying the conditions in soil solution. Microbial activity raises the CO_2 concentration in soil air, and substances secreted by microbes may affect precipitation (Section 1.3.3).

Research was conducted to investigate the role played by the soil microbial community on the precipitation of $CaCO_3$ in a soil environment where there are natural constraints on microbial growth and solute movement, and to investigate whether different components of the community affected such processes in different ways.

The hypotheses tested were:

1. The microbial community composition, specifically with respect to bacteria and fungi, of a soil does not affect the overall direction of the movement of ions in a $CaCO_3$ precipitation zone at the vicinity of a source of alkalinity. Cl^- exchange with HCO_3^- into the anion-exchange resin, inducing parallel movement of Ca^{2+} and H^+ (Figure 2.1).

2. The nature of the microbial community will impact upon the rate of $CaCO_3$ precipitation.

3. The polymorph of $CaCO_3$ precipitated in soil is affected by the nature of the microbial community.

One of the objectives was to conduct the study keeping soil conditions in the experimental system as realistic as possible, and to involve whole microbial communities rather than single species. This is because in natural systems, microbes never exist in isolation and always function in the context of a more or less diverse community. As explained above, most precedent studies have focused on the artificial situation of single species. Soil was thus treated with spe-

cific antibiotics to engender eukaryotic- (i.e. fungal) or prokaryotic- (i.e. bacterial) dominated systems.

The hypotheses were tested by both quantitative and qualitative approaches. Similar reactants and precipitation concentration-distance profiles as presented in the previous chapter were established for experimental systems where the soil biological communities were manipulated. The morphology of crystals of $CaCO_3$ can indicate the kinetics and thermodynamics of the precipitation reaction that can not be detected through chemical methods. Hence manipulated systems were observed using an environmental scanning electron microscope (ESEM) and the nature of calcium carbonate crystals thus observed were analysed by X-ray diffraction.

5.2 Materials and methods

5.2.1 Experimental soil

For this experiment, the experimental soil Ti (Section 3.2.1) was resampled, to provide a fresh soil with a representative microbial community. It was prepared as previously described using $CaCl_2$ to homogenise the exchange complex and the soil solution ionic composition (see Section 4.2.1).

It was then treated with specific biocides to produce four treatments:

- Reference*: not modified after the $CaCl_2$ wash
- Sterile
- Prokaryote inhibited: treated with a bactericide
- Eukaryote inhibited: treated with a fungicide

5.2.2 Preparation of the experimental soil

Sterilisation

Nine of the cells described in previous chapter (Section 4.2.2) were packed with soil at a bulk density of 1.0 g cm^{-3} and brought to 0.50 cm cm^{-3} volumetric moisture content with a 10 mM $CaCl_2$ solution. Each soil column was then individually wrapped in hermetically sealed plastic bags, and subjected to a charge of gamma rays of 25-40 kGy (Isotron Irradiation Laboratory, Swindon SN3 4TA, UK). After sterilisation and until they were put into contact with anion exchange resin, irradiated soils were stored in their sealed containers at 4°C.

*This term is adopted to avoid confusion with 'Control' which is used in a different context where no resin was involved - See Section 5.2.3

Eukaryote inhibition

Cycloheximide is the most commonly used and accepted fungicide in microbial studies. It has a limited effect on bacterial growth for concentrations under 10 mg g^{-1} (Rousk et al., 2009). Based on the literature (Velvis, 1997; Rousk et al., 2009), eukaryotes were inhibited by application of cycloheximide (Sigma Aldrich CAS 66-81-9) at a concentration of 0.95 mg g^{-1} soil, sufficient to modify the microbial community towards being predominantly bacterial, while limiting the adverse effects on bacterial growth.

Prokaryote inhibition

Of the numerous existing prokaryote inhibitors, the most widely used in the literature is streptomycin. However recent papers have found streptomycin to be "particularly impotent" in certain soils, and also to affect fungal communities (Rousk et al., 2009, 2010).

Bronopol, a more specific and potent alternative proposed (Rousk et al., 2010), was used in this research. Bronopol (Sigma Aldrich CAS 52-51-7) was applied at a rate of 1.0 mg g^{-1} soil, sufficient to modify the soil microbial community by inhibiting bacterial while having no negative effect on the fungal population.

5.2.3 Measurement of solutes movement

The soil was packed in collars at bulk density $\rho = 1.0$ g cm^{-3}, then each collar was brought to 50% volumetric moisture content with a $CaCl_2$ 10 mM solution in which the antibiotics were dissolved at the prescribed concentrations. To get conditions as homogeneous as possible, soil collars were left to settle in water-saturated incubation chambers for 5 days before contact with the anion exchange resin loaded with bicarbonate ions (HCO_3^-).

For each microbiological treatment, two diffusion times were tested, viz. 1 and 5 days. Control

soil columns were additionally prepared following the same procedure, then put in contact with upper collars devoid of resin, in order to check that in the absence of the source of base, the system remained at equilibrium and no solute movement occurred. Three replicates of each treatment were established.

After each diffusion period, the cores of soil were sliced and analysed for pH, $Ca^{2+}_{(L)}$, $Cl^{-}_{(L)}$ and precipitated $CaCO_3$ following the analysis sequence detailed in Section 4.2.3.

5.2.4 Data analysis

Concentration-distance profiles were established as previously (Section 4.2.3), and each concentration-distance profile was fitted with a model calculated for each data sets to test the hypothesis that the four treatments applied to the experimental soil induced significant differences in the behaviour of soil solutes in and near a $CaCO_3$ precipitation zone.

The linear model was of the form:

$$P = T_{effect} + T_{effect}.x + \epsilon$$

where P is the parameter of interest (P = pH, $Ca^{2+}_{(L)}$, $Cl^{-}_{(L)}$ or $CaCO_3$), T_{effect} the effect of treatment (reference, sterile, eukaryote- or prokaryote inhibited), x the distance to the soil-resin interface (cm), and ϵ a constant. This was calculated using Statistica 9.0, assuming the data normally distributed and after identifying and eliminating any outliers in the datasets.

A non-linear logistic model was used for pH and Ca^{2+} and Cl^{-} profiles after one day, when the linear model did not account for a satisfactory percentage of the variation in the data. The four-parameter logistical model was of the form:

$$pH = pH_0 + \frac{pH_{max} - pH_0}{1 - \left(\frac{x}{x_0}\right)^s}$$

where pH_0 is the soil pH at the opposite end of the soil column to the resin, pH_{max} the soil pH at the soil-resin interface, x the distance to the soil-resin interface (cm), s the slope and x_0 the indent which give an idea of the spread over which changes occur in soil.

The increase in $CaCO_3$ at the soil-resin interface was fitted with an exponential decay curve of the form:

$$CaCO_3 = CaCO_{3_0} + CaCO_{3_{max}} e^{sx} \tag{5.1}$$

where $CaCO_{3_0}$ is the intial content of $CaCO_3$ in soil, $CaCO_{3_{max}}$ the amount precipitated at the soil-resin interface (both in mmol kg^{-1} soil), s the slope and x the distance to the soil-resin interface (cm).

Significant differences between treatments were calculated using an analysis of variance (ANOVA) on the parameters of the linear and non-linear models, assuming the data normally distributed and eliminating any outliers in the data set. The linear models were compared using Statistica, while for the non-linear models, the parameters (minimum and maximum value, slope and indent) were compared individually for each treatment using a single factor ANOVA in Microsoft Excel.

Crystal morphology and $CaCO_3$ polymorphism

The crystalline form of $CaCO_3$ precipitated under different circumstances was established using an environmental scanning electron microscope (ESEM) and X-ray diffraction (XRD).

Supplementary soil columns were prepared following the protocol described above. At the end of a five-day contact period with the bicarbonate-loaded anion exchange resin, the nylon mesh filters were removed and observed under an ESEM.

Observations were made of the nylon mesh at the interface of soil and resin, and in the first 5 mm of soil from the interface where precipitation was likely more abundant, in both vacuum and environmental modes. The latter allows observations in a hydrated state, without vacuum

in the chamber of the microscope. This means that features such as fungal hyphae are preserved in a more or less intact state.

After observation under the microscope, the filters were attached to aluminium-backed sample holders using carbon-tabs. In addition, attempts were made to remove material from the surface of one of the filters (Reference soil) using a scalpel blade. The material liberated was mounted directly on the surface of a "zero background" silicon crystal substrate.

XRD analysis was carried out using a PANalytical X'Pert Pro series diffractometer equipped with a cobalt-target tube (wavelength $\lambda = 1.78896$ Å), X'Celerator detector and operated at 45 kV and 40 mA. The samples were scanned from 4.5-85°2q at 2.76°2q min^{-1}.

The diffraction data were then analysed using PANalytical X'Pert Pro software coupled to the 2009 version of the International Centre for Diffraction Data (ICDD) database, to identify the mineral species present in the samples. Using a cobalt target tube, the peaks for calcite, aragonite and vaterite are expected at diffraction angles 2θ 34.28°, 30.53° and 31.57° respectively.

5.3 Results

5.3.1 Diffusion of solutes

Control - no contact with anion exchange resin

All treatments showed an overall constant concentration-distance profile for pH. The reference system pH was 6.0, while pH was altered by the treatments and fluctuated between 5.5 and 6.5 in the three treated soils (Figure 5.2 (b), (c) and (d)). The pH profile in the eukaryote-inhibited system (Figure 5.2 (c)) also showed greater variation around the overall mean, which was not apparent in any of the other three systems.

Likewise, profiles for $Ca^{2+}_{(L)}$ and $Cl^{-}_{(L)}$ were constant across the distance range tested in the

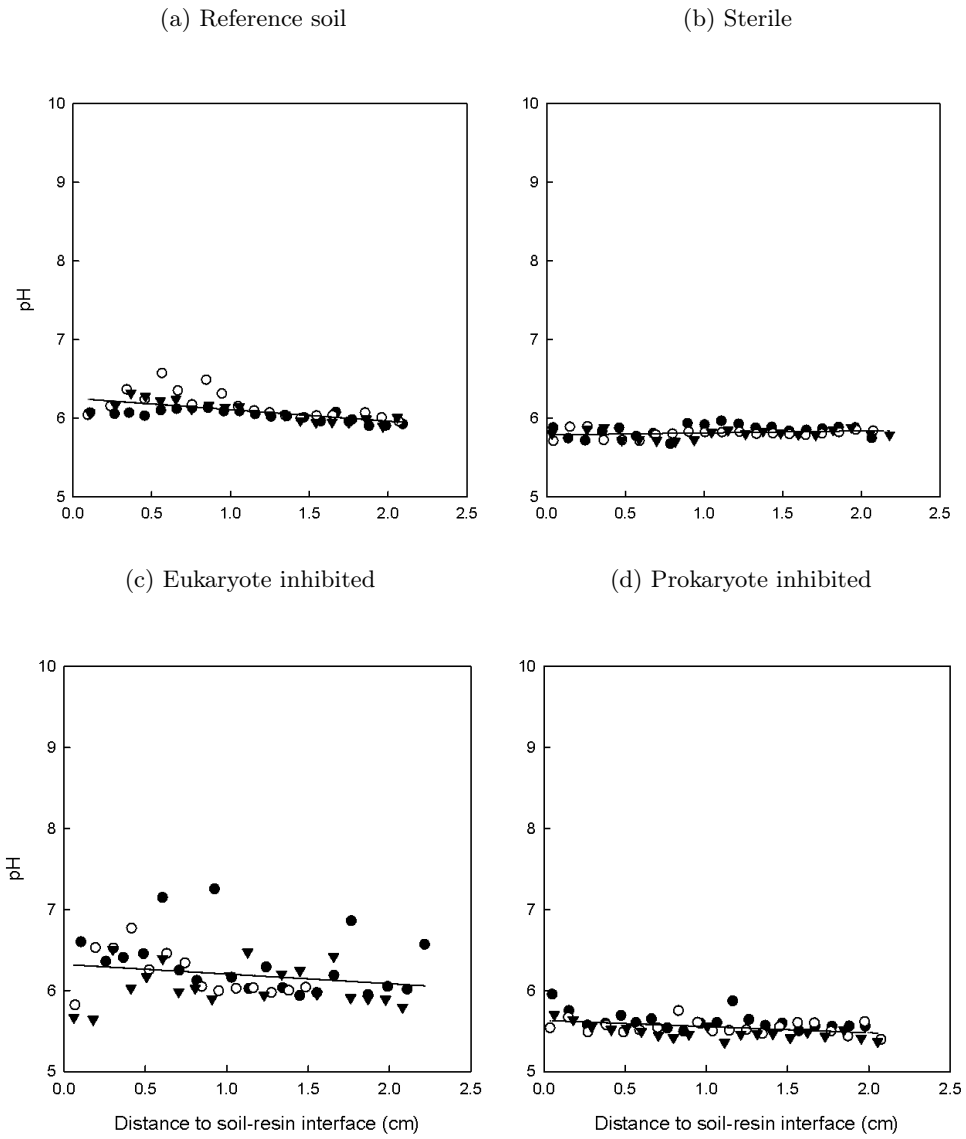

Figure 5.2: *pH-distance profiles in the control cells, where there is no contact with anion exchange resin, referenced by treatment. The different symbols denote different replicates. The linear model fitted accounted for 75% of variation in the data (R^2 = 0.7488).*

three treated systems. While the concentration values did not exactly match in all four treatments, the chloride concentration was found to be double that of calcium (Figure 5.3 (b), (c) and (d)). The profiles in the reference system however did not appear as constant, and showed an apparent concentration increase in both ion concentrations closer to the top of the soil collar

(Figure 5.3 (a)). The same was not observed in any other control profile which would indicate a human error.

There was no calcium carbonate precipitation for any of the four treatments (Figure 5.4). The basal value for solid $CaCO_3$ in the soil was measured at 1.1 mmol kg^{-1} soil.

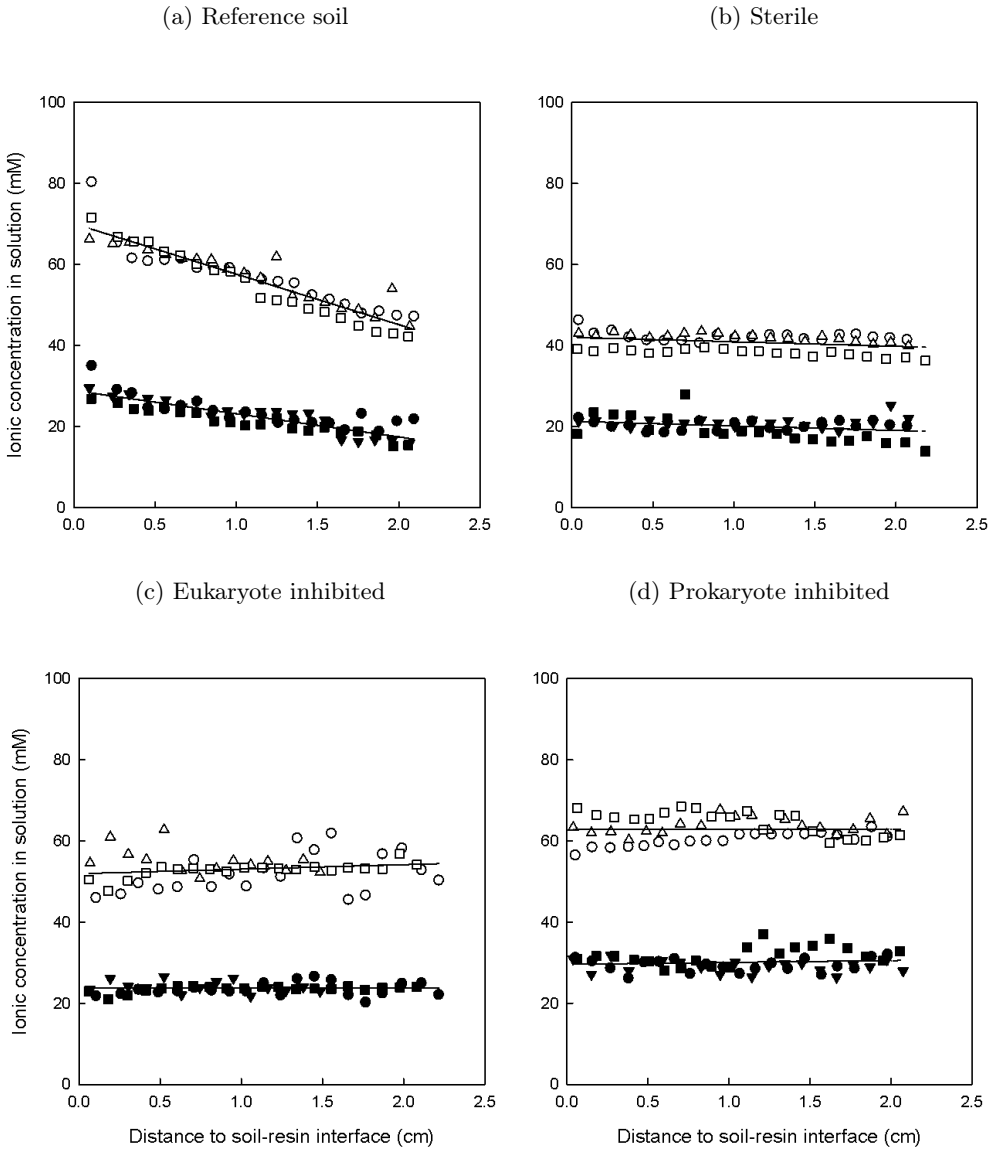

Figure 5.3: *Calcium and chloride concentration-distance profiles in the control cells, where there is no contact with anion exchange resin, with respect to treatment. The different symbols denote different replicates. The linear model fitted to* Ca^{2+} *and* Cl^{-} *accounted for 81% and 91% of variation in the data respectively (*$R^2_{Ca} = 0.8131$ *and* $R^2_{Cl} = 0.9056$*).*

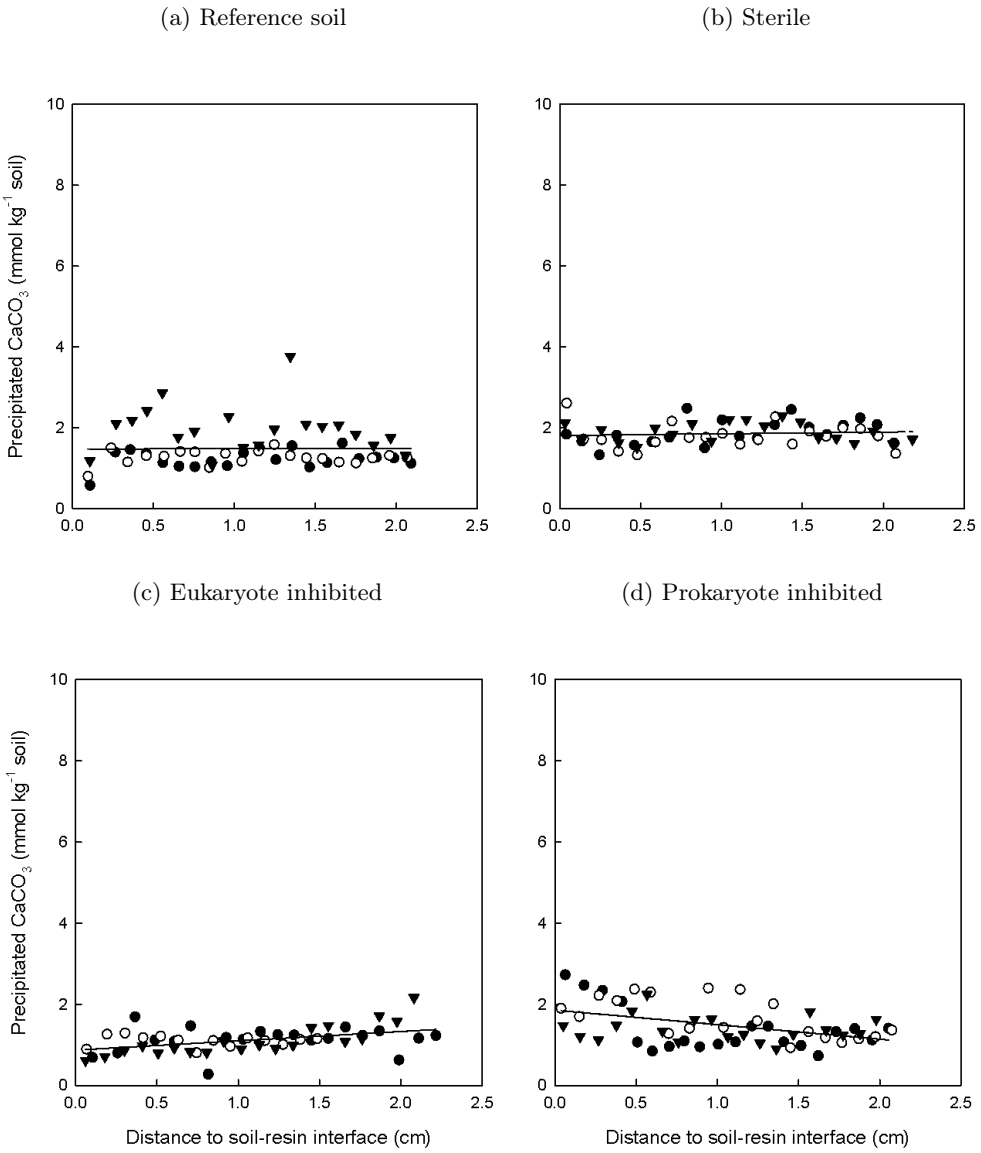

Figure 5.4: *Precipitated $CaCO_3$ concentration-distance profiles in the control cells, where there is no contact with anion exchange resin, with respect to treatment. The different symbols denote different replicates.*

Contact with a source of bicarbonate ions

After one day and five days of contact with the source of base, the concentration-distance profiles for all species significantly varied from the observations in the control. The distance travelled by solutes and changes in pH differed between treatments, reaching 1 to 1.5 cm after one day and going through the length of the block of soil after five days, with further changes closer to the source of alkalinity.

The contact between the flat surface of the block of soil and the malleable mass of resin beads was effective and homogeneous between replicates, based upon the impression of the nylon mesh into the soil surfaces.

The regression lines fitted on each concentration-distance profile are the results of the statistical analysis run for each parameter and each diffusion time. The R^2 value for each statistical run is given in the captions of the figure to quantify the amount of variation in the datasets taken into account by the model. Statistically, the soil treatment was found to have a significant impact on pH, $CaCO_3$ precipitated and both Ca^{2+}[†] and Cl^-.

After one day of contact with the anion exchange resin, the pH in soils increased at the vicinity of the soil-resin interface. The reference soil reached a pH of 9.5 at the point of contact with the resin and settled under 6.0 at the other end (Figure 5.5 (a)). The pH measured at the soil-resin interface in the other treatments was found to be significantly different ($p < 0.05$) from the value in the reference soil (Figures 5.5 (b), (c) and (d)). However, the value of the minimum plateau at the opposite extremity of the soil columns did not vary significantly between treatments ($p \geq 0.05$). The slope between the two plateau was similar for all treatments but the prokaryote-inhibited system, where the rise in pH was not as sharp with distance to the soil-resin interface, and thus found to be significantly different from the other three treatments (Figure 5.5 (d)).

After five days, the pH concentration-distance profiles became more linear in both sterile and prokaryote dominated systems (Figures 5.6 (b) and (c)), despite what appeared to be an

[†]A summary of p values from the statistical analysis of data is given in Appendix B.3.

(a) Reference soil

(b) Sterile

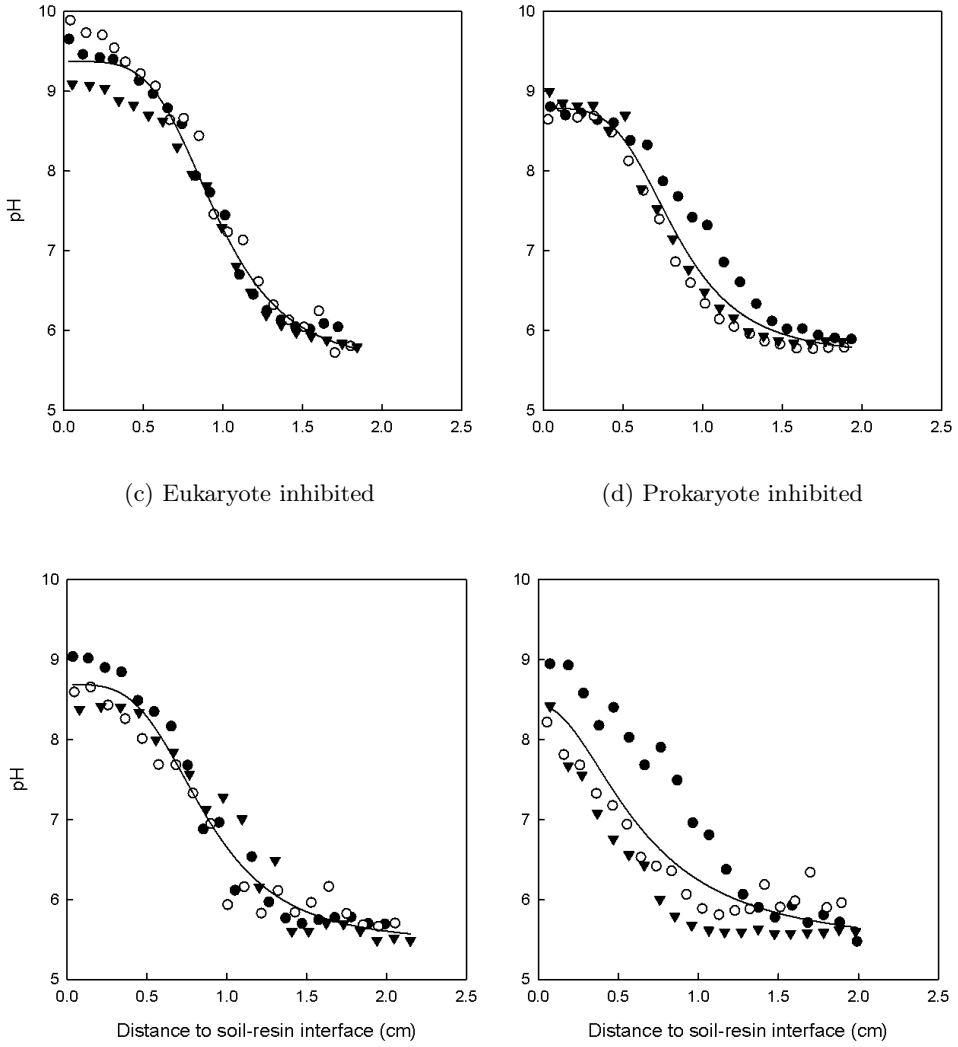

(c) Eukaryote inhibited

(d) Prokaryote inhibited

Figure 5.5: *pH-distance profiles after one day of contact with anion exchange resin, with respect to treatment. The different symbols denote different replicates. The non- linear models fitted accounted for over 96% of variation in the data for every replicate.*

(a) Reference soil

(b) Sterile

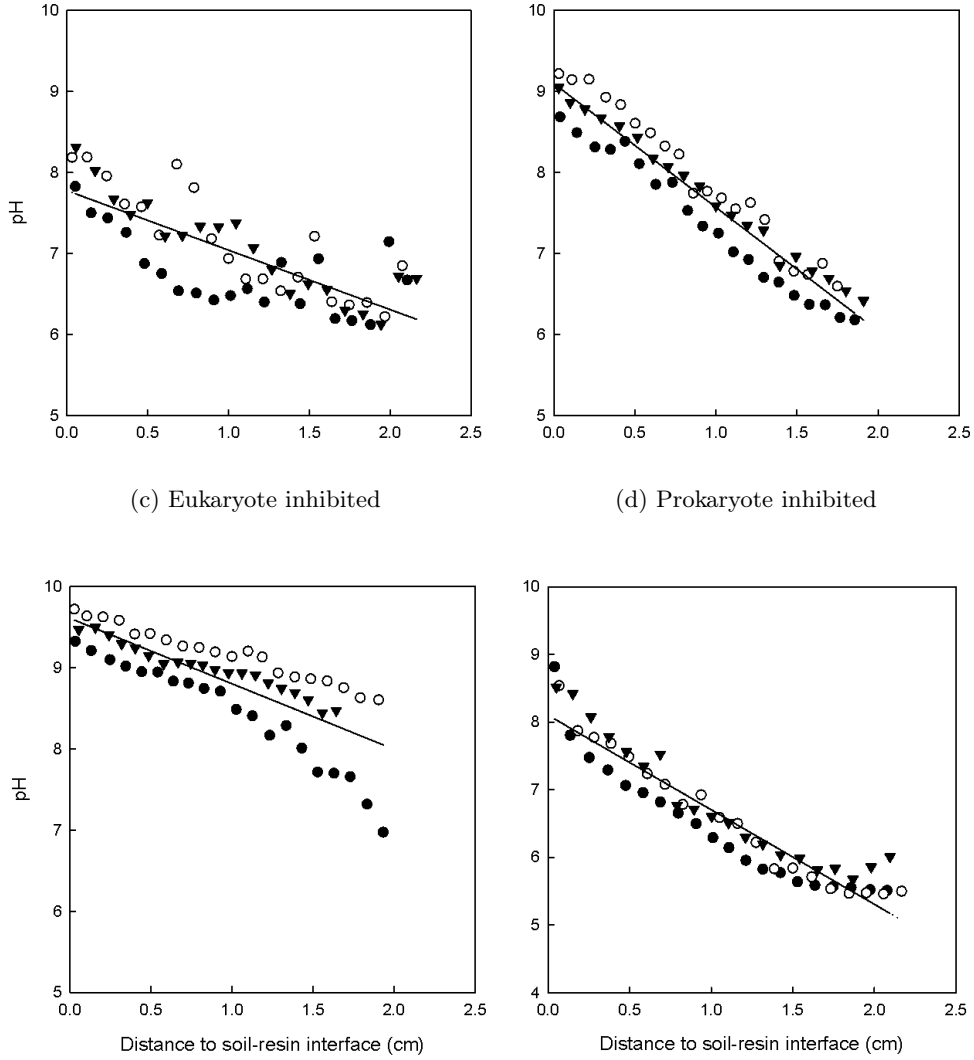

(c) Eukaryote inhibited

(d) Prokaryote inhibited

Figure 5.6: *pH-distance profiles after five days of contact with anion exchange resin, with respect to treatment. The different symbols denote different replicates. The linear model fitted accounted for 92% of variation in the data (R^2 = 0.9210).*

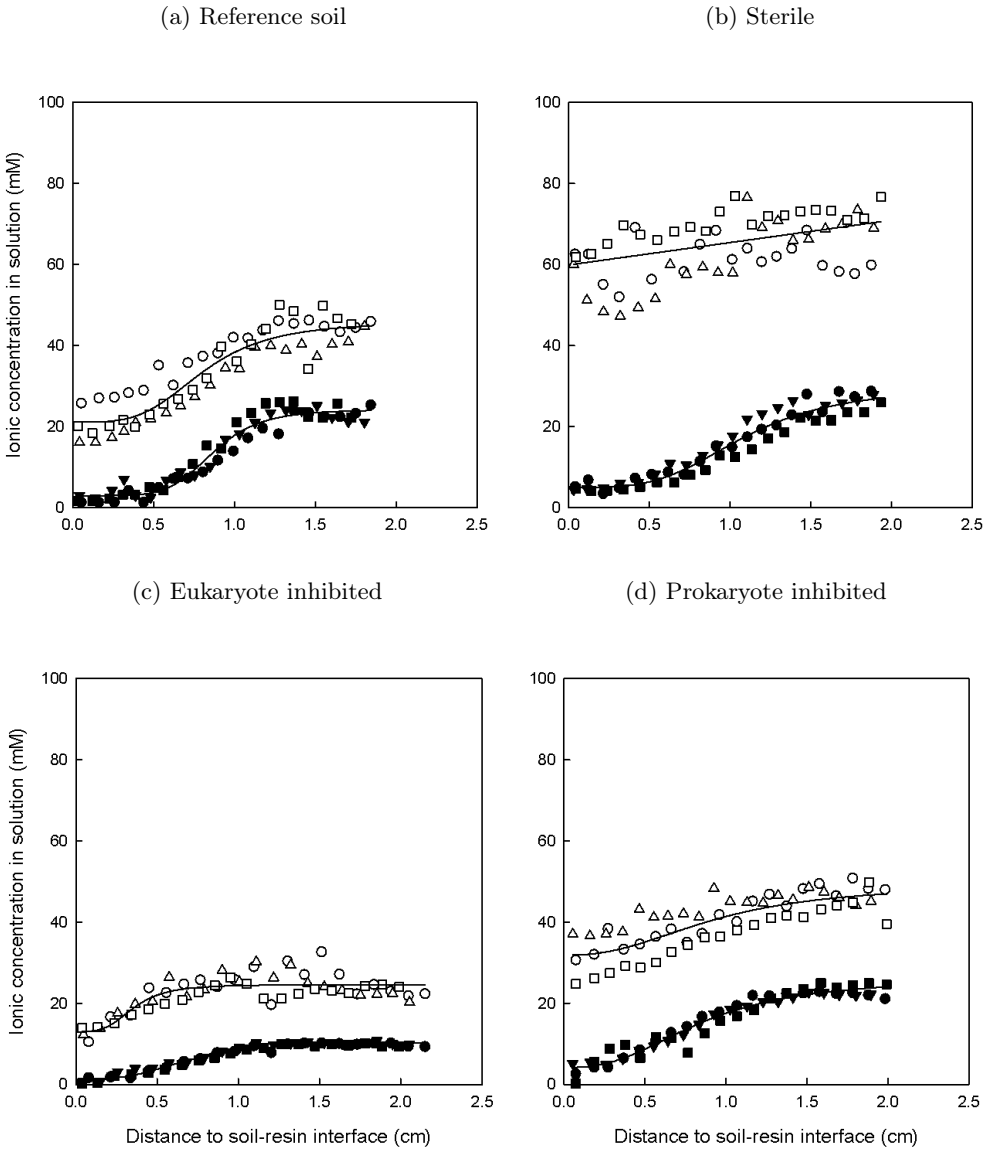

Figure 5.7: *Calcium (black markers) and chloride (white markers) concentration-distance profiles after one day of contact with anion exchange resin, with respect to treatment. The different symbols denote different replicates. The linear model fitted to* Ca^{2+} *and* Cl^{-} *accounted for 91% and 92% of variation in the data respectively* ($R^2_{Ca} = 0.9082$ *and* $R^2_{Cl} = 0.9167$).

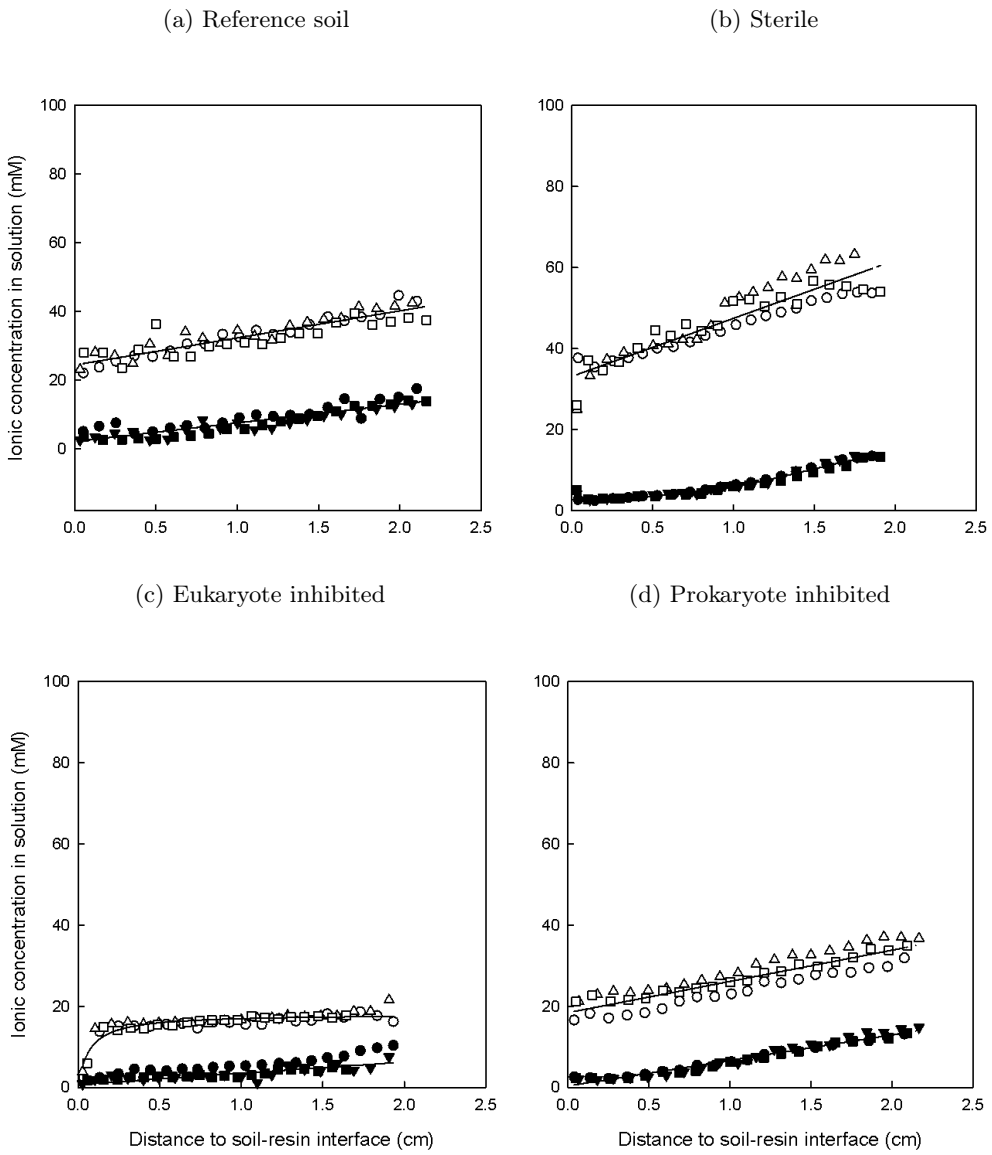

Figure 5.8: *Calcium (black markers) and chloride (white markers) concentration-distance profiles after five days of contact with anion exchange resin, with respect to treatment. The different symbols denote different replicates. The linear model fitted to* Ca^{2+} *and* Cl^{-} *accounted for 88% and 97% of variation in the data respectively (*R^2_{Ca} *= 0.8821 and* R^2_{Cl} *= 0.9710).*

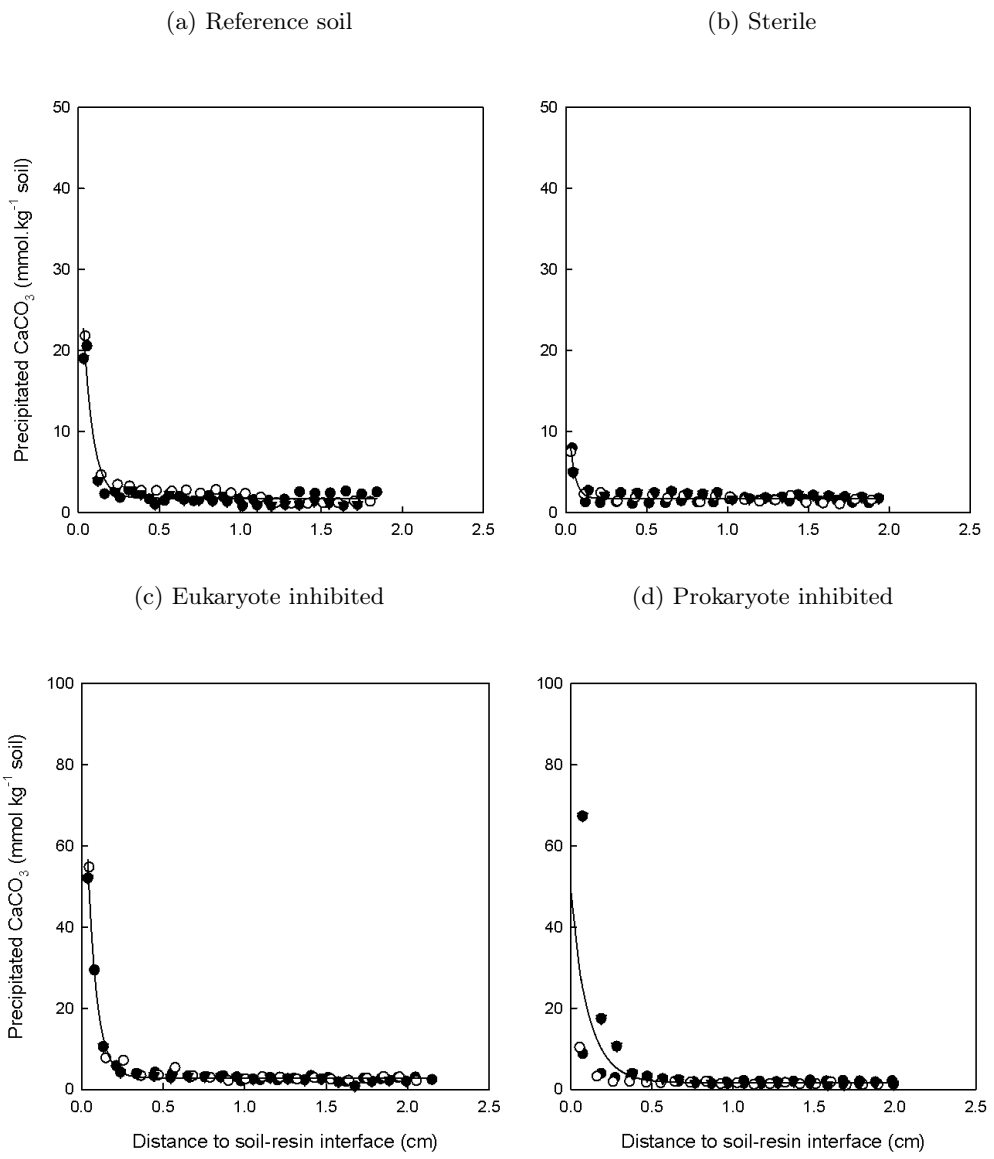

Figure 5.9: *Precipitated $CaCO_3$ concentration-distance profiles after one day of contact with anion exchange resin, with respect to treatment. The different symbols denote different replicates. Note the difference in scale between (a),(b) and (c),(d).*

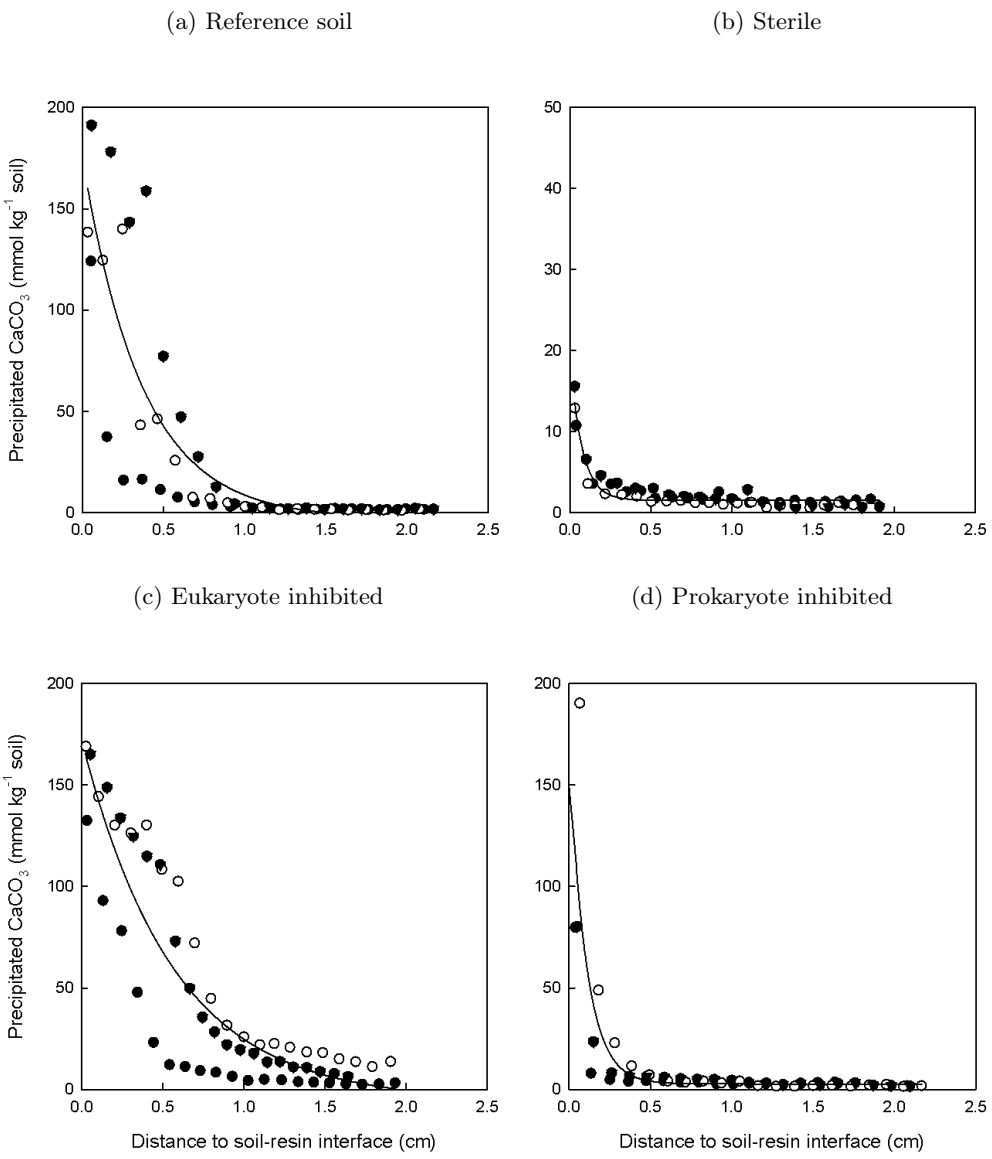

Figure 5.10: *Precipitated $CaCO_3$ concentration-distance profiles after five days of contact with anion exchange resin, with respect to treatment. The different symbols denote different replicates. Note the difference in scale for (b).*

anomalous replicate in the latter. In the prokaryote-inhibited system (Figure 5.6 (d)) the profile appeared also more linear over an increased depth of 1.5 cm, and then plateaued at its initial value of 5.5. The pH in the reference system appeared more variable between replicates (Figure 5.6 (a)), and not as obviously linear with depth; the pH at the soil-resin interface had decreased to 8.0, while in the bacterial system it had increased from 9.0 after one day to 9.5 (Figure 5.6 (c)). Both the sterile and fungal-dominated systems soil-resin interface were observed at the same pH as after one day of contact (Figures 5.6 (b), (d)). The fungal system was the only treatment where the pH was not only constant at the soil-resin interface after one and five days, but also still plateauing at its initial value (5.5) at the opposite extremity of the sliced soil column.

The concentration-distance profiles for the ions in solution also showed changes from the concentration-distance profiles in the absence of a source of HCO_3^-. After one day diffusion, all three live systems showed a drop in chloride concentration near the soil-resin interface accompanied by a drop in calcium ions concentration (Figure 5.7). The concentration in Cl^- remained double that of Ca^{2+} throughout the sliced soil columns in the three live systems (Figures 5.7 (a), (b), (c)). In the sterile treatment however, while the concentration of calcium in solution dropped over the same distance as in the reference soil, the chloride concentration did not drop from its initial value of 60 mM.

As highlighted in the absence of contact with anion exchange resin, the concentrations of solutes in the eukaryote-inhibited system (Figure 5.7 (c)) was again found to be less than those measured in both the reference and prokaryote-inhibited systems (Figures 5.7 (a) and (d)).

After five days, the profiles in the live systems were all found to be linear across the distance of soil studied, and dropped to about half of their overall concentration value for both Ca^{2+} and Cl^- after one day of diffusion (Figures 5.8 (a), (c) and (d)). The Cl^- concentration plateau at the opposite extremity of the soil column was however found at a similar value as after one day for both treatments (Figures 5.8 (a), (c)).

In the prokaryote-inhibited soil however, the changes in concentrations of ions were observed

over the same 1 cm-distance from the resin as after one day diffusion, however the overall value of the profiles dropped by half in both cases (Figure 5.8 (d)).

Similar observations were made on the Ca^{2+} concentration-distance profile in a sterile system, which featured both an increase in the diffusion distance and a plateau in concentration at the opposite end of the experimental soil column (Figure 5.8 (b)). Cl^- had diffused into the resin more after five days than after one, however its movement was found to be very limited in comparison to the live treatments. Its value at the end extremity of the sliced soil column was still above 50 mM.

The amount of precipitated $CaCO_3$ differed significantly between treatments. After one day of contact with resin, the amount of precipitation in the sterile soils was less than 10 mmol kg^{-1} soil at the soil-resin interface (Figure 5.9 (b)). After five days, it was less than 20 mmol kg^{-1} soil (Figure 5.10 (b)), only 10% of the amount of precipitated $CaCO_3$ found in the reference soil (Figure 5.10 (a)).

Both prokaryote- and eukaryote-inhibited systems showed approximately double the precipitation found in the reference system after one day diffusion (Figure 5.9 (c) and (d)). After five days, the $CaCO_3$ concentration-distance profiles in the live systems were also significantly different ($p < 0.05$). The amount of precipitation was the highest in the reference system, and precipitation occurred over similar distances away from the soil-resin interface for both the reference and eukaryote-inhibited systems (Figure 5.10 (a) and (c)). However, $CaCO_3$ formed only in the direct vicinity of the soil-resin interface in the prokaryote-inhibited soil (Figure 5.10 (d)). The latter was found to present more homogeneity between replicates than both the reference and bacterial-dominated treatments.

5.3.2 Crystal morphology and $CaCO_3$ polymorph

General observations

Overview observation of the meshes at low magnification from the different treatments (Figure 5.11) revealed the increased development of hyphae resulting from inhibition of the soil's bacterial population (Figure 5.11 (d)), highlighting the differences in microbial communities between treatments.

Sterile system

No sign of life was detected under the microscope in the irradiated soils. The crystals observed in the abiotic system were generally sparsely distributed with smooth surfaces (Figure 5.12). The rhombohedral arrangement of single crystals observed suggested that the single crystals were shaped as needles, or "trigonal" i.e. with three faces and one axis of symmetry (Figures 5.12 (c) and (d)).

Prokaryote-inhibited system

In the prokaryote-inhibited system, the crystals were characterised as being arranged in floret-like shapes, with individual crystals showing blunt orthorhombic faces (Figure 5.13 (b), (c)), as well as some with smoother surfaces (Figure 5.13 (d)). Both arrangements appeared to be more numerous on the nylon fibres, and the fungal hyphae were notably not coated by the precipitate.

(a) Reference

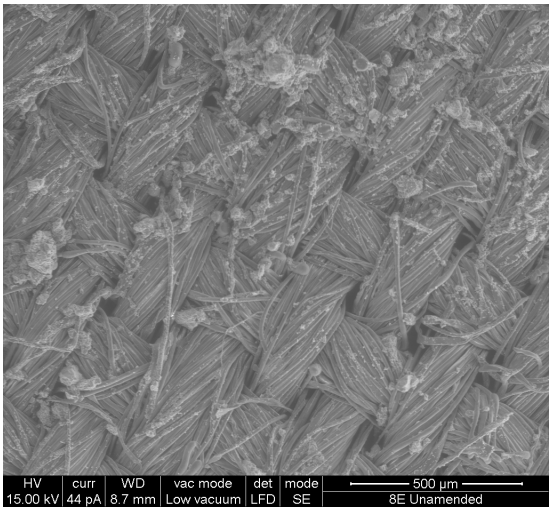

(b) Sterile

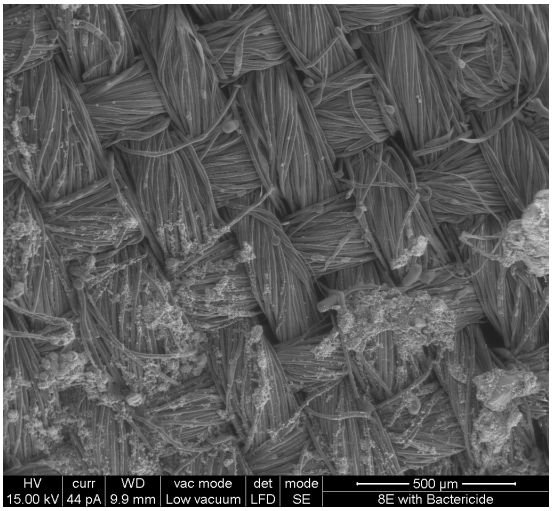

(c) Eukaryote-inhibited

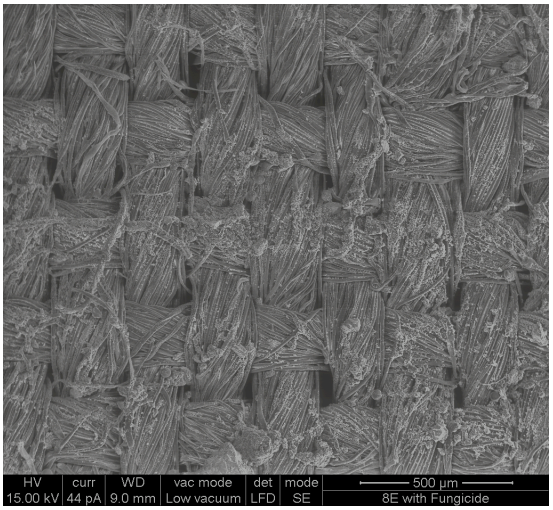

(d) Prokaryote-inhibited

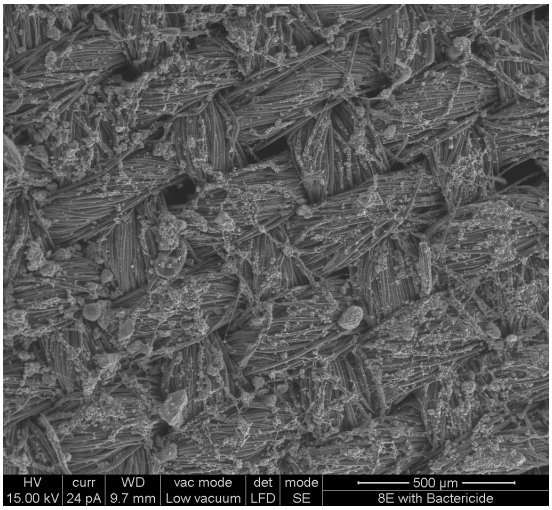

Figure 5.11: *Overview observation of the meshes from the different treatments showing the distribution of crystals and fungal hyphae (bacteria invisible at this scale).*

(a) (b) (c)

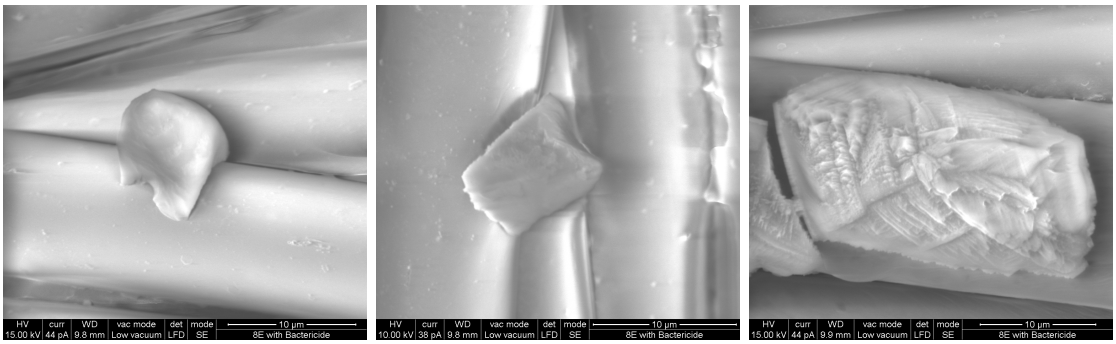

(d) Rhombohedral arrangement of crystals

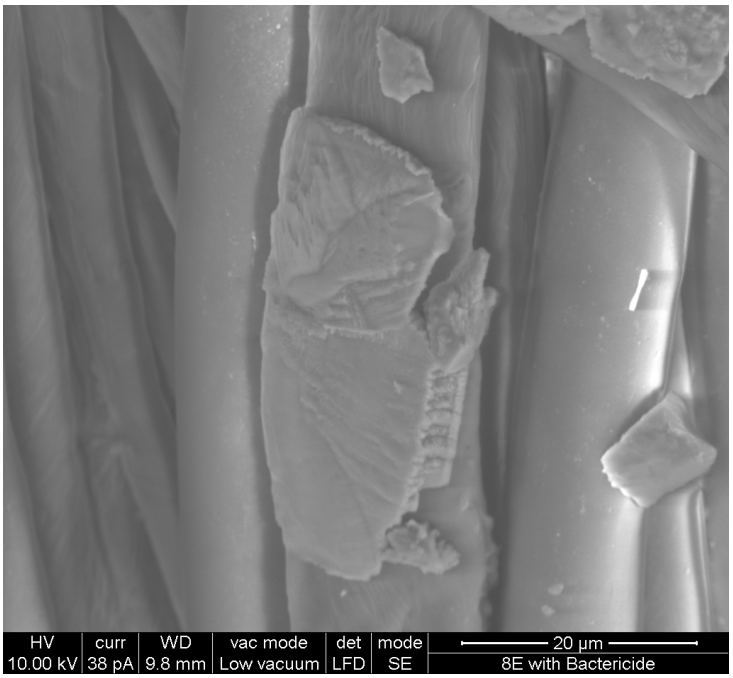

(e) Crystals elemental composition

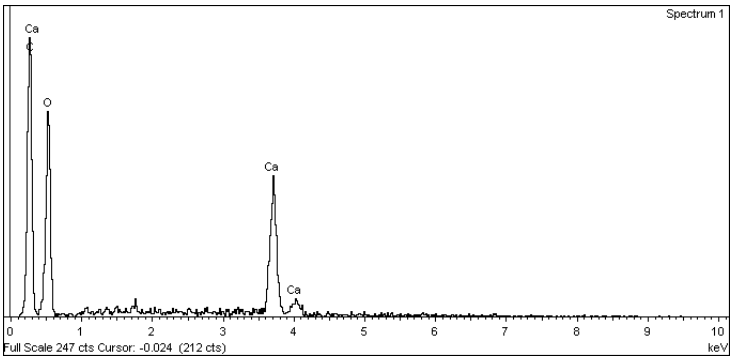

Figure 5.12: *Smooth $CaCO_3$ crystal shapes and arrangements found in a sterile system (a,b,c,d). (e) shows the result of the elemental composition analysis.*

(a)

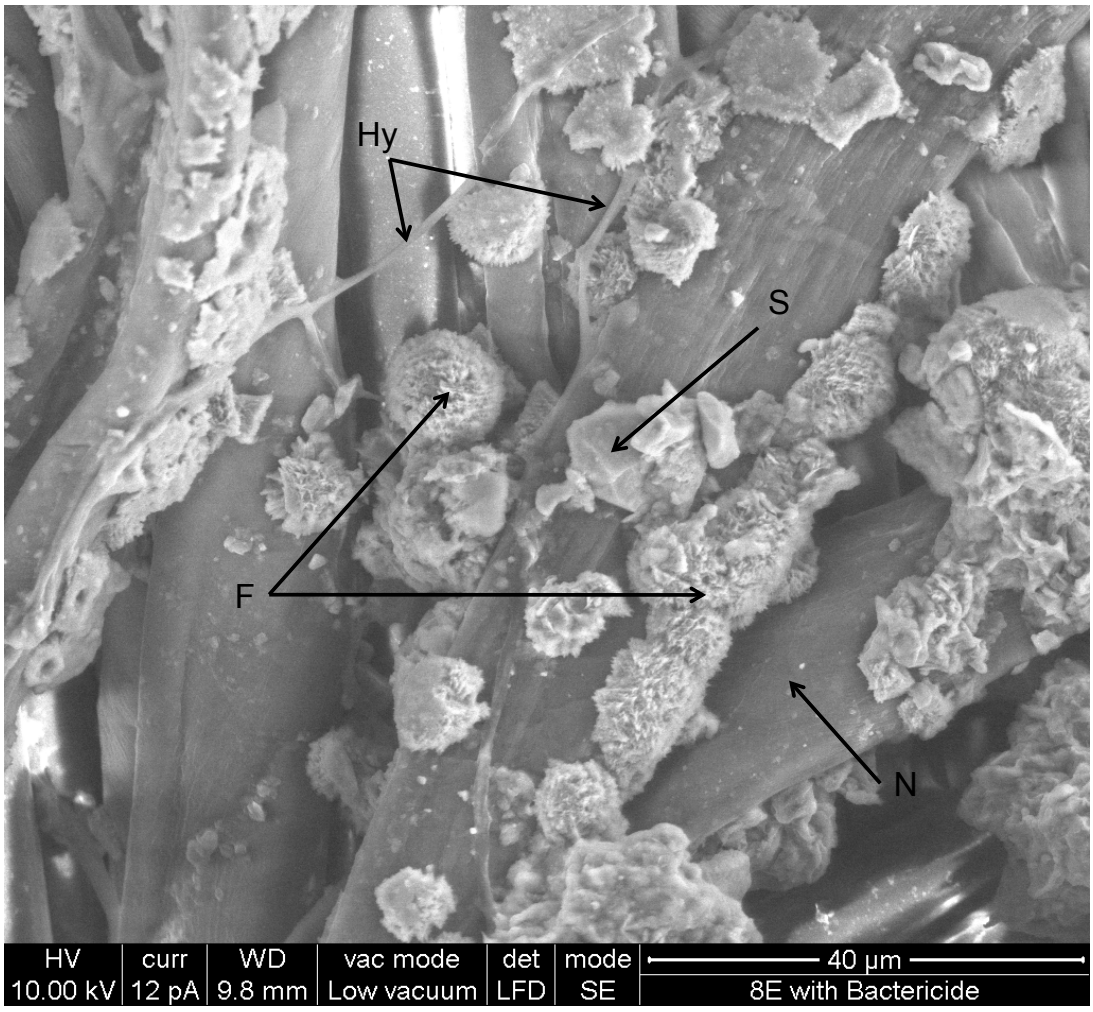

(b) (c) (d)

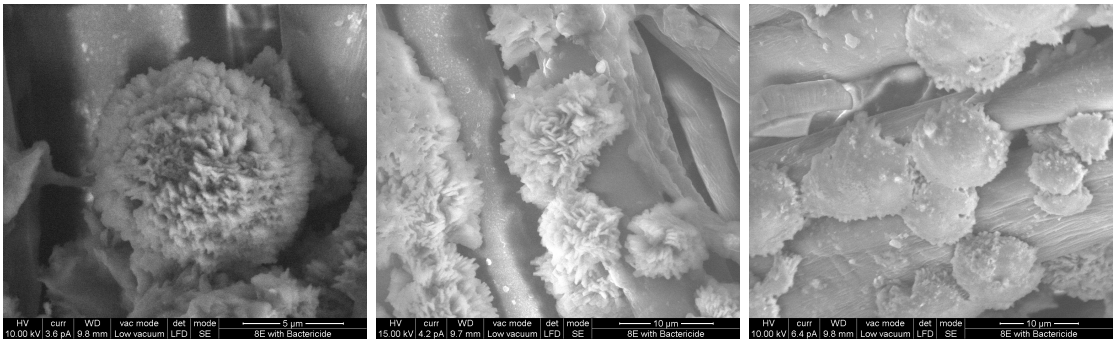

Figure 5.13: *Abundance (a) of $CaCO_3$ precipitation in a prokaryote inhibited system (Hy = fungal hypha, F = floret-like crystal arrangement, S = smooth $CaCO_3$ crystal arrangement, N = nylon fibre). The details show floret-like (b,c) and smooth (d) crystal arrangements.*

Eukaryote-inhibited system

The crystals observed in a bacterial dominated system (Figure 5.14) were much smaller than those observed in the prokaryote-inhibited treatment (Figure 5.13), and resembled bow-ties, or wheat sheaves.

Reference non-manipulated system

The sheaves and floret shapes observed in each manipulated live system were also observed to occur in the unamended 'reference' soil. However, the most predominant structure took the form of a $CaCO_3$ sphere surrounded by a crown of irregular crystals (Figure 5.15).

ESEM Environmental mode

The observation of the reference soil in a hydrated state allowed the study of the close interaction between fungal hyphae and $CaCO_3$ crystals. Fungal hyphae were observed to be pulled from their trajectory by crystals growing along their surface (Figure 5.16 (a), (b), (c)) and in some instances completely embedded in $CaCO_3$ crystals (Figure 5.16 (d)).

The composition of the crystals observed were confirmed as $CaCO_3$ with elemental composition determination (Figure 5.16 (e)).

X-ray diffraction analysis

The X-ray diffraction analysis of the reference system nylon mesh mounted on a zero background silicon mount detected only calcite as the polymorph of $CaCO_3$ precipitated (Figure 5.17). The reference nylon mesh was re-analysed at the same time as the other treatments mounted on an aluminium mount (Figure 5.18). All diffractograms for every treatment only detected calcite as the $CaCO_3$ polymorph precipitated.

(a)

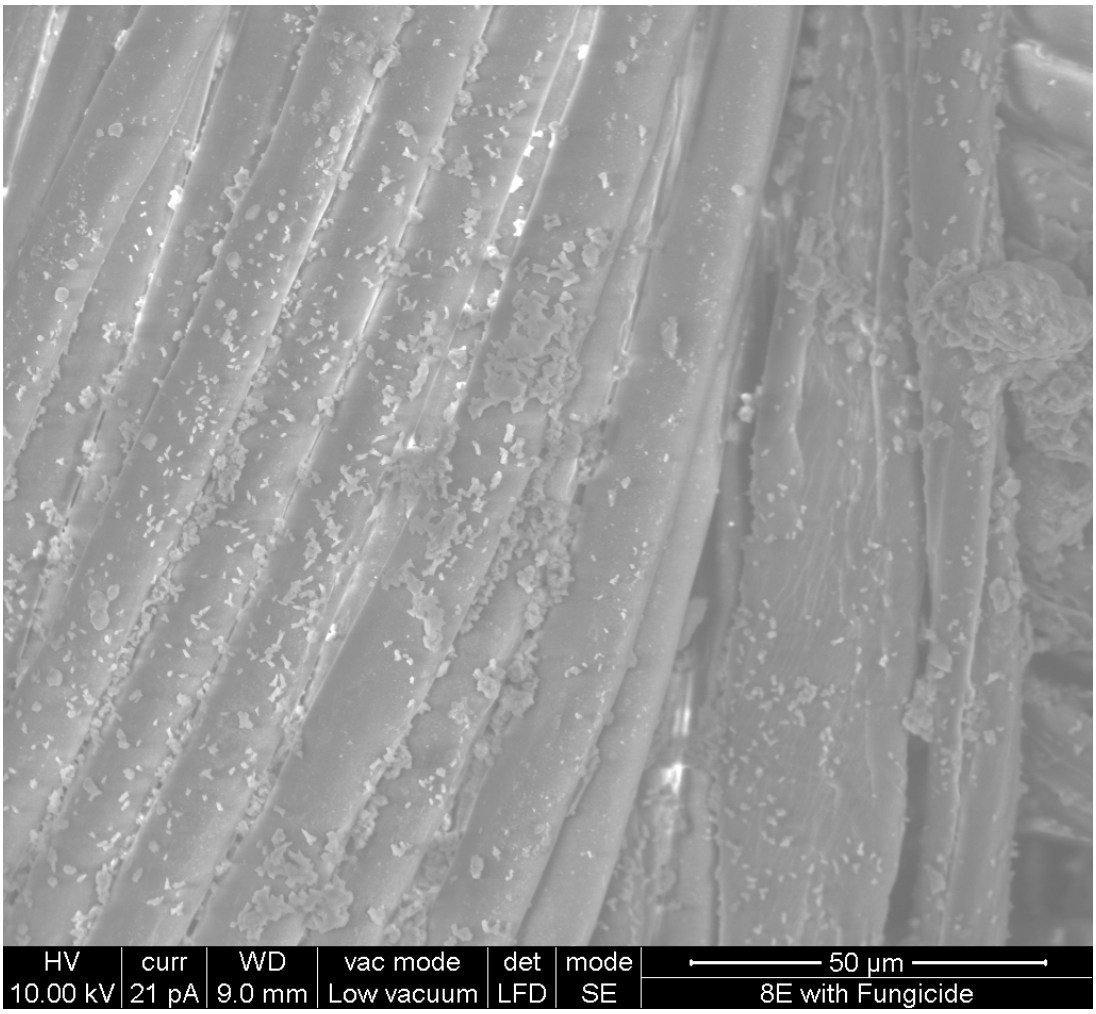

(b)

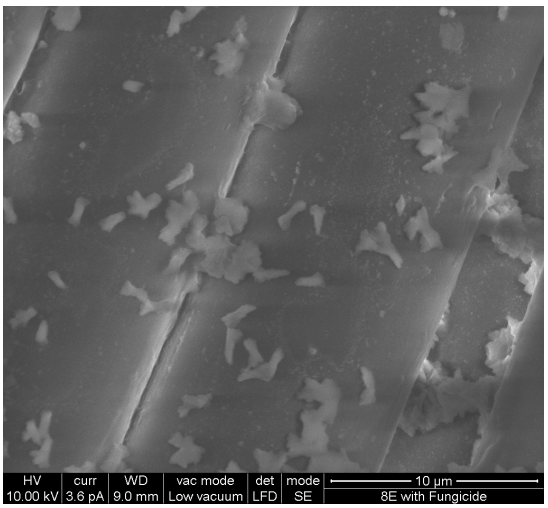

(c)

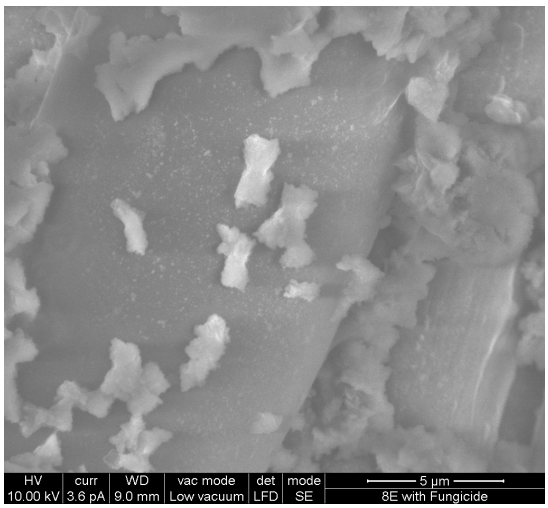

Figure 5.14: *Abundance (a) and details (b,c) crystal arrangements in a eukaryote inhibited system.*

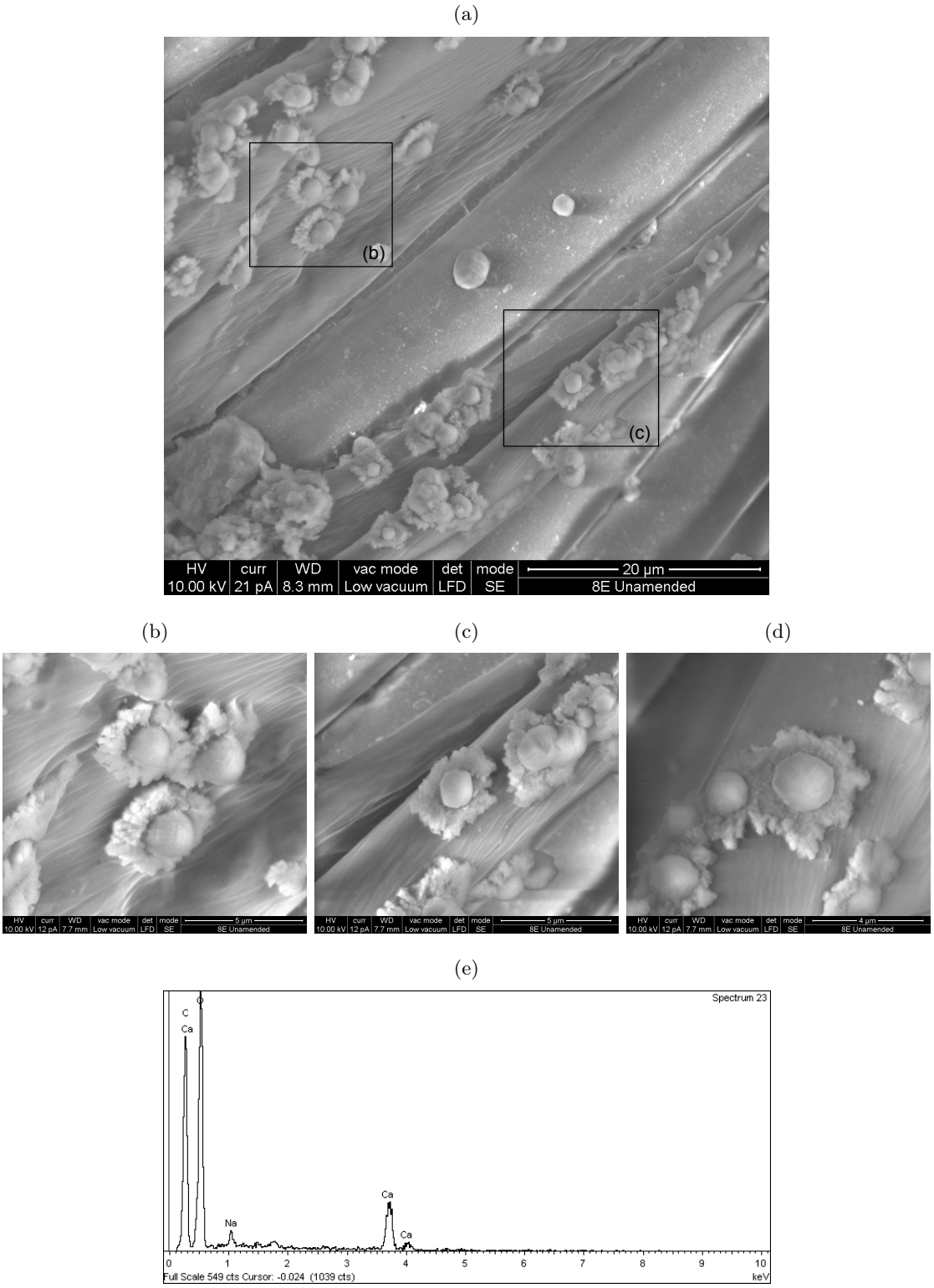

Figure 5.15: *Abundance (a), details (b,c,d) and elemental composition (e) of new crystal arrangements found in the reference system.*

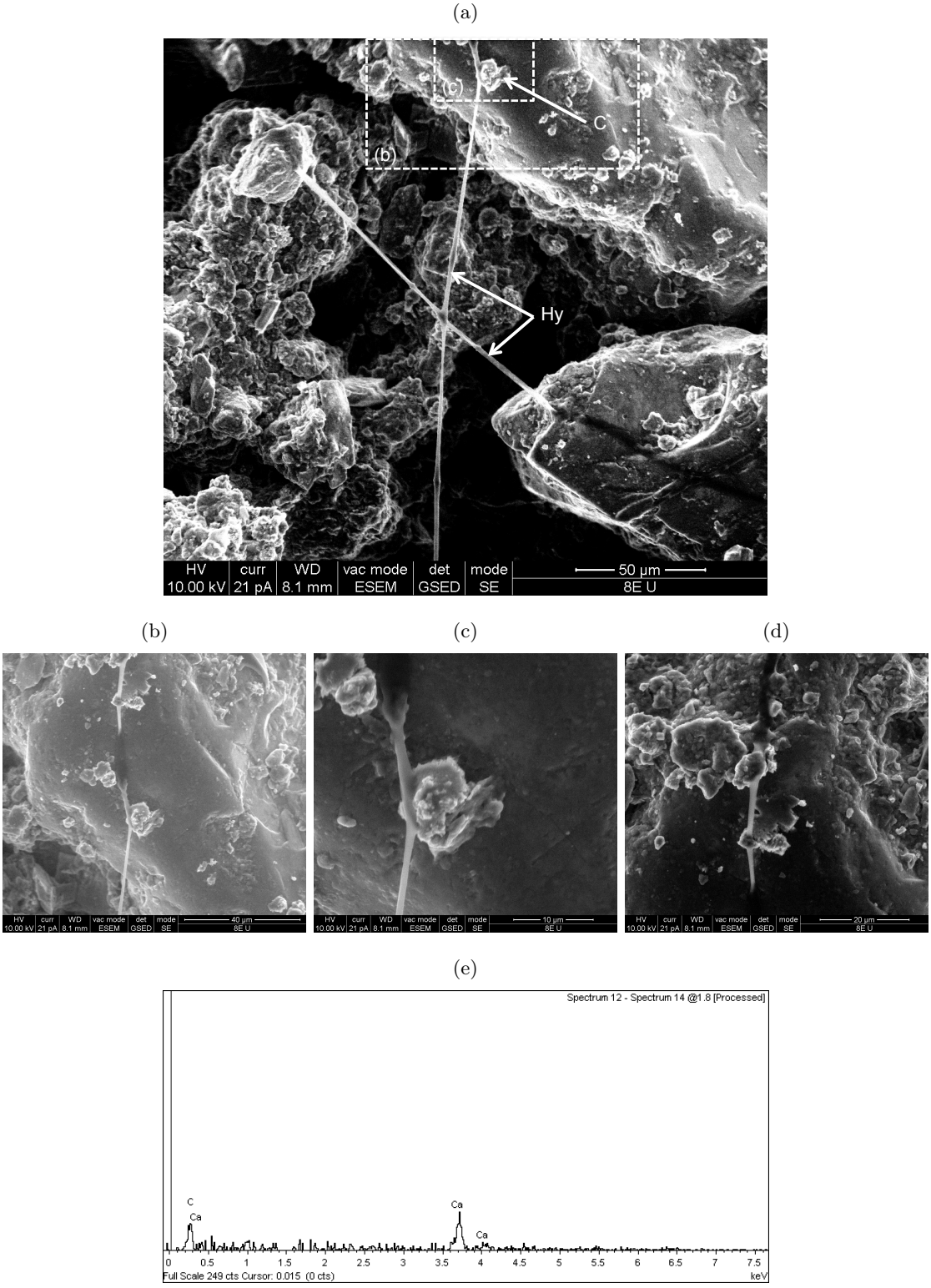

Figure 5.16: *Interaction between a fungal hypha (Hy) and $CaCO_3$ crystals (C) in the reference soil observed in the ESEM environmental mode (a,b,c). (d) shows the result of the elemental analysis of the crystal (C) attached to the fungal hypha in (a).*

(a)

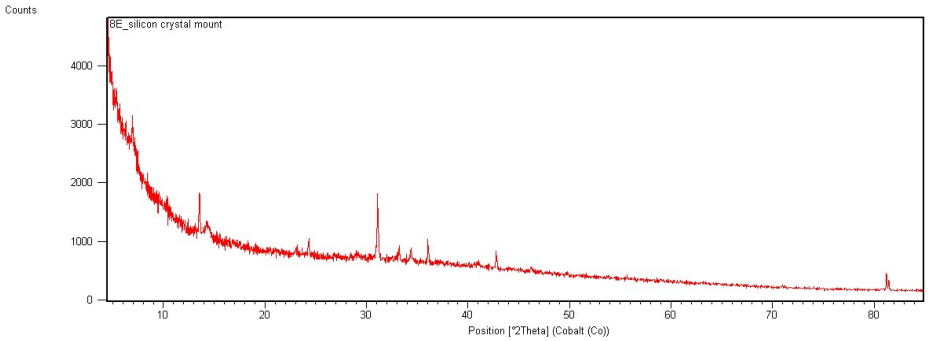

(b)

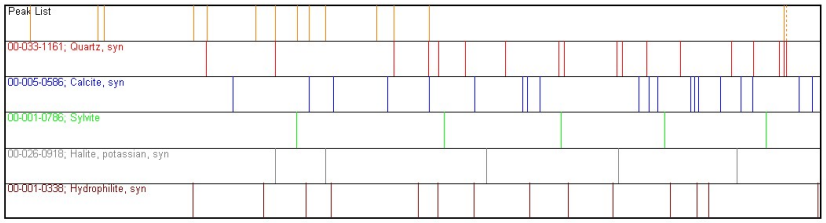

Figure 5.17: *X-ray diffraction result spectrum (a) for the reference soil mounted on a zero background silicon mount and the peak interpretation table (b).*

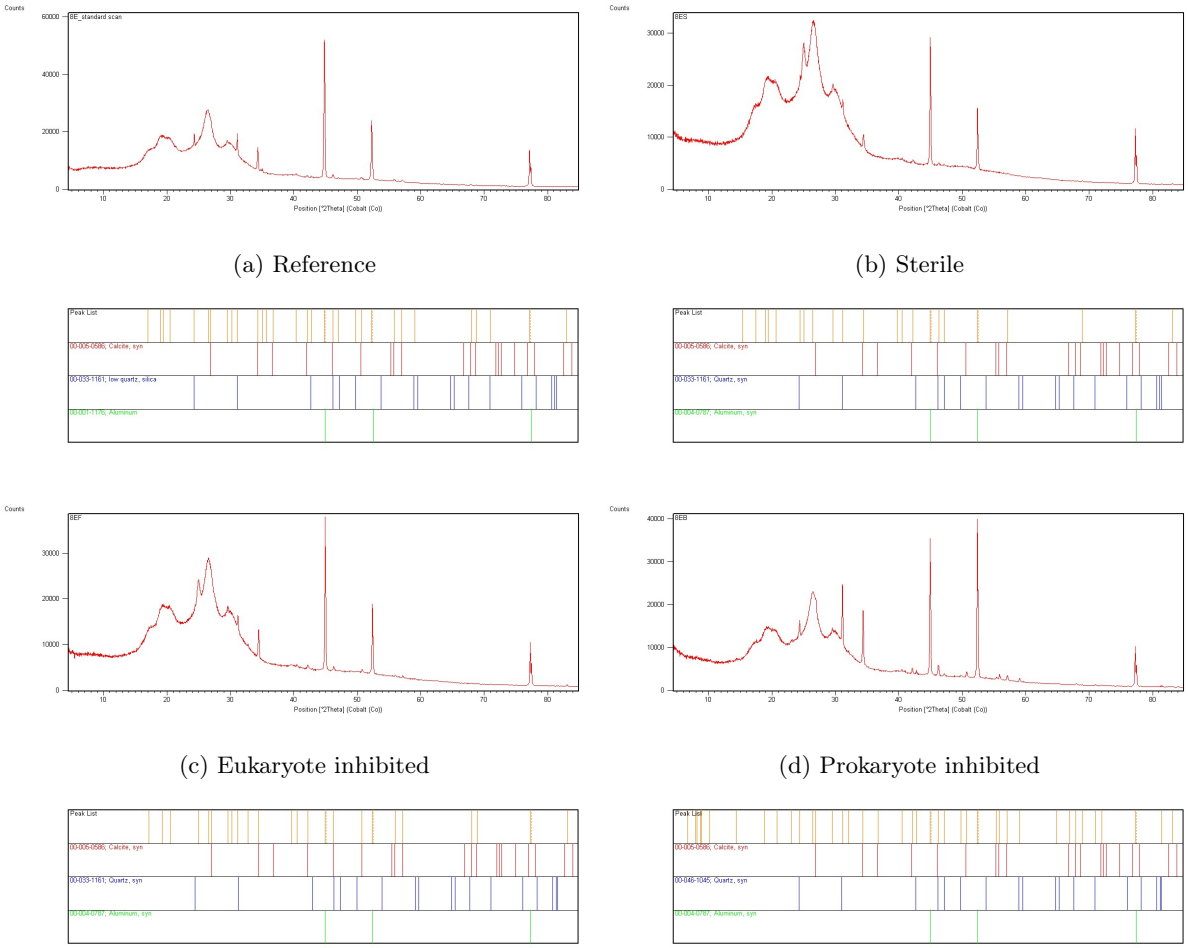

(a) Reference

(b) Sterile

(c) Eukaryote inhibited

(d) Prokaryote inhibited

Figure 5.18: *X-ray diffraction results for the four treatments interface nylon meshes mounted on aluminium mounts. The top part of each figure shows the resultant spectrum after diffraction, the bottom part is the peak interpretation table, showing the crystalline species related to each peak in the corresponding spectrum.*

5.4 Discussion

The influence of both fungal and bacterial communities on the precipitation reaction has widely been investigated on growing media, e.g. Buczynski and Chafetz (1991); Stocks-Fischer et al. (1999); Bachmeier et al. (2002); Mitchell and Ferris (2006); Rivadeneyra et al. (2006); Rogerson et al. (2008); Dupraz et al. (2009); Masaphy et al. (2009). The interest of this study however lies in the interaction within and between whole microbial communities rather than a study into the effect of single microbial species removed from field conditions.

To achieve this approach, the experimental soil was treated with cycloheximide or bronopol to achieve an inhibition of the targeted microbial community, either fungal or bacterial, while limiting non target-specific effects on the rest of the soil biota. Direct and microscopic observations confirmed the different nature of microbial communities developing as a result of the treatments, with a notable explosive hyphal growth in the prokaryote-inhibited soils. Further, the observation of obviously different behaviours for each parameter measured in the different soil treatments provides indirect evidence that the antibiotics concentrations applied were appropriate to lead to a substantial modification of the experimental soil microbial community composition.

The soil pH recorded in the reference system was 6.0, which was coherent with the initial soil physicochemical properties measured on the natural soil (Table 3.1). In all systems the concentrations in Ca^{2+} and Cl^{-} verify the stochiometry of the initial $CaCl_2$ solution used to bring the soil columns to the desired moisture content. However in the control reference system, the rise in Ca^{2+} and Cl^{-} concentrations near the soil-resin interface was not expected. It could have been due to an evaporation of water from the incubation chambers if the seal was not appropriately hermetic, preventing the atmosphere inside the chambers from saturating with water and leading to the soil columns slowly drying and the soil solution getting increasingly concentrated. This was assumed not to happen in the presence of resin since the resin moisture

content was adjusted on sand tables to match that of the soil and thus prevent mass flows of water between the two collars.

The initial soil conditions were affected both by irradiation and antibiotics. However there is no agreement in the literature on the effect of gamma irradiation on soil pH. McNamara et al. (2003) review several publications which have published contradicting results for the effect of gamma rays on soil pH over the last 50 years. While other authors report that pH was increased after sterilisation by irradiation, Hartel and Alexander (1983) report that a higher dose of irradiation lowered the pH of their soil by up to 0.2 units. By comparing the effect of irradiation on two soils, they highlighted the possibility that soils of different texture are not affected the same way by gamma rays, a sandy clay loam sample seemingly being more affected with respect to pH than a silty loam.

The experimental soil Ti used in the study of soil biota on $CaCO_3$ precipitation is a loamy sand, which could be linked to the 0.2 unit drop in pH observed in the sterile system.

The typical production of organic acids - citric, oxalic and malic acids in particular (Gadd, 2007) - by fungi during their growth can explain the lower pH recorded in the prokaryote-inhibited system compared to either three other treatments, including the sterile soil. In a calcium-rich environment, oxalic acid can release two protons to form oxalate and chelate a divalent cation such as calcium. It can thus pull calcium from the soil exchange complex into solution. Calcium ions thus complexed are detected by AAS, even if they are not available for $CaCO_3$ precipitation.

Gadd (2007) also highlights that during growth, fungi foraging for nutrients can release elements from precipitated phases. A portion of these elements can be stored in the fungal hyphae, but this action can also lead to supersaturation of the microenvironment around the hyphae, and hence sometimes the formation of calcium-rich deposits.

The concentration-distance profiles which were measured support Hypothesis 1 that the particular composition of the soil microbial community does not affect the expected direction of the ions' movement in the vicinity of a source of alkalinity. pH was indeed observed to increase

near a source of alkalinity, while Ca^{2+} concentration in solution decreased, and $CaCO_3$ was precipitated.

The difference in the values and overall shapes of measured concentration-distance profiles does however lead to the further assumption that microbial activity influences the composition of soil environments, and thus the behaviour and fate of the elements involved in a reaction such as $CaCO_3$ precipitation. Key elements involved in the precipitation of $CaCO_3$ are Ca^{2+} and carbonate species. In this experimental system, the movement of Ca^{2+} would be regulated by the diffusion of HCO_3^- into the soil and corresponding diffusion of Cl^- out of the soil. The diffusion of HCO_3^- into the soil and the soil pH affects the availability of carbonate ions for precipitation. The movement of solutes such as Ca^{2+} and OH^- ions to the site of precipitation have been assumed to occur partly by acid-base transfer, mainly H_2CO_3-HCO_3^- derived from dissolved CO_2, as in the model presented in Chapter 4.

Thus there is evidence here that changing the composition of the microbial community within a natural soil had an influence on the diffusion of said solutes and ultimately on the rate and profile of $CaCO_3$ precipitation, as was detected here and confirmed by the statistical analysis. Linear models could be fitted to all pH, Ca^{2+} and Cl^- profiles but four, with the linear models accounting for enough of the variations in the datasets. For the linear models, taking into account the variations in the data due to the differences in moisture content and bulk density between replicates accounted only for 0.4% variation in the datasets more than if they were not considered. Their effect was thus deemed negligible, and the effect of the distance to the soil-resin interface predominant: this allowed to fit one model for the three replicates. The four pH profiles after one day of diffusion were analysed using logistic curves.

In a sterile system, the CO_2 concentration in soil air would not be significantly raised above that of the atmosphere (0.039%), because the additional source of CO_2 from living organisms' respiration would be absent. This would represent a strong limitation on $CaCO_3$ precipitation, and in turn on the buffering of the pH increase caused by the vicinity with the source of alkalinity. Both after 1 and 5 days of contact with resin, the amount of Cl^- having left the soil in exchange

for HCO_3^- is lower than in the other three treatments. The limited quantity of bicarbonate ions from the resin would have reacted with protons in solution and from the soil exchange complex to form H_2O and CO_2, which would be enough to limit the increase in pH through the soil column. The main portion of CO_2 produced by the abiotic reaction would escape the soil column, however at the close vicinity of the resin, some would dissolve in solution and lead to the limited amount of precipitation observed (Figures 5.9 and 5.10 (b)).

Depletion of Ca^{2+} from the soil solution resulted again from an increase in pH-dependent cation exchange sites on the soil solid due to the increase in soil pH (Equation 4.a). The concentration in Cl^- is moderately modified by comparison with the live treatments, indicating a limited exchange of Cl^- for HCO_3^- (Figures 5.7 and 5.8 (b)). The stochiometry of a $CaCl_2$ solution was not preserved in the sterile system, which would indicate that the movement of Ca^{2+} was not parallel to that of Cl^-, and corroborate the fact that a portion of Ca^{2+} gets sorbed onto the soil solid. Other cations would have to balance the electroneutrality of the soil solution.

In a eukaryote-inhibited system, pH through the soil column depth showed more variation around a mean value. The system appeared less homogeneous than the reference or the prokaryote-inhibited soils. The dispersed spatial distribution of bacterial cells in the eukaryote-inhibited treatment may have created pockets of localised microbial activity where higher rates of respiration lead to higher CO_2 concentration in soil air. By comparison, fungal mycelial would be distributed in a different manner, via interconnected networks, leading to different, more homogeneous, patterns of CO_2, ions and nucleation sites distribution, arguably at a larger scale than with bacteria alone.

Fungal hyphae would be expected to ramify throughout the soil cores, but typically also show preferential growth in zones of least resistance, e.g. soil surfaces or planes (Harris et al., 2003; Otten et al., 2004). In the system here, hyphae proliferation might be expected to occur at the soil-resin junction.

This could explain a smaller plateau of pH at the soil-resin interface and smaller slope in the fungal-dominated system by comparison with the other three treatments (Figure 5.5 (d)),

as well as the location of $CaCO_3$ formation (Figure 5.10 (d)). A zone of high fungal activity at the soil-resin interface would indicate high rates of respiratory CO_2 production, which in turn increase acid-base transfers in the soil solution to neutralise HCO_3^- entering the soil. If $CaCO_3$ precipitation can be triggered using microbial surfaces as nucleation points, it would also create a localised availability of suitable nucleation surfaces, which would explain $CaCO_3$ precipitation remaining localised at the direct vicinity of the soil-resin interface (Figure 5.10 (d)).

By comparison, both experimental systems where bacteria would have been present throughout the soil column (reference and eukaryote-inhibited) showed $CaCO_3$ precipitated up to 1 cm deep into the soil profile (Figures 5.10 (a) and (c)), potentially explained by the more widespread distribution of microbial activity.

Such localised pockets of CO_2 would also facilitate the movement of reactants to appropriate nucleation sites by acid-base transfers. As higher concentrations of CO_2 would be present through the soil column, it would make more solutes available for precipitation, and their movement more rapid, in turn potentially explaining the consistently lower profiles for both Ca^{2+} and Cl^- in solution in eukaryote-inhibited systems. The presence of microbial surfaces suitable for nucleation through the soil would also allow for the spread of $CaCO_3$ formation observed.

In the reference system, where soil biota has not been modified, it was assumed that both fungi and bacteria would still be present and functional with fungi growing preferentially at the soil-resin interface and bacteria through its depth. $CaCO_3$ would thus also precipitate over a bigger depth of soil than in a solely fungal system, although not as deep as in a solely bacterial system, the rate of precipitation being potentially higher at the soil-resin interface creating competition for solutes at depth.

The precipitation patterns observed and discussed above in terms of CO_2 concentration and distribution could also corroborate the hypothesis made at the beginning of the study that microbial surfaces act as nucleation sites for crystallisation, thus catalysing the reaction further. Some interactions between fungal hyphae and $CaCO_3$ crystals were observed (Figure 5.16), while

the observation of a eukaryote-inhibited system revealed sheaf-like structures around 3 μm long that could have arisen as a result of bacteria acting as dispersed nucleation sites.

Microbes playing a role as nucleation sites could further explain the difference in crystal morphologies observed between live and sterile soils. Indeed, the presence of diverse nucleation sites in a live system creates high competition for the solutes in solution in supersaturated systems. This leads to a fast initial precipitation in random arrangements such as the florets observed in the fungal soil. Such rapid precipitation could also lead to the formation of less crystalline forms, or even amorphous gels which would quickly lower the supersaturation of the surrounding solution. At a micro-scale level, the solution would then not be supersaturated around the amorphous balls of calcium carbonate formed, which would then slowly re-dissolve to allow for a slower re-precipitation of the amorphous material into crystalline phases to occur. This process would result in the structures observed in the reference system (Figure 5.15). In a sterile system however, less diffusion of the solutes towards the depth of the soil column and the limited amount of nucleation sites leads to a much slower precipitation and thus the formation of the smoother and more regular crystal arrangements observed.

It was expected that the observed crystalline shapes could also be explained by the precipitation of different polymorphs. Triclinic crystals smoothly arranged in the sterile system are typically associated with calcite, while blunt orthorhombic faced crystals chaotically precipitated in florets in the prokaryote-inhibited system would likely be aragonite. However the XRD analysis did not reveal any polymorph other than calcite. The XRD analysis was realised on the same material as the ESEM observations, but the three week interval between the two observations might explain the absence of either aragonite or vaterite, which tend to re-precipitate as calcite, the most stable polymorph at standard temperature and pressure. Were there any amorphous $CaCO_3$ present, further than being unstable and rapidly re-precipitating into calcite, its presence would result in a rise of the baseline rather than sharp peaks in an XRD spectrum, making it hard to isolate from a heterogeneous medium like soil. The observation of the experimental soil on a zero background as part of this study (Figure 5.17) confirmed the rise of the baseline in

the XRD analyses as a diffraction from the aluminium background (Figure 5.18), thus ruling out the presence of amorphous calcium carbonate. However, the presence of amorphous calcium carbonate could potentially be confirmed directly after the observation of structures of interest (Figure 5.15) by combining infrared and Raman spectroscopy of the samples: such techniques have been used in the studies into the stabilisation of amorphous calcium carbonate in living organisms have used a mixture of infrared and Raman spectroscopy to identify the phase of $CaCO_3$ observed (Raz et al., 2002).

5.4.1 Conclusion

The comparison between a microbiologically active system and a sterile soil confirmed that microbial activity does not affect the direction of solute diffusion at the vicinity of a source of alkalinity. This experiment showed that it does however influence the precipitation of calcium carbonate quite substantially. It is then hypothesised further that microbial respiration creates localised zones of high CO_2 pressure in the soil air compared to atmospheric levels. This in turn tends to increase the concentration of CO_3^{2-} in the soil solution, thus increasing the rate of $CaCO_3$ precipitation. This same mechanism was highlighted in Chapter 3 as the potential explanation for the difference in the capacity of two soils with different microbial biomass to buffer an artificial increase in their pH.

The surface of microbial cells providing suitable nucleation sites for the initiation of $CaCO_3$ crystal growth, which could potentially instigate an additional mechanism for the role played by microorganisms was highlighted in this section through the observation of undisturbed samples under ESEM.

The composition of the microbial community was not only found to affect the magnitude but also the spread of the observed changes in the soil environment near a source of alkalinity. This could be due to the difference in growth mechanisms between fungi and bacteria, but

also to the suitability of their surfaces as nucleation sites, and in particular the nature of the compounds each community exudes. Fungi for instance release dissolved organic C compounds in solution, particularly low molecular weight organic anions such as oxalate, that may decrease the concentration of Ca^{2+} available in solution for, or have other inhibitory effects on, precipitation. This complicates the relation between microbial activities and precipitation, and the functioning of associated microorganisms, and would need further study in order to be elucidated.

However, microscopic observations confirmed the occurrence of precipitation at the soil-fungi interface. There was circumstantial evidence for a similar scenario in the case of bacteria in this study, which is corroborated in the literature (Rodriguez-Navarro et al., 2007; Mitchell and Ferris, 2006; Lian et al., 2006). Single-species studies indeed conclude that the presence of bacteria lead to bigger, more numerous and more stable crystals of calcite than precipitated in bacteria-free solutions (Mitchell and Ferris, 2006), and confirmed the presence of two mechanisms by which bacteria influence $CaCO_3$ precipitation: "active" where microbes surfaces act as nucleation sites and "passive" when the metabolism of microbes modify their micro-environment to create conditions favourable to $CaCO_3$ precipitation. Both mechanisms could occur simultaneously.

By comparison with observations of the original samples of soil derived from the field (Figure 5.1), $CaCO_3$ precipitation in the experimental systems was less abundant and no such microfine structures were found. The different amounts of precipitation could simply be due to the time over which it was allowed to occur, but also to the limited amount of reactants in the experimental systems compared to natural field conditions. Indeed, the phenomenon clearly appeared to be sensitive to the microbial community's structure: there could be an even greater range of crystallisation forms than those observed in this study.

Indeed, the fungi manifest in the experimental system here would have been saprophytes. One hypothesis could be that in the soil sampled in the field, the presence of a vegetation cover would potentially lead to a fungal community dominated by mycorrhizal fungi. Such fungi live in symbiosis with an autotrophic organism which would provide it with more substantial sources

of carbon substrate than saprophytes, potentially enhancing their activity and metabolism. This would increase the influence of the fungi on its environment, and potentially fuel the precipitation of $CaCO_3$ on a scale orders of magnitude higher than that observed in this experimental system where mycorrhizae would not be functioning at all. Comparing the precipitates occurring in mycorrhizal- or saprophyte-dominated communities could thus be a start to continue this exploration and check whether the mycelial structure coated in acicular $CaCO_3$ crystals observed in Figure 5.1 would be that of a mycorrhizal fungi.

Chapter 6

Conclusion and Future Work

This study aimed to provide a better quantitative understanding of the precipitation of $CaCO_3$ in soils, and the physicochemical and biological processes involved in $CaCO_3$ formation were investigated. It was hypothesised that, as in aqueous media, increased availability of CO_2 in the soil atmosphere would increase the rate of $CaCO_3$ formation, while the presence of P and DOC in solution would inhibit the precipitation reaction. The existence of a structure in natural soils would further modulate the rate of $CaCO_3$ formation by influencing the rate of delivery of reactants through the soil profile to a crystal nucleation site. Microbial communities in soils were hypothesised to affect both the availability of reactants and inhibitors, and the way diffusion through the soil pore network would impede $CaCO_3$ precipitation. Furthermore, $CaCO_3$ precipitation would occur as a result of metabolic processes at a variety of soil-microbe interfaces.

Accordingly, a model of $CaCO_3$ precipitation in soils was successfully developed based on the properties of soils, and without arbitrary assumptions. The mechanisms of precipitation of $CaCO_3$ are more complicated in soil than in aqueous media. The good agreement between the model and experimental results shows that the model accounts correctly for the important abiotic processes involved in $CaCO_3$ precipitation in soils. Thus, it provides a valid physicochemical framework for further study of $CaCO_3$ formation in soils. While the process of $CaCO_3$ formation obeys the same basic physicochemical principles as precipitation in solution, it was shown that many additional processes interact in natural soils to influence the rate and spread of $CaCO_3$ formation. In particular this study highlighted how the concentration of CO_2 in soil air influences the rate of precipitation.

The simplified system used in this study simulated the production of alkalinity in the rhizosphere by plants and microbes, via a planar source of bicarbonate ions. However, in field conditions the dissolution of respiratory CO_2 into soil solution would occur in the vicinity roots, fungal hyphae and other soil microbes. The source of bicarbonate would thus be more limited than in this study, and the transport limitations different than for a planar source.

In addition to transport-based constraints, the soil biota has been confirmed to play an important role in the formation of $CaCO_3$ in soils. The limited test of the model sensitivity done as part of this study suggests that both the kinetics of the precipitation reaction and the transport of reactants through the soil structure play important roles in determining the rate of $CaCO_3$ precipitation, and the soil microbiology is hypothesised to play an important role in both these processes. Conclusions drawn throughout this study confirmed the importance of soil biota in the precipitation reaction. It was hypothesised that soil microbes would affect the rate of $CaCO_3$ precipitation through respiratory production of CO_2, and by providing physical surfaces as nucleation sites. Lower rates of precipitation were recorded in stored compared to freshly-sampled soil, where microbes would be more abundant and active, corroborating this hypothesis. Also, measurements of $CaCO_3$ precipitated in soil microcosms displayed major differences between a soil freshly sampled that had undergone no microbial manipulation (Reference) and the same soil sterilised by gamma-irradiation: less than 10% of the total amount of precipitation occurring in the live soil was observed in the sterile soil. The microscopic observation of the soils manipulated by biocides and irradiation with an associated reference soil also showed differences in the morphology of $CaCO_3$ crystals formed. Thus the status, and specifically the composition, of the microbial community appears to play a particular role in the phenomenon of calcrete formation. From the observation of Nottinghamshire soil samples, one of the hypotheses at the beginning of this study stipulated that there was a particularly strong association between soil fungi and the formation of $CaCO_3$ crystals, that was confirmed by microscopic observations of experimental systems in the last part of this study. However, the amounts of precipitation observed in the field could not be reproduced in laboratory experiments.

The experimental and modelled observations in this study provide the basis for the hypothesis that increases in CO_2 in the atmosphere may affect calcrete formation in soils. Increases in atmospheric CO_2 are indirectly linked to an increase in CO_2 concentrations in the rhizosphere, since higher atmospheric CO_2 has been shown to generally increase the amount of carbon deposited below ground by plants (Smith et al., 2008; Chapin et al., 2009). It is hypothesised that

such material may increase microbial activity and hence respiration, the concentration of CO_2 in soil air, and hence the rate of inorganic C precipitation in soils, particularly in localised zones within the soil. Also, an increase in CO_2 would increase the diffusion of solutes by acid-base transfers. The presence of a vegetation cover could thus partially explain the higher amounts of $CaCO_3$ precipitated in natural conditions and observed in the soils sampled from both Pegwell Bay, Kent and Nottinghamshire at the beginning of this study.

This hypothesis could be tested experimentally by growing plants in ambient and elevated atmospheric concentrations of CO_2, and measuring $CaCO_3$ formation, in the context of manipulated microbial communities.

Additionally to the production of CO_2, microbes are known to act as potential nucleation sites for $CaCO_3$ crystal formation, thus lowering the energy demanding initial step of $CaCO_3$ precipitation. The microfine structures of $CaCO_3$ deposits typically found in UK soils (Figure 5.1) suggests that fungal mycelia play a crucial role in $CaCO_3$ crystal growth in natural conditions. However, precipitation was also important in experimental systems dominated by bacteria. The different morphologies of crystals observed in the experiments could thus be explained by the differences in growth and propagation mechanisms between different microbial communities found in soils. Fungal hyphae would be expected to ramify through the soil, but will grow preferentially in zones of least resistance. In contrast, in a system dominated by bacteria, localised pockets of high activity would be expected to form through the soil profile, modulated by soil structure. This would have as consequences: (i) that respiration patterns, and thus spatial distribution of CO_2 differed between systems, (ii) that the availability of reaction surfaces for heterogeneous nucleation differed between microcosms.

Further to the differences in $CaCO_3$ precipitation patterns in soils resulting from community-scale manipulation of the microbiology, it could be that some bacterial or fungal species have varying effects on the precipitation reaction in certain soils. Thus, the abundance of microfine structures sampled in the field could be due to different types of fungi catalysing the reaction than those observed in this experimental system. Indeed, in the presence of vegetation, myc-

orrhizal fungi would be present. Since these fungi associate with autotrophic plants, they will acquire substantially greater quantities of C-substrate than many soil heterotrophs, resulting in much greater relative activity. In the experimental system considered in this study, the only type of fungi present would have been saprophytes, and hence likely to have been respiring relatively slowly compared to mycorrhizae. This hypothesis could be readily tested experimentally by measuring calcrete formation in soils supporting plants in mycorrhizal and non-mycorrhizal states.

Additionally, in the process of $CaCO_3$ precipitation, microbes would also have to be considered as sources of substances potentially inhibiting the precipitation reaction. The diversity and nature of soil microbial populations would thus need further investigation to complete the physicochemical framework of the model.

Whilst the potential role of the soil biota in calcrete formation is clear from this study, there are also likely to be substantial consequences to organisms which become encased in $CaCO_3$ via the reactions demonstrated. However, it is not always obvious why calcification should be beneficial to soil biota; in some cases, it may impair vital functions. A beneficial outcome to the organism actually seems rather unlikely for calcified bacteria and fungal hyphae, and the consequences of a $CaCO_3$ encasement on microbial activity needs further consideration and clarification. Likewise, it has been suggested that the intensive calcification in soils would have consequences for soil structure and porosity. Because it would fill soil pores, microbially-induced $CaCO_3$ precipitation would strengthen the soil fabric, and has thus been investigated both in laboratory experiments and *in situ* to stabilise sand and control its resilience to shear stress (DeJong et al., 2006; Van der Ruyt and van der Zon, 2009). This would have applications to strengthen construction foundations or control soil erosion in areas of the planet prone to earthquakes or extreme weather events, as well as to reinforce near-shore areas. However, it would change the water infiltration capacity of soils and may have potential negative outcomes in relation to flood prevention.

Surface mineral carbonation is one of the three techniques of Carbon Capture and Storage (CCS) considered by scientists of the Royal Society in the report on "Geoengineering the climate" (2009); however, the eventual use of $CaCO_3$ formation as a geoengineering technique would require further investigation into the potential environmental consequences of triggering widespread precipitation. Renforth et al. (2009) confirmed the suitability of construction and brownfield sites for intensive $CaCO_3$ precipitation, which would limit negative consequences on arable land and flood plains. However, while it has been established that pedogenic carbonates are durable in soils, further work is necessary to establish the stability of such artificially-induced secondary $CaCO_3$ structures.

Bibliography

V. Achal, A. Mukherjee, P. C. Basu, and M. S. Reddy. Strain improvement of *Sporosarcina pasteurii* for enhanced urease and calcite production. *Journal of Industrial Microbiology and Biotechnology*, 36(7):981–988, 2009.

L. Addadi, S. Raz, and S. Weiner. Taking advantage of disorder: Amorphous calcium carbonate and its roles in biomineralization. *Advanced Materials*, 15(12):959–970, 2003.

J. Aizenberg, G. Lambert, L. Addadi, and S. Weiner. Stabilization of amorphous calcium carbonate by specialized macromolecules in biological and synthetic precipitates. *Advanced Materials*, 8(3):222, 1996.

J. Aizenberg, D. A. Muller, J. L. Grazul, and D. R. Hamann. Direct fabrication of large micropatterned single crystals. *Science*, 299(5610):1205–1208, 2003.

A.M. Alonso-Zarza, M.E. Sanz, and J.P. Calvo. Calcified root cells in Miocene pedogenic carbonates of the Madrid Basin. Evidence for the origin of Microcodium b. *Sedimentary Geology*, 116(1-2):81–97, 1998.

L. Ammann, F. Bergaya, and G. Lagaly. Determination of the cation exchange capacity of clays with copper complexes revisited. *Clay Minerals*, 40(4):441–453, 2005.

C. Amrhein and D. L. Suarez. Calcite supersaturation in soils as a result of organic matter mineralization. *Soil Science Society of America Journal*, 51(4):932–937, 1987.

F. Anter, M. H. Hilal, and A. H. El Damaty. A chemical and biological approach towards the definition of calcareous soils - II. Plant growth, P32 and Fe uptake as affected by percentage of calcium carbonate fraction. *Plant and Soil*, 39(3):479–486, 1973.

P. W. Atkins. *Physical chemistry*. Oxford University Press, 6th edition, 1998.

K. L. Bachmeier, A. E. Williams, J. R. Warmington, and S. S. Bang. Urease activity in microbiologically-induced calcite precipitation. *Journal of Biotechnology*, 93(2):171–181, 2002.

S. Bachu. Carbon dioxide storage in geological media: Role, means, status and barriers to deployment. *Progress in Energy and Combustion Science*, 34(2):254–273, 2008.

B. Bajnoczi and V. Kovacs-Kis. Origin of pedogenic needle-fiber calcite revealed by micromorphology and stable isotope composition - A case study of a Quaternary paleosol from Hungary. *Chemie der Erde-Geochemistry*, 66(3):203–212, 2006.

J. F. Banfield and R. J. Hamers. *Processes at minerals surfaces with relevance to microorganisms and prebiotic synthesis*, volume Geomicrobiology: interactions between microbes and minerals, vol. 35, chapter 25, pages 81–122. Mineralogical Society of America, 1997.

J. BeczeDeak, R. Langohr, and E. P. Verrecchia. Small scale secondary $CaCO_3$ accumulations in selected sections of the European loess belt. Morphological forms and potential for paleoenvironmental reconstruction. *Geoderma*, 76(3-4):221–252, 1997.

P.H. Bellamy, P.J. Loveland, R.I. Bradley, R.M. Lark, and G.J.D. Kirk. Carbon losses from all soils across England and Wales 1978-2003. *Nature*, 437(7056):245–248, 2005.

F. Bergaya and M. Vayer. CEC of clays: Measurement by adsorption of a copper ethylenediamine complex. *Applied Clay Science*, 12(3):275–280, 1997.

D. Beruto and M. Giordani. Calcite and aragonite formation from aqueous calcium hydrogencarbonate solutions - Effect of induced electromagnetic field on the activity of $CaCO_3$ nuclei precursors. *Journal of the Chemical Society-Faraday Transactions*, 89(14):2457–2461, 1993.

P. W. Birkeland. *Pedology, Weathering, and Geomorphological research.* Oxford University Press, New York, 1974.

L. Brecevic and D. Kralj. On calcium carbonates: from fundamental research to application. *Croatica Chemica Acta*, 80(3-4):467–484, 2007.

L. Brecevic and A.E. Nielsen. Solubility of amorphous calcium carbonate. *Journal of Crystal Growth*, 98(3):504–510, 1989.

A. Bruand and O. Duval. Calcified fungal filaments in the petrocalcic horizon of Eutrochrepts in Beauce, France. *Soil Science Society of America Journal*, 63(1):164–169, 1999.

C. Buczynski and H. S. Chafetz. Habit of bacterially induced precipitates of calcium carbonate and the influence of medium viscosity on mineralogy. *Journal of Sedimentary Petrology*, 61 (2):226–233, 1991.

E. P. Burford, S. Hillier, and G. M. Gadd. Biomineralization of fungal hyphae with calcite ($CaCO_3$) and calcium oxalate mono- and dihydrate in carboniferous limestone microcosms. *Geomicrobiology Journal*, 23(8):599–611, 2006.

G. Cailleau, O. Braissant, C. Dupraz, M. Aragno, and E. P. Verrecchia. Biologically induced accumulations of $CaCO_3$ in orthox soils of Biga, Ivory Coast. *Catena*, 59(1):1–17, 2005.

M.G. Canti and T.G. Piearce. Morphology and dynamics of calcium carbonate granules produced by different earthworm species. *Pedobiologia*, 47:511–521, 2003.

D. Carpenter, M. E. Hodson, P. Eggleton, and C. Kirk. Earthworm induced mineral weathering: Preliminary results. *European Journal of Soil Biology*, 43(48):S176–S183, 2007.

T. E. Cerling. The stable isotopic composition of modern soil carbonate and its relationship to climate. *Earth and Planetary Science Letters*, 71(2):229–240, 1984.

F.S. Chapin, J. McFarland, A.D. McGuire, E.S. Euskirchen, R.W. Ruess, and K. Kielland.

The changing global carbon cycle: linking plant-soil carbon dynamics to global consequences. *Journal of Ecology*, 97(5):840–850, 2009.

M. L. Clarke, A. E. Milodowski, J. E. Bouch, M. J. Leng, and K. J. Northmore. New OSL dating of UK loess: indications of two phases of Lateglacial dust accretion in SE England and climate implications. *Journal of Quaternary Science*, 21(6645):1–11, 2006.

A. R. Conklin. *Introduction to soil chemistry. Analysis and Instrumentation.* John Wiley & sons, Inc., 2005.

R. Corstanje, G. J. D. Kirk, M. Pawlett, R. Read, and R. M. Lark. Spatial variation of ammonia volatilization from soil and its scale-dependent correlation with soil properties. *European Journal of Soil Science*, 59(6):1260–1270, 2008.

M. D. Cramer and H. J. Hawkins. A physiological mechanism for the formation of root casts. *Palaeogeography Palaeoclimatology Palaeoecology*, 274(3-4):125–133, 2009.

N. H. de Leeuw and T. G. Cooper. A computer modeling study of the inhibiting effect of organic adsorbates on calcite crystal growth. *Crystal Growth and Design*, 4(1):123–133, 2004.

J. T. DeJong, M. B. Fritzges, and K. Nusslein. Microbially induced cementation to control sand response to undrained shear. *Journal of Geotechnical and Geoenvironmental Engineering*, 132 (11):1381–1392, 2006.

R. Dohrmann. Cation exchange capacity methodology II: A modified silver-thiourea method. *Applied Clay Science*, 34(1-4):38–46, 2006a.

R. Dohrmann. Cation exchange capacity methodology III: Correct exchangeable calcium determination of calcareous clays using a new silver-thiourea method. *Applied Clay Science*, 34 (1-4):47–57, 2006b.

R. Dohrmann. Cation exchange capacity methodology I: An efficient model for the detection of

incorrect cation exchange capacity and exchangeable cation results. *Applied Clay Science*, 34 (1-4):31–37, 2006c.

S. Dupraz, M. Parmentier, B. Menez, and F. Guyot. Experimental and numerical modeling of bacterially induced pH increase and calcite precipitation in saline aquifers. *Chemical Geology*, 265(1-2):44–53, 2009.

B. Dupre, C. Dessert, P. Oliva, Y. Godderis, J. Viers, L. Francois, R. Millot, and J. Gaillardet. Rivers, chemical weathering and Earth's climate. *Comptes Rendus Geoscience*, 335(16):1141–1160, 2003.

H.L. Ehrlich. Geomicrobiology: its significance for geology. *Earth-Science Reviews*, 45(1-2): 45–60, 1998.

V. Ettler, O. Zelena, M. Mihaljevic, O. Sebek, and L. Strnad. Removal of trace elements from landfill leachate by calcite precipitation. *Journal of Geochemical Exploration*, 88(1-3):28–31, 2006.

E. Flugel. *Microfacies of carbonate rocks. Analysis, interpretation and application.* Springer, 2009.

P. Freytet, J.C. Plaziat, and E.P. Verrecchia. A classification of rhizogenic calcretes, with examples from the upper Jurassic lower Cretaceous of Spain and upper Cretaceous of southern France - Discussion. *Sedimentary Geology*, 110(3-4):299–303, 1997.

Y. Fujita, E. G. Ferris, R. D. Lawson, F. S. Colwell, and R. W. Smith. Calcium carbonate precipitation by ureolytic subsurface bacteria. *Geomicrobiology Journal*, 17(4):305–318, 2000.

G.M. Gadd. Geomycology. Biogeochemical transformations of rocks, minerals, metals and radionuclides by fungi, bioweathering and bioremediation. *Mycological Research*, 111(1-2):3–49, 2007.

A. S. Goudie. Organic agency in calcrete development. *Journal of Arid Environments*, 32(2): 103–110, 1996.

F. Hammes and W. Verstraete. Key roles of pH and calcium metabolism in microbial carbonate precipitation. *Reviews in Environmental Science and Biotechnology*, 1(6645):3–7, 2002.

T. Y. J. Han and J. Aizenberg. Calcium carbonate storage in amorphous form and its template-induced crystallization. *Chemistry of Materials*, 20(3):1064–1068, 2008.

K. Harris, I.M. Young, C.A. Gilligan, W. Otten, and K. Ritz. Effect of bulk density on the spatial organisation of the fungus *Rhizoctonia solani* in soil. *Microbiology Ecology*, 44:45–56, 2003.

P.G. Hartel and M. Alexander. Decline of cowpea rhizobia in acid soils after gamma-irradiation. *Soil Biology and Biochemistry*, 15(4):489–490, 1983.

J. Hartmann and S. Kempe. What is the maximum potential for carbon dioxide sequestration by stimulated weathering on the global scale? *Naturwissenschaften*, 95:1159–1164, 2008.

J. J. Hassett, D. W. Gregg, and J. B. Fehrenbacher. Formation of calcium carbonate concretions in natric horizons of Illinois soils. *Soil Science*, 122(4):202–205, 1976.

Y.-M. Huang. *The effect of precipitation of calcium carbonate on soil pH following urea application.* PhD thesis, University of Oxford, 1990.

W. P. Inskeep and P. R. Bloom. Calcium carbonate supersaturation in soil solutions of Calciaquolls. *Soil Science Society of America Journal*, 50(6):1431–1437, 1986a.

W. P. Inskeep and P. R. Bloom. Kinetics of calcite precipitation in the presence of water-soluble organic ligands. *Soil Science Society of America Journal*, 50(5):1167–1172, 1986b.

B. Jaillard, A. Guyon, and A. F. Maurin. Structure and composition of calcified roots, and their identification in calcareous soils. *Geoderma*, 50(3):197–210, 1991.

N. J. Karberg, K. S. Pregitzer, J. S. King, A. L. Friend, and J. R. Wood. Soil CO_2 partial pressure and dissolved inorganic carbonate chemistry under elevated CO_2 and ozone. *Oecologia*, 142 (2):296–306, 2005.

R. A. Kemp, E. Derbyshire, F. H. Chen, and H. Z. Ma. Pedosedimentary development and palaeoenvironmental significance of the S1 palaeosol on the northeastern margin of the Qinghai-Xizang (Tibetan) Plateau. *Journal of Quaternary Science*, 11(2):95–106, 1996.

R.A. Kemp. Distribution and genesis of calcitic pedofeatures within a rapidly aggrading Loess-paleosol sequence in China. *Geoderma*, 65(3-4):303–316, 1995.

A.S. Khadkikar, L.S. Chamyal, and R. Ramesh. The character and genesis of calcrete in Late Quaternary alluvial deposits, Gujarat, western India, and its bearing on the interpretation of ancient climates. *Palaeogeography Palaeoclimatology Palaeoecology*, 162(3-4):239–261, 2000.

D. E. Kile, D. D. Eberl, A. R. Hoch, and M. M. Reddy. An assessment of calcite crystal growth mechanisms based on crystal size distributions. *Geochimica et Cosmochimica Acta*, 64(17): 2937–2950, 2000.

N. Koga, Y. Z. Nakagoe, and H. Tanaka. Crystallization of amorphous calcium carbonate. *Thermochimica Acta*, 318(1-2):239–244, 1998.

K. Kusa, T. Sawamoto, R. Hu, and R. Hatano. Comparison of N_2O and CO_2 concentrations and fluxes in the soil profile between a Gray Lowland soil and an Andosol. *Soil Science and Plant Nutrition*, 56(1):186–199, 2010.

R. Lal. Global potential of soil carbon sequestration to mitigate the greenhouse effect. *Critical Reviews in Plant Sciences*, 22(2):151–184, 2003.

I. Lebron and D. L. Suarez. Calcite nucleation and precipitation kinetics as affected by dissolved organic matter at 25°C and pH>7.5. *Geochimica et Cosmochimica Acta*, 60(15):2765–2776, 1996.

I. Lebron and D. L. Suarez. Kinetics and mechanisms of precipitation of calcite as affected by P_{CO_2} and organic ligands at 25℃. *Geochimica et Cosmochimica Acta*, 62(3):405–416, 1998.

H.S. Lee, T.H. Ha, and K. Kim. Fabrication of unusually stable amorphous calcium carbonate in an ethanol medium. *Materials Chemistry and Physics*, 93(2-3):376–382, 2005.

M. R. Lee, M. E. Hodson, and G. Langworthy. Earthworms produce granules of intricately zoned calcite. *Geology*, 36(12):943–946, 2008.

N. N. Levina, R. R. Lew, G. J. Hyde, and I. B. Heath. The roles of calcium and plasma membrane ion channels in hyphal tip growth of *Neurospora crassa*. *Journal of Cell Science*, 108(6645): 3405–3417, 1995.

W. Li, P.P. Zhou, L.P. Jia, L.J. Yu, X. Li, and M. Zhu. Limestone dissolution induced by fungal mycelia, acidic materials, and carbonic anhydrase from fungi. *Mycopathologia*, 167(1):37–46, 2009.

B. Lian, Q. N. Hu, J. Chen, J. F. Ji, and H. H. Teng. Carbonate biomineralization induced by soil bacterium *Bacillus megaterium*. *Geochimica et Cosmochimica Acta*, 70(22):5522–5535, 2006.

Y. P. Lin and P. C. Singer. Inhibition of calcite crystal growth by polyphosphates. *Water Research*, 39(19):4835–4843, 2005a.

Y. P. Lin and P. C. Singer. Effects of seed material and solution composition on calcite precipitation. *Geochimica et Cosmochimica Acta*, 69(18):4495–4504, 2005b.

Y. P. Lin, P. C. Singer, and G. R. Aiken. Inhibition of calcite precipitation by natural organic material: Kinetics, mechanism, and thermodynamics. *Environmental Science & Technology*, 39(17):6420–6428, 2005.

Y.P. Lin and P.C. Singer. Inhibition of calcite precipitation by orthophosphate: Speciation and thermodynamic considerations. *Geochimica et Cosmochimica Acta*, 70(10):2530–2539, 2006.

M. G. Lioliou, C. A. Paraskeva, P. G. Koutsoukos, and A. C. Payatakes. Heterogeneous nucleation and growth of calcium carbonate on calcite and quartz. *Journal of Colloid and Interface Science*, 308(2):421–428, 2007.

A. Luttge and P. G. Conrad. Direct observation of microbial inhibition of calcite dissolution. *Applied and Environmental Microbiology*, 70(3):1627–1632, 2004.

D. A. C. Manning. Calcite precipitation in landfills: an essential product of waste stabilization. *Mineralogical Magazine*, 65(5):603–610, 2001.

D.A.C. Manning. Biological enhancement of soil carbonate precipitation. Passive removal of atmospheric carbon dioxide. *Mineralogical Magazine*, 72:639–649, 2008.

F. Manoli, S. Koutsopoulos, and E. Dalas. Crystallization of calcite on chitin. *Journal of Crystal Growth*, 182(1-2):116–124, 1997.

F. Manoli, J. Kanakis, P. Malkaj, and E. Dalas. The effect of aminoacids on the crystal growth of calcium carbonate. *Journal of Crystal Growth*, 236(1-3):363–370, 2002.

S. Masaphy, L. Zabari, J. Pastrana, and S. Dultz. Role of fungal mycelium in the formation of carbonate concretions in growing media. An investigation by SEM and Synchrotron-based X-ray tomographic microscopy. *Geomicrobiology Journal*, 26(7):442–450, 2009.

M. B. McBride. *Environmental chemistry of soils*. Oxford University Press, 1994.

T.A. McConnaughey and J.F. Whelan. Calcification generates protons for nutrient and bicarbonate uptake. *Earth-Science Reviews*, 42(1-2):95–117, 1997.

S. B. McLaughlin and R. Wimmer. Tansley Review No. 104 - Calcium physiology and terrestrial ecosystem processes. *New Phytologist*, 142(3):373–417, 1999.

N.P. McNamara, H.I.J. Black, N.A. Beresford, and N.R. Parekh. Effects of acute gamma irradiation on chemical, physical and biological properties of soils. *Applied Soil Ecology*, 24(2): 117–132, 2003.

A. J. Miller, G. Vogg, and D. Sanders. Cytosolic calcium homeostasis in fungi - Roles of plasma membrane transport and intracellular sequestration of calcium. *Proceedings of the National Academy of Sciences of the United States of America*, 87(23):9348–9352, 1990.

N. D. Misopolinos and J. M. Kalovoulos. Determination of CEC and exchangeable Ca and Mg in non-saline calcareous soils. *Journal of Soil Science*, 35(1):93–98, 1984.

A. C. Mitchell and F. G. Ferris. The influence of *Bacillus pasteurii* on the nucleation and growth of calcium carbonate. *Geomicrobiology Journal*, 23:213–226, 2006.

A. Miyawaki, J. Llopis, R. Heim, J. M. McCaffery, J. A. Adams, M. Ikura, and R. Y. Tsien. Fluorescent indicators for calcium based on green fluorescent proteins and calmodulin. *Nature*, 388(6645):882–887, 1997.

G. Nelson, O. Kozlova-Zwinderman, A. J. Collis, M. R. Knight, J. R. S. Fincham, C. P. Stanger, A. Renwick, J. G. M. Hessing, P. J. Punt, C. A. M. J. van den Hondel, and N. D. Read. Calcium measurement in living filamentous fungi expressing codon-optimized aequorin. *Molecular Microbiology*, 5(23):1437–1450, 2004.

P.H. Nye. Measurement and mechanism of ion diffusion in soils .VII. Theory for propagation of changes of pH in soils. *Journal of Soil Science*, 23(1):82–92, 1972.

P.H. Nye. Diffusion of ions and uncharged solutes in soils and soil clays. *Advances in Agronomy*, 31:225–272, 1979.

P.H. Nye and A. Ameloko. A comparison of measured and theoretical soil acidity diffusion coefficients over a wide range of pH. *Journal of Soil Science*, 37(2):191–196, 1986.

P.H. Nye and M. Ramzan. Measurement and mechanism of ion diffusion in soil. X. Prediction of soil acidity gradients in acid-base transfers. *Journal of Soil Science*, 30(1):43–51, 1979.

W. Otten, K. Harris, I.M. Young, K. Ritz, and C.A. Gilligan. Preferential spread of the

pathogenic fungus *Rhizoctonia solani* through structured soil. *Soil Biology and Biochemistry*, 36(2):203–210, 2004.

S. E. Phillips and P. G. Self. Morphology, crystallography and origin of needle-fiber calcite in Quaternary pedogenic calcretes of South Australia. *Australian Journal of Soil Research*, 25 (4):429–444, 1987.

A. Pinner and P.H. Nye. A pulse method for studying effects of dead-end pores, slow equilibration and soil structure on diffusion of solutes in soil. *Journal of Soil Science*, 33(1):25–35, 1982.

S. G. Pritchard and J. S. Amthor. *Crops and environmental change*. Haworth Press, 2005.

M. Ptashnyk, T. Roose, and G.J.D. Kirk. Diffusion of strongly-sorbed solutes in soil - a dual porosity model allowing for slow access to sorption sites and time-dependent sorption reactions. *European Journal of Soil Science*, 61:108–119, 2010.

K. Pustovoytov and B. Terhorst. An isotopic study of a late Quaternary loess-paleosol sequence in SW Germany. *Revista Mexicana de Ciencas Geologicas*, 21(1):88–93, 2004.

M. Ramzan and P.H. Nye. Measurement and mechanism of ion diffusion in soils - IX Changes in soil acidity near a source of bicarbonate ions. *Journal of Soil Science*, 29(2):184–194, 1978.

D. Rautaray, A. Ahmad, and M. Sastry. Biosynthesis of $CaCO_3$ crystals of complex morphology using a fungus and an actinomycete. *Journal of the American Chemical Society*, 125(48): 14656–14657, 2003.

S. Raz, O. Testeniere, A. Hecker, S. Weiner, and G. Luquet. Stable amorphous calcium carbonate is the main component of the calcium storage structures of the crustacean Orchestia cavimana. *Biological Bulletin*, 203(3):269–274, 2002.

F. Reith, S. A. Wakelin, A. L. Gregg, and A. S. Mumm. A microbial pathway for the formation of gold-anomalous calcrete. *Chemical Geology*, 258(3-4):315–326, 2009.

P. Renforth, D. A. C. Manning, and E. Lopez-Capel. Carbonate precipitation in artificial soils as a sink for atmospheric carbon dioxide. *Applied Geochemistry*, 24(9):1757–1764, 2009.

K. Ritz. Fungi. (unpublished), 2004.

K. Ritz and I.M. Young. Interactions between soil structure and fungi. *Mycologist*, 18(2):52–59, 2004.

M. A. Rivadeneyra, A. Martin-Algarra, A. Sanchez-Navas, and D. Martin-Ramos. Carbonate and phosphate precipitation by *Chromohalobacter marismortui*. *Geomicrobiology Journal*, 23 (2):89–101, 2006.

C. Rodriguez-Navarro, C. Jimenez-Lopez, A. Rodriguez-Navarro, M. T. Gonzalez-Munoz, and M. Rodriguez-Gallego. Bacterially mediated mineralization of vaterite. *Geochimica et Cosmochimica Acta*, 71(5):1197–1213, 2007.

M. Rogerson, H. M. Pedley, J. D. Wadhawan, and R. Middleton. New insights into biological influence on the geochemistry of freshwater carbonate deposits. *Geochimica et Cosmochimica Acta*, 72(20):4976–4987, 2008.

J. Rousk, L.A. Demoling, and E. Baath. Contrasting short-term antibiotic effects on respiration and bacterial growth compromises the validity of the selective respiratory inhibition technique to distinguish fungi and bacteria. *Microbial Ecology*, 58(1):75–85, 2009.

J. Rousk, L. A. Demoling, A. Bahr, and E. Baath. Examining the fungal and bacterial niche overlap using selective inhibitors in soil. 2010.

Royal Society. The role of land carbon in mitigating global climate change. Technical report, Royal Society, London, 2001.

Royal Society. Geoengineering the climate. Science, governance and uncertainty. Technical report, Royal Society, London, 2009.

S. Sanchez-Moral, J. C. Canaveras, L. Laiz, C. Saiz-Jimenez, J. Bedoya, and L. Luque. Biomediated precipitation of calcium carbonate metastable phases in hypogean environments: A short review. *Geomicrobiology Journal*, 20(5):491–500, 2003.

K. Sawada. The mechanisms of crystallization and transformation of calcium carbonates. *Pure and Applied Chemistry*, 69(5):921–928, 97.

K. E. Schmittner and P. Giresse. Micro-environmental controls on biomineralization: superficial processes of apatite and calcite precipitation in Quaternary soils, Roussillon, France. *Sedimentology*, 46(3):463–476, 1999.

R. D. Schuiling and P. Krijgsman. Enhanced weathering. An effective and cheap tool to sequester carbon dioxide. *Climate Change*, 74:349–354, 2006.

P. Smith, C.M. Fang, J.J.C. Dawson, and J.B. Moncrieff. Impact of global warming on soil organic carbon. *Advances in Agronomy*, 97:1–43, 2008.

I. Sondi and B. Salopek-Sondi. Influence of the primary structure of enzymes on the formation of $CaCO_3$ polymorphs: A comparison of plant (*Canavalia ensiformis*) and bacterial (*Bacillus pasteurii*) ureases. *Langmuir*, 21(19):8876–8882, 2005.

S. Stocks-Fischer, J. K. Galinat, and S. S. Bang. Microbiological precipitation of calcium carbonate. *Soil Biology and Biochemistry*, 31(11):1563–1571, 1999.

G. E. Strong, J. R. A. Giles, and V. P. Wright. A Holocene calcrete from North Yorkshire, England - Implications for interpreting paleoclimates using calcretes. *Sedimentology*, 39(2): 333–347, 1992.

W. Stumm and J.J. Morgan. *Aquatic Chemistry. Chemical Equilibria and Rates in Natural Waters.* John Wiley & Sons, Inc., 3 edition, 1996.

K. H. Tan. *Gas phase in soils*, volume Environmental soil science, chapter 4. CRC Press, 2 edition, 2000.

A. Tang and O.C. Sandall. Diffusion coefficient of chlorine in water at 25-60℃. *Journal of chemical and engineering data*, 30(2):189–191, 1985. ISSN 0021-9568.

P. B. Tinker and P. H. Nye. *Solute movement in the rhizosphere*. Oxford University Press, 2000.

B. M. Tucker. The determination of exchangeable calcium and magnesium in carbonate soils. *Australian Journal of Soil Research*, 5(4):706–715, 1954.

M. Van der Ruyt and W. van der Zon. Biological *in situ* reinforcement of sand in near-shore areas. *Proceedings of the Institution of Civil Engineers-Geotechnical Engineering*, 162(1):81–83, 2009.

H. Velvis. Evaluation of the selective respiratory inhibition method for measuring the ratio of fungal:bacterial activity in acid agricultural soils. *Biology and Fertility of Soils*, 25(4):354–360, 1997.

E. P. Verrecchia and J. L. Dumont. A biogeochemical model for chalk alteration by fungi in semiarid environments. *Biogeochemistry*, 35(3):447–470, 1996.

E. P. Verrecchia and K. E. Verrechia. Needle-fiber calcite - A critical review and a proposed classification. *Journal of Sedimentary Research Section A-Sedimentary Petrology and Processes*, 64(3):650–664, 1994.

E. P. Verrecchia, C. Loisy, O. Braissant, and A. A. Gorbushina. *The role of fungal biofilm and networks in the terrestrial calcium carbonate cycle*, volume Fossils and recent biofilms - A natural history of life on Earth, chapter 25, pages 363–369. Kluwer Academic Publisher, 2003.

F. Visconti, J. M. de Paz, and J. L. Rubio. Principal component analysis of chemical properties of soil saturation extracts from an irrigated Mediterranean area: Implications for calcite equilibrium in soil solutions. *Geoderma*, 151(3-4):407–416, 2009.

F. Visconti, J.M. DePaz, and J.L. Rubio. Calcite and gypsum solubility products in water-

saturated salt-affected soil samples at 25°C and at least up to 14 dS m^{-1}. *European Journal of Soil Science*, 61:255–270, April 2010.

W. B. Wang, Y. D. Liu, D. H. Li, C. X. Hu, and B. Q. Rao. Feasibility of cyanobacterial inoculation for biological soil crusts formation in desert area. *Soil Biology and Biochemistry*, 41(5):926–929, 2009.

L. A. Warren, P. A. Maurice, N. Parmar, and F. G. Ferris. Microbially mediated calcium carbonate precipitation: Implications for interpreting calcite precipitation and for solid-phase capture of inorganic contaminants. *Geomicrobiology Journal*, 18(1):93–115, 2001.

K. Westin and A. C. Rasmuson. Crystal growth of aragonite and calcite in presence of citric acid, DTPA, EDTA and pyromellitic acid. *Journal of Colloid and Interface Science*, 282(2): 359–369, 2005.

V. S. Whiffin, L. A. van Paassen, and M. P. Harkes. Microbial carbonate precipitation as a soil improvement technique. *Geomicrobiology Journal*, 24(5):417–423, 2007.

A. Whitmore, G.J.D. Kirk, and B. Rawlins. Carbon storage in soils. In London DEFRA, editor, *Final Report of DEFRA Project SP1605. Studies in support of the Soil Strategy*, 2010.

V. P. Wright. The role of fungal biomineralization in the formation of early Carboniferous soil fabrics. *Sedimentology*, 33(6):831–838, 1986.

A. G. Xyla, E. K. Giannimaras, and P. G. Koutsoukos. The precipitation of calcium carbonate in aqueous solutions. *Colloids and Surfaces*, 53:241–255, 1991.

D. H. Yaalon. Problems of soil testing on calcareous soils. *Plant and Soil*, 8(3):275–288, 1957.

K. K. Yates and L. L. Robbins. Radioisotope tracer studies of inorganic carbon and Ca in microbially derived $CaCO_3$. *Geochimica et Cosmochimica Acta*, 63(1):129–136, 1999.

I. M. Young and K. Ritz. *The habitat of soil microbes*, volume Biological Diversity and Function in soils, pages 31–43. Cambridge University Press, 2005.

M. Zavarin and H. E. Doner. Effect of P and Se(IV) on calcite precipitation inhibition. *Soil Science*, 170(8):612–623, 2005.

B. B. Zhou, M. A. Shao, and H. B. Shao. Effects of rock fragments on water movement and solute transport in a Loess plateau soil. *Comptes Rendus Geoscience*, 341(6):462–472, 2009.

Appendix A

Model and Speciation FORTRAN transcripts

Appendix B

Experimental Data

B.1 Influence of P and DOC as inhibitors of $CaCO_3$ precipitation in the absence of transport limitations

The following graphs B1 to B6 are referred to in Chapter 3.

B.2 Mass flow transfers between anion exchange resin and soil

In the investigation of reactants diffusion from a source of alkalinity through the soil structure in a $CaCO_3$ precipitation zone, the experimental system had to ensure that there was no mass flow of water between soil and resin. The moisture content of the experimental soils were chosen to facilitate handling, and the moisture content of the anion exchange resin adjusted so that its water potential matched that of the soil.

Experimental systems were prepared following the same protocol detailed in Chapter 4. Resins were adjusted at three ranging moisture contents on sand tables, and the movement of water checked by measuring the moisture content of soil slices after five days of contact between soil and resin.

For both soils, at the two lower resin moisture contents, there was a slight decrease in soil moisture content at the soil-resin interface, which would indicate that there was movement of water from the soil to the resin (Figure B.7). Both soils were thus put in contact with a layer of anion-exchange resin saturated with water in the final experimental system (Chapter 4).

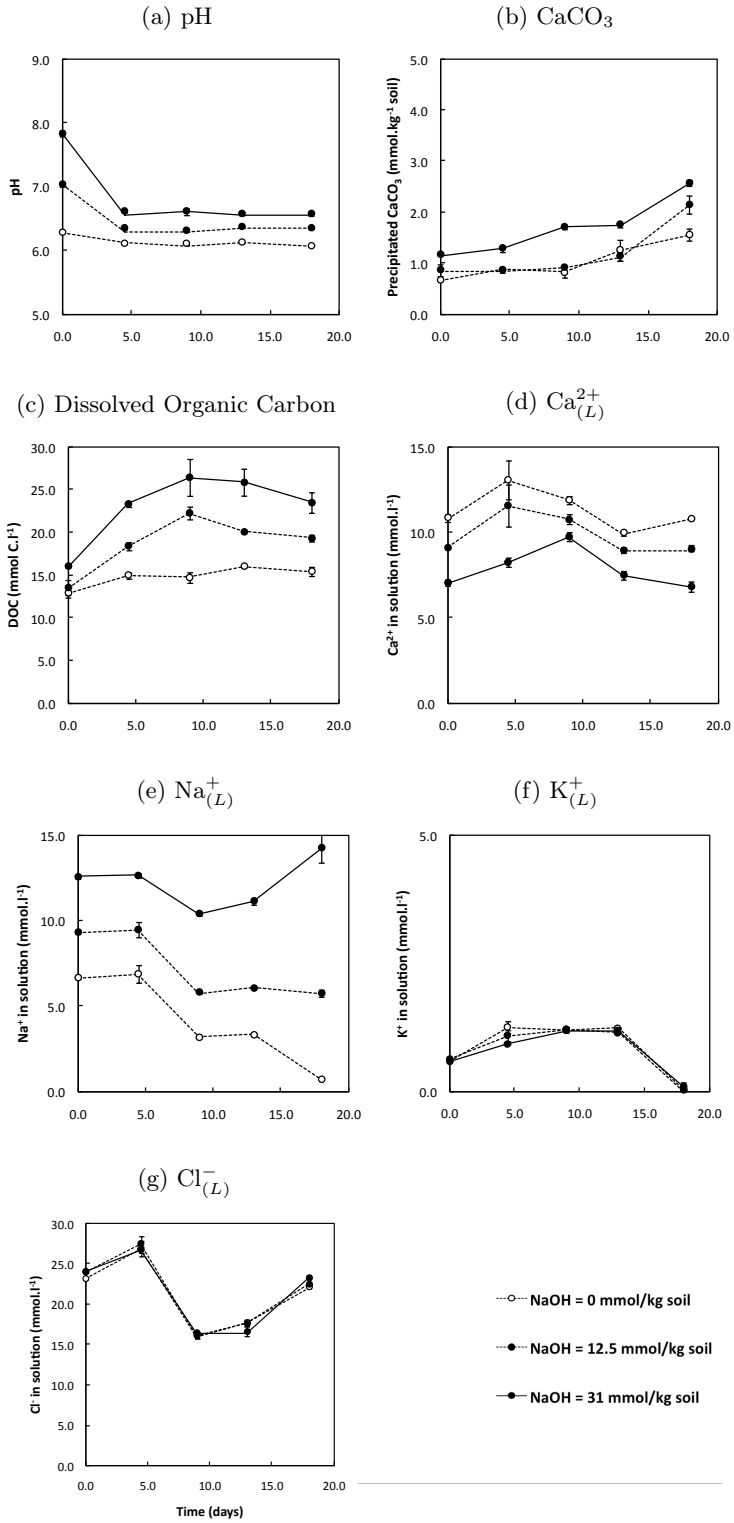

Figure B.1: *Changes over time in experimental soil Ti suspensions with added P = 0.25 mmol.kg^{-1}, after different additions of base (see legend), under 4% carbon dioxide partial pressure. (Points show means (n = 3). When error bars are not visible they are smaller than the data points.)*

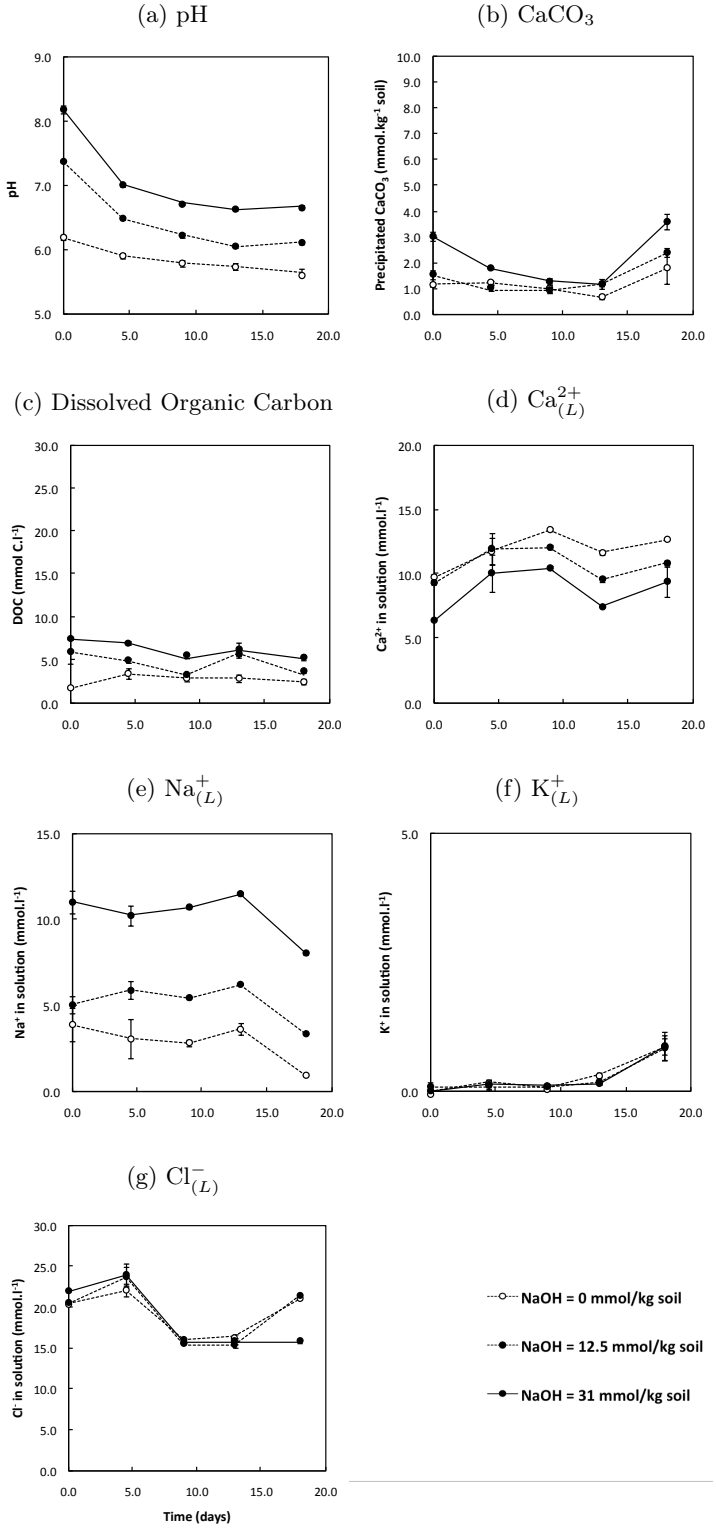

Figure B.2: *Changes over time in experimental soil G suspensions with added P = 0.25 mmol.kg^{-1}, after different additions of base (see legend), under 4% carbon dioxide partial pressure. (Points show means (n = 3). When error bars are not visible they are smaller than the data points.)*

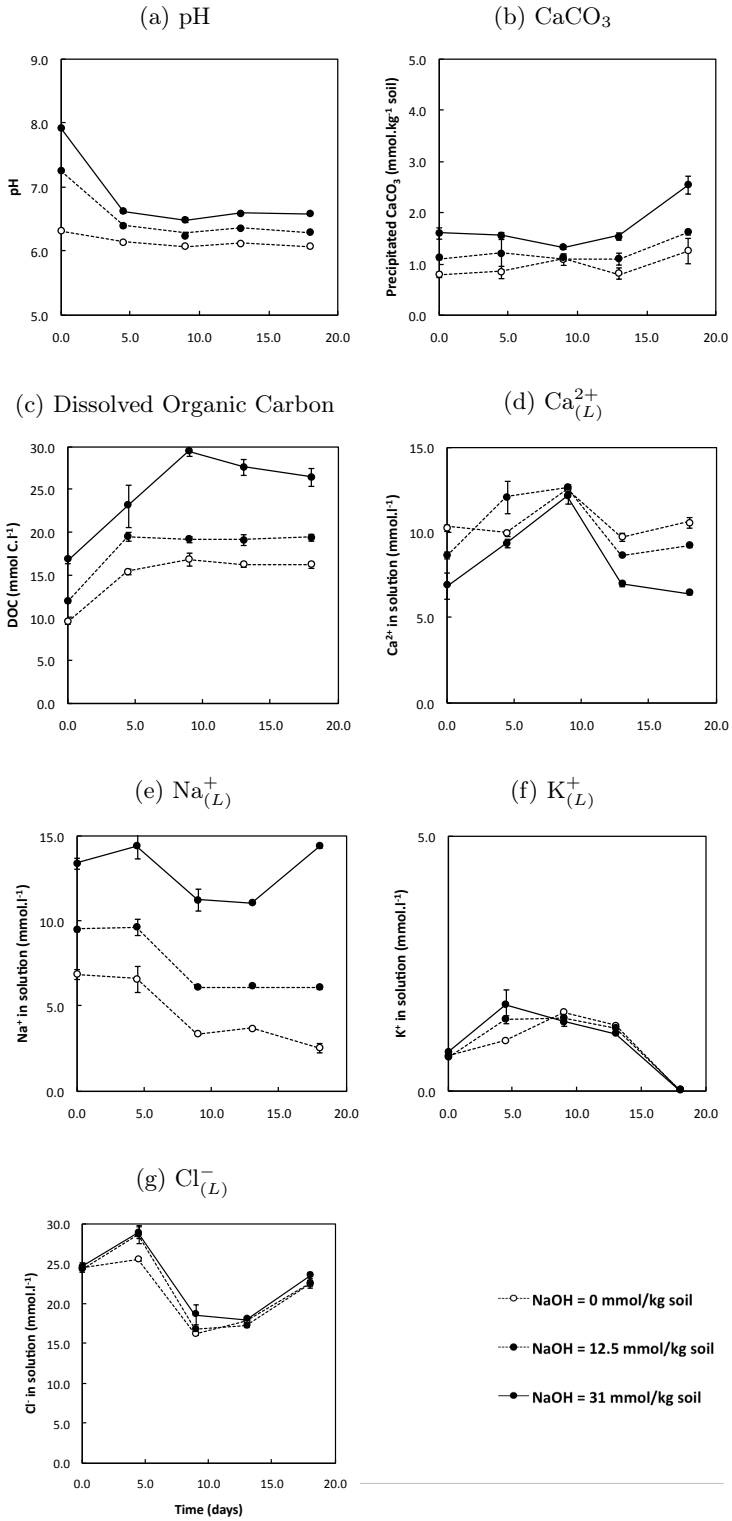

Figure B.3: *Changes over time in experimental soil Ti suspensions with added P = 0.50 mmol.kg^{-1}, after different additions of base (see legend), under 4% carbon dioxide partial pressure. (Points show means (n = 3). When error bars are not visible they are smaller than the data points.)*

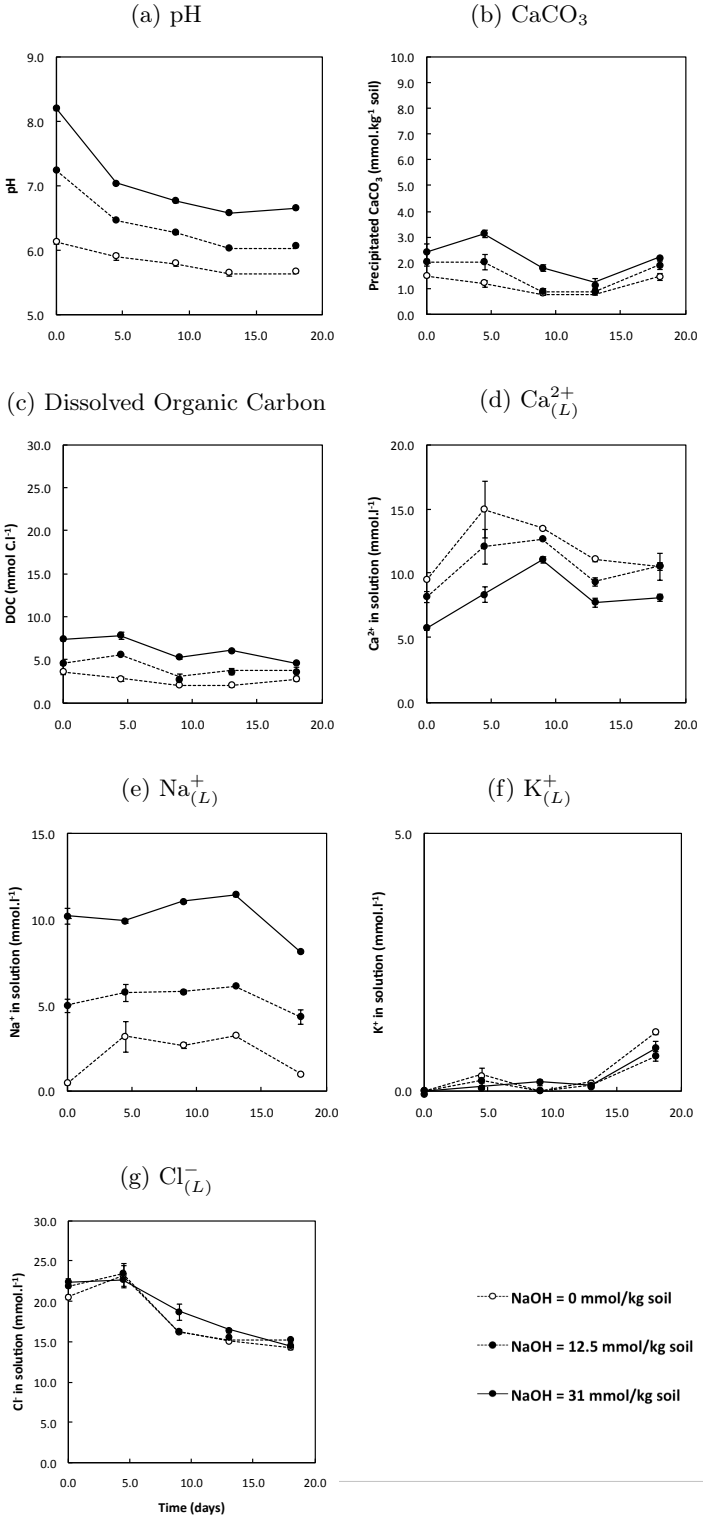

Figure B.4: *Changes over time in experimental soil G suspensions with added P = 0.50 mmol.kg^{-1}, after different additions of base (see legend), under 4% carbon dioxide partial pressure. (Points show means (n = 3). When error bars are not visible they are smaller than the data points.)*

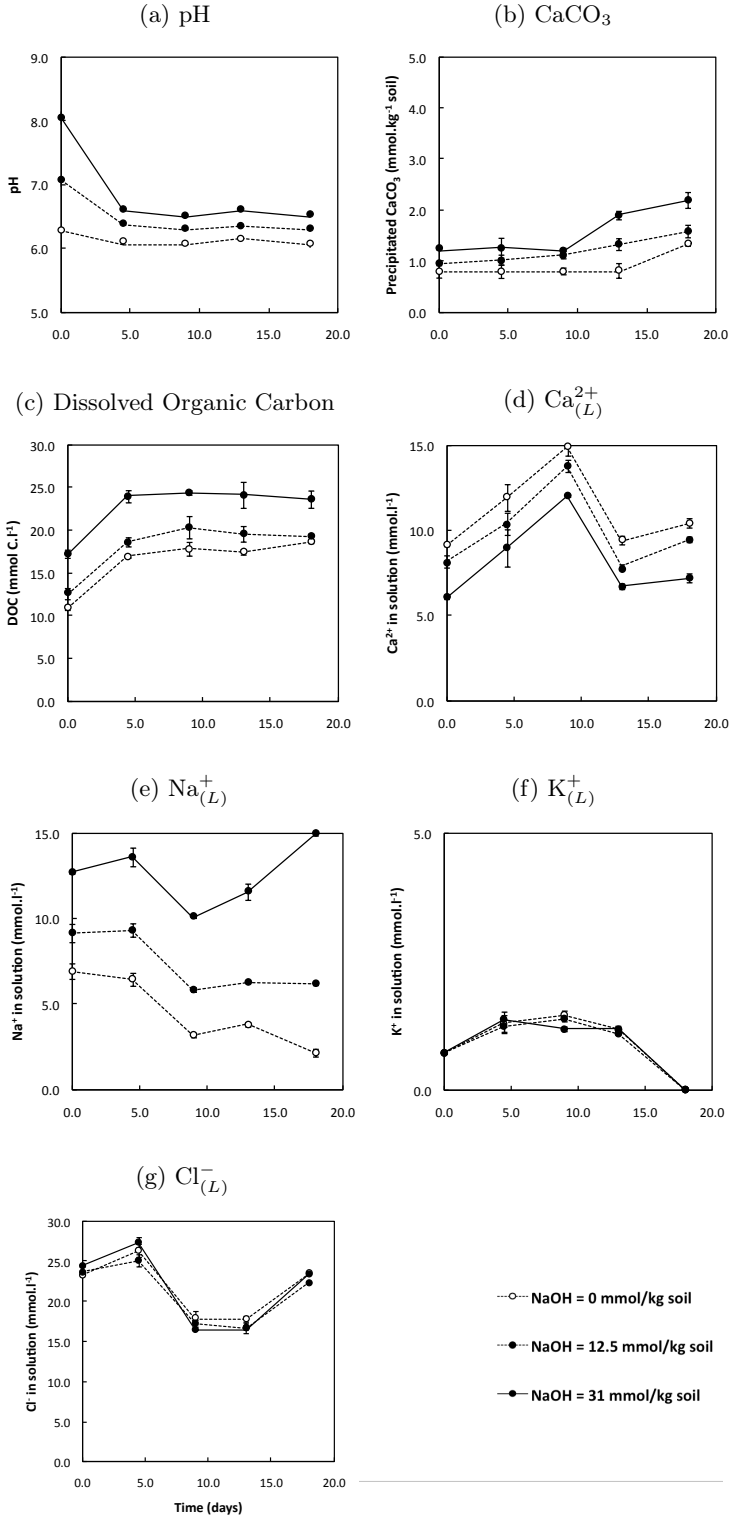

Figure B.5: *Changes over time in experimental soil Ti suspensions with added P = 1.50 mmol.kg^{-1}, after different additions of base (see legend), under 4% carbon dioxide partial pressure. (Points show means (n = 3). When error bars are not visible they are smaller than the data points.)*

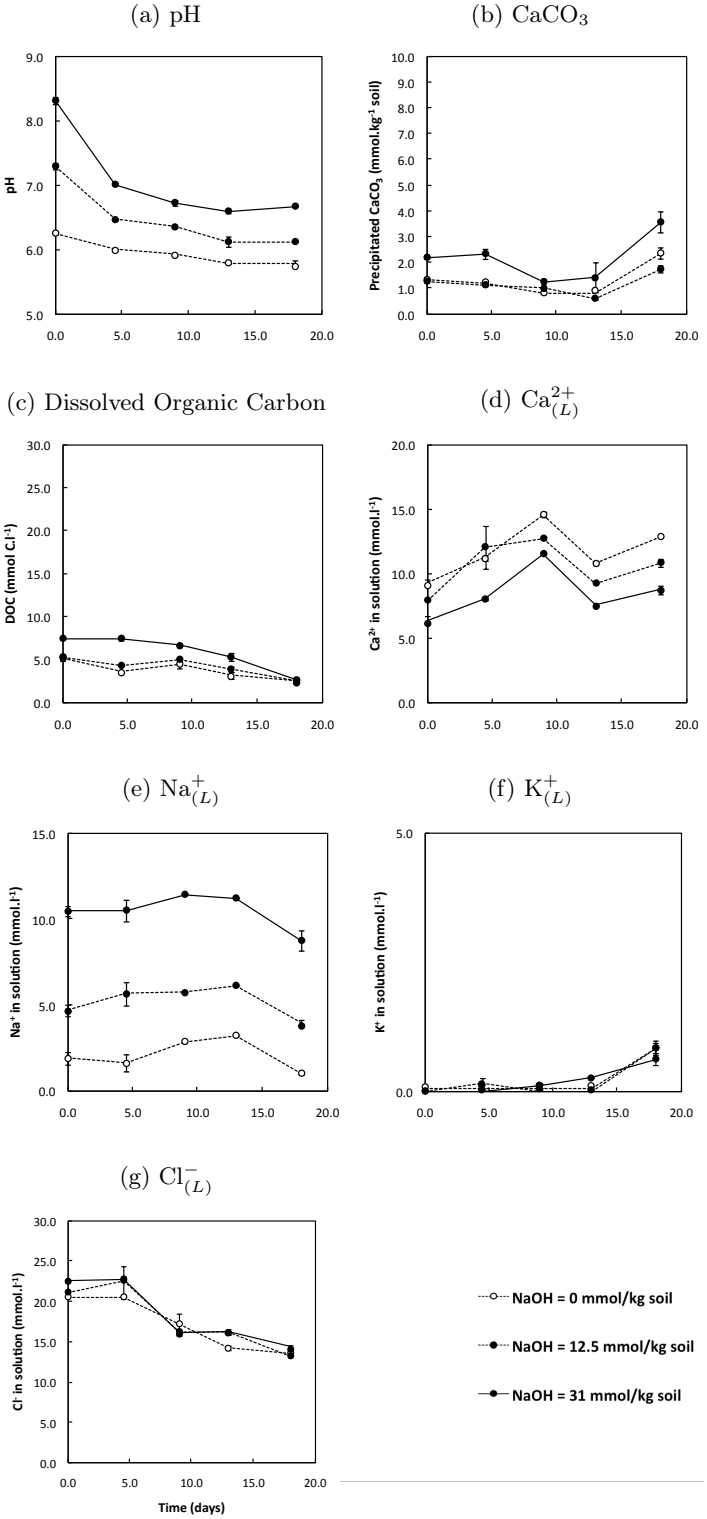

Figure B.6: *Changes over time in experimental soil G suspensions with added P = 1.50 mmol.kg^{-1}, after different additions of base (see legend), under 4% carbon dioxide partial pressure. (Points show means (n = 3). When error bars are not visible they are smaller than the data points.)*

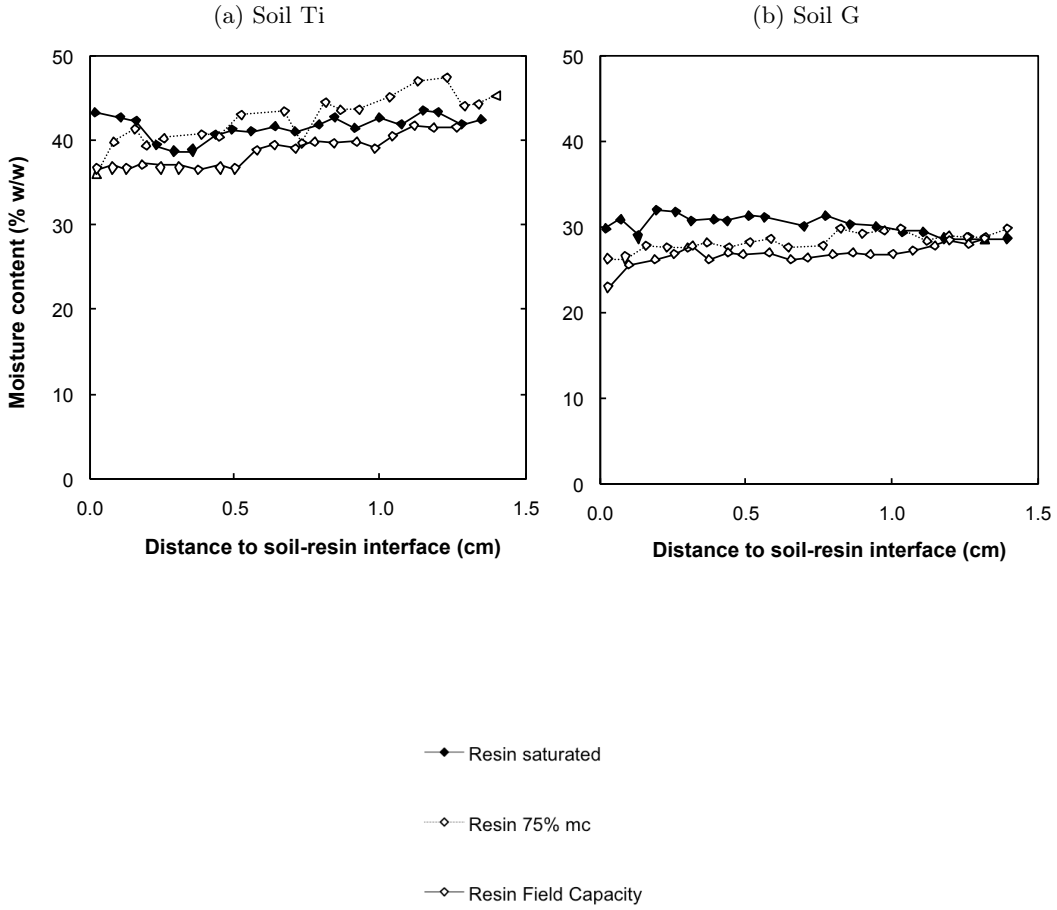

Figure B.7: *Changes in moisture content through sliced soil columns in contact with anion-exchange resin adjusted to three moisture contents: saturated, 75%, and field capacity. (Points show means (n = 3). When error bars are not visible they are smaller than the data points.)*

B.3 Statistical Analysis of the results of community-scale manipulation of soil biota

One day diffusion

Table B.1: *Regression parameters for the concentration-distance profiles after one day diffusion in the Reference soil.*

	Minimum	Maximum	Slope	Spread
pH	5.53	9.37	-4.42	0.95
Ca^{2+}	2.94	24.18	5.94	0.87
Cl^{-}	21.08	45.90	3.77	0.81
$CaCO_3$	1.75	36.83	-16.91	n.a

Table B.2: *Regression parameters for the concentration-distance profiles after one day diffusion in the Sterile soil.*

	Minimum	Maximum	Slope	Spread
pH	5.66	8.77	-4.18	0.85
Ca^{2+}	4.91	29.68	3.62	1.09
Cl^{-}	n.a	n.a	n.a	n.a
$CaCO_3$	1.71	15.97	-30.21	n.a

Table B.3: *Regression parameters for the concentration-distance profiles after one day diffusion in the Prokaryote-inhibited soil.*

	Minimum	Maximum	Slope	Spread
pH	5.45	8.38	-2.70	0.64
Ca^{2+}	4.14	26.24	2.57	0.85
Cl^{-}	31.85	49.40	2.39	0.93
$CaCO_3$	1.62	44.75	-8.85	n.a

Table B.4: *Regression parameters for the concentration-distance profiles after one day diffusion in the Eukaryote-inhibited soil.*

	Minimum	Maximum	Slope	Spread
pH	5.49	8.60	-4.07	0.88
Ca^{2+}	1.29	10.49	3.22	0.69
Cl^{-}	13.05	24.61	3.59	0.36
$CaCO_3$	2.86	105.81	-17.92.n	a.

p-values

Table B.5: *Significant difference between minimum values of pH for each treatment after 1 day diffusion*

	Reference	Sterile	Prokaryote-inhibited	Eukaryote-inhibited
Reference	n/a			
Sterile	0.459	n/a		
Prokaryote-inhibited	0.797	0.440	n/a	
Eukaryote-inhibited	0.873	0.321	0.883	n/a

Table B.6: *Significant difference between maximum values of pH for each treatment after 1 day diffusion*

	Reference	Sterile	Prokaryote-inhibited	Eukaryote-inhibited
Reference	n/a			
Sterile	0.050	n/a		
Prokaryote-inhibited	0.031	0.166	n/a	
Eukaryote-inhibited	0.044	0.395	0.474	n/a

Table B.7: *Significant difference between slopes of pH for each treatment after 1 day diffusion*

	Reference	Sterile	Prokaryote-inhibited	Eukaryote-inhibited
Reference	n/a			
Sterile	0.676	n/a		
Prokaryote-inhibited	0.040	0.012	n/a	
Eukaryote-inhibited	0.530	0.610	0.015	n/a

Table B.8: *Significant difference between spread of pH change through soil for each treatment after 1 day diffusion*

	Reference	Sterile	Prokaryote-inhibited	Eukaryote-inhibited
Reference	n/a			
Sterile	0.310	n/a		
Prokaryote-inhibited	0.147	0.341	n/a	
Eukaryote-inhibited	0.445	0.789	0.272	

Table B.9: *Significant difference between minimum values of Ca^{2+} for each treatment after 1 day diffusion*

	Reference	Sterile	Prokaryote-inhibited	Eukaryote-inhibited
Reference	n/a			
Sterile	0.060	n/a		
Prokaryote-inhibited	0.893	0.262	n/a	
Eukaryote-inhibited	0.090	0.001	0.241	n/a

Table B.10: *Significant difference between maximum values of Ca^{2+} for each treatment after 1 day diffusion*

	Reference	Sterile	Prokaryote-inhibited	Eukaryote-inhibited
Reference	n/a			
Sterile	0.060	n/a		
Prokaryote-inhibited	0.397	0.509	n/a	
Eukaryote-inhibited	0.000	0.000	0.215	n/a

Table B.11: *Significant difference between slopes of Ca^{2+} for each treatment after 1 day diffusion*

	Reference	Sterile	Prokaryote-inhibited	Eukaryote-inhibited
Reference	n/a			
Sterile	0.110	n/a		
Prokaryote-inhibited	0.073	0.303	n/a	
Eukaryote-inhibited	0.079	0.378	0.581	n/a

Table B.12: *Significant difference between spread of Ca^{2+} change through soil for each treatment after 1 day diffusion*

	Reference	Sterile	Prokaryote-inhibited	Eukaryote-inhibited
Reference	n/a			
Sterile	0.089	n/a		
Prokaryote-inhibited	0.411	0.472	n/a	
Eukaryote-inhibited	0.013	0.009	0.362	

Table B.13: *Significant difference between minimum values of Cl^- for each treatment after 1 day diffusion*

	Reference	Prokaryote-inhibited	Eukaryote-inhibited
Reference	n/a		
Prokaryote-inhibited	0.074	n/a	
Eukaryote-inhibited	0.052	0.005	n/a

Table B.14: *Significant difference between maximum values of Cl^- for each treatment after 1 day diffusion*

	Reference	Prokaryote-inhibited	Eukaryote-inhibited
Reference	n/a		
Prokaryote-inhibited	0.152	n/a	
Eukaryote-inhibited	0.000	0.000	n/a

Table B.15: *Significant difference between slopes of Cl^- for each treatment after 1 day diffusion*

	Reference	Prokaryote-inhibited	Eukaryote-inhibited
Reference	n/a		
Prokaryote-inhibited	0.410	n/a	
Eukaryote-inhibited	0.801	0.641	n/a

Table B.16: *Significant difference between spread of Cl^- changes for each treatment after 1 day diffusion*

	Reference	Prokaryote-inhibited	Eukaryote-inhibited
Reference	n/a		
Prokaryote-inhibited	0.720	n/a	
Eukaryote-inhibited	0.001	0.031	n/a

Table B.17: *Significant difference between maximum values of $CaCO_3$ for each treatment after 1 day diffusion*

	Reference	Sterile	Prokaryote-inhibited	Eukaryote-inhibited
Reference	n/a			
Sterile	0.002	n/a		
Prokaryote-inhibited	0.454	0.206	n/a	
Eukaryote-inhibited	0.005	0.002	0.340	n/a

Table B.18: *Significant difference between slopes of $CaCO_3$ for each treatment after 1 day diffusion*

	Reference	Sterile	Prokaryote-inhibited	Eukaryote-inhibited
Reference	n/a			
Sterile	0.296	n/a		
Prokaryote-inhibited	0.032	0.052	n/a	
Eukaryote-inhibited	0.679	0.372	0.026	n/a

Five days diffusion

Table B.19: *Regression parameters for the $CaCO_3$ concentration-distance profiles after five days diffusion*

	Reference	Sterile	Prokaryote-inhibited	Eukaryote Inhibited
$CaCO_{3_0}$	1.564	1.503	2.682	1.672
$CaCO_{3_{max}}$	178.482	18.014	165.341	177.930
Slope	-2.723	-13.349	-9.551	-1.773

Table B.20: *Significant difference between maximum values of $CaCO_3$ for each treatment after 5 days diffusion*

	Reference	Sterile	Prokaryote-inhibited	Eukaryote-inhibited
Reference	n/a			
Sterile	0.001	n/a		
Prokaryote-inhibited	0.611	0.031	n/a	
Eukaryote-inhibited	0.399	0.271	0.437	n/a

Table B.21: *Significant difference between slopes of $CaCO_3$ for each treatment after 5 days diffusion*

	Reference	Sterile	Prokaryote-inhibited	Eukaryote-inhibited
Reference	n/a			
Sterile	0.125	n/a		
Prokaryote-inhibited	0.121	0.493	n/a	
Eukaryote-inhibited	0.349	0.013	0.044	n/a

After a five-day diffusion time, profiles of pH, Ca^{2+} and Cl^{-} were found to be significantly different (Figures B.8)

Cell No.	Treatement	{1} 6.9849	{2} 7.6655	{3} 6.5974	{4} 8.8596
1	Reference		0.00	0.000000	0.00
2	Sterile	0.000000		0.000000	0.00
3	Bactericide	0.000000	0.00		0.00
4	Fungicide	0.000000	0.00	0.000000	

Cell No.	Treatement	{1} 7.9299	{2} 6.6239	{3} 7.2137	{4} 4.0392
1	Reference		0.000000	0.002356	0.00
2	Sterile	0.000000		0.011988	0.00
3	Bactericide	0.002356	0.011988		0.00
4	Fungicide	0.000000	0.000000	0.000000	

Cell No.	Treatement	{1} 32.887	{2} 46.538	{3} 26.798	{4} 65.761
1	Reference		0.00	0.00	0.00
2	Sterile	0.00		0.00	0.00
3	Bactericide	0.00	0.00		0.00
4	Fungicide	0.00	0.00	0.00	

Figure B.8: *ANOVA results for pH- and solutes concentration-distance profiles using Statistica to compare microbial treatments. The table show p-values.*

Appendix C

Exchangeable Calcium in Calcareous Soils

C.1 Introduction

Several attempts have been made at defining the properties of calcareous soils and the influence of calcium carbonate on biochemical reactions in soils (Anter et al., 1973). Whether the focus of the studies is the sorption of heavy metals, plant growth or their nutrients (such as phosphorus and iron) uptake, and whatever their results, the general agreement is that calcium carbonate has a major role to play in different reactions in soils, mainly due to its very reactive surface and its role as a source of very common and reactive ions.

Many loess soils and soils derived from calcareous parent materials such as the ones found on top of the white cliffs on the South coast of England can contain 30% of calcium carbonate (Yaalon, 1957). This poses a problem when analysing the common properties of these soils as most common soil testing methods have not been developed for highly calcareous soils and applying such methods to highly calcareous soils can easily lead to erroneous results.

Measuring the cation exchange capacity (CEC) of a soil and its exchangeable cation content is fundamental to assessing the amount of cations that can readily be desorbed from the soil exchange complex and by doing so, compete with other ions, and take part in equilibria of interest. It is however difficult to accurately assess as the sorbtion of ions to soil particles is a reversible parameter.

All methods developed to measure CEC and the exchangeable cations content of soils rely on solutions saturated with ions such as barium which will compete with and eventually displace cations sorbed on soil particles. In such highly electrolyte solutions, the solubility of carbonate minerals is highly increased. In calcareous soil, precipitated calcium carbonate can be dissolved during the steps necessary to extract calcium and other cations from soils cation exchange complex. This leads to erroneous, often overestimated, results, as it is impossible to distinguish between calcium desorbed from soil particles and calcium ions dissolved from calcium carbonate after the extraction steps in the final measurement.

There have been several attempts by soil scientists at developing other methods than the standard ones to accurately measure calcareous soils exchangeable calcium content and cation exchange capacity.

After a quick review of some of the most popular existing methods, the two objectives of this section are to verify the accuracy and reliability of exchangeable calcium measurements using a selected method, then to investigate the possibility of combining the measurement of calcium carbonate and exchangeable calcium in a single method. This is imperative if the two analyses are to be performed on the small samples produced with the diffusion experimental system introduced in previous sections of this chapter.

C.2 Existing methods

Ammonium salts (Tucker 1954)

Using ammonium salts (such as ammonium chloride or ammonium acetate) in alcoholic solution (generally 60% ethanol) is one of the first method described as suitable to get accurate results for exchangeable ions in calcareous soils (Tucker, 1954).

Ammonium acetate and the triethanolamine buffered barium chloride extraction solutions are the two most common and widely used methods for non calcareous soils. They are often used as reference methods.

However the ammonium acetate washing step is followed by a rinse in deionised water which has to be carefully performed to remove excess ammonium acetate before the exchange with sodium ions. The displaced ammonium ions are then measured to estimate cation exchange characteristics. The numerous successive steps make the method output results variable, dependent on the rinsing conditions (Ammann et al., 2005).

Tucker (1954) nevertheless insists that ammonium chloride is better than ammonium acetate

as an exchange ion, stating that if the ammonium chloride extraction solution (in 60% ethanol) is buffered at pH 8.5 with ammonia, the solubilities of both calcite and dolomite are limited. The method was tested on soils in equilibrium with carbonates though, as opposed to soils containing any mineral phase.

Since then, several papers have found that this method is not adapted to soils containing any carbonate minerals (Dohrmann, 2006c). Indeed, the method relies on a high surplus of ammonium ion to get a complete exchange with cations adsorbed onto soil particles, and the stability of minerals such as $CaCO_3$ decreases in an electrolyte rich solution.

Lithium formate and lithium acetate

In the same way Tucker (1954) compares ammonium chloride and acetate, the method presented by Misopolinos and Kalovoulos (1983) using lithium (as lithium formate) as exchange cation is compared in their paper with another method using lithium as the exchange cation in a lithium acetate solution.

Their results suggest that the dissolution of calcium carbonate during saturation process is higher when using a lithium acetate exchange solution buffered at pH = 8.2, and that a lithium formate exchange solution is a reliable method to evaluate exchangeable cations contents and the cation exchange capacity of non saline calcareous soils.

However, lithium modifies the density of charge at the particles surface by moving between clay platelets, leading to erroneous results for cation exchange capacity and exchangeable cations content .

Barium Chloride in triethanolamine buffered solution

The barium chloride ($BaCl_2$) method is the most widely accepted method as the British Standard (BS 7755-3.12:1996) *Determination of the potential cation exchange capacity and exchangeable cations using barium chloride solution buffered at pH = 8.1.*

However, the extraction of exchangeable cations from a calcareous soil exchange complex is notoriously as problematic with this method as with the previous four. Calcium carbonate reacts with barium in the extraction solution to precipitate witherite ($BaCO_3$), leading to overestimation of both CEC and exchangeable calcium.

Adaptations of this method have been tried to overcome the problem, mainly by attempting to minimise the dissolution of carbonates, however only successful in certain types of samples. Reducing the extraction steps length for instance, lead to a partial extraction of exchangeable calcium from samples rich in vermiculite and illite, while the "compulsive exchange method" tried to minimise exchange competition in the reexchange step with magnesium (Mg^{2+}) by washing samples in an excess of barium, but relied heavily on a precise measurement of Mg^{2+} (Dohrmann, 2006b), which proved the method unreliable too.

An adaptation of the barium chloride extraction method is however attractive because it is, as previously mentioned, the most widely accepted and successful method.

Cationic exchange complexes

Rather than flushing soils exchange complex with a high surplus of exchange cation like Ba^{2+}, some more recent methods tried and rely on cationic exchange complexes with an affinity for soils exchange sites higher than that of cations such as Ca^{2+} and Ba^{2+}. Such exchange complexes include silver thiourea (Dohrmann, 2006c,a,b) and copper complexes (Bergaya and Vayer, 1997;

Ammann et al., 2005), such as Cobalt (III) hexamine, Copper (II) ethylenediamine, Copper (II) triethylenetetramine and Copper (II) tetraethylenepentamine.

Because of the high affinity of such molecules for soil exchange sites, the extraction protocol is relatively simple, and consists in a single exchange step, followed by centrifugation and the measurement of the final exchange molecule concentration in the supernatant by spectrophotometry.

C.3 Method investigation - Silver thiourea

Introduction

The silver thiourea (Ag-TU) method was developed and readjusted in three consecutive papers written by Dohrmann (2006a, b, c), to allow accurate measurements of soil cation exchange capacity and exchangeable cations in calcareous soils and clay minerals.

The aim of this subsection is to quantify the influence of soluble $CaCO_3$ minerals on the silver thiourea method described by Dohrmann (2006b) by testing it on a non-calcareous soil amended with increasing amounts of $CaCO_3$. Silver thiourea (AgTU), a metal-organic complex has been chosen for its particularly high selectivity for soils exchange sites, and the further absence of stable complexation between uncharged thiourea and more basic cations such as Ca^{2+} after the exchange step of the method. Ca^{2+} on exchange sites is displaced by Ag^{2+} and saturate the soil solution preventing any precipitated $CaCO_3$ present from dissolving. The extraction solution is also saturated with calcite to shift the equilibrium of the calcium carbonate precipitation reaction and thus prevent any $CaCO_3$ from precipitating.

The aim of this experiment is to check that the calcite silver thiourea method can be used with more accuracy than the standard $BaCl_2$ method in calcareous samples. Additionally, the experiment will be used to check a method for measuring $CaCO_3$ in the soil following the exchangeable Ca^{2+} determination with silver thiourea.

If the method presented by Dohrmann in his three consecutive papers is reliable on calcareous samples, this experiment will verify the two hypotheses below:

1. the result for sample 1 (non calcareous) using a Ag-TU extraction solution agrees with the British Standard barium chloride method.
2. the calcite saturated Ag-TU method does not dissolve $CaCO_3$ in the sample tested, hence the addition of $CaCO_3$ to the soil does not influence the measurement of exchangeable calcium. The content in exchangeable calcium in samples 2 to 6 thus correspond with sample 1 and the initial amount extracted using $BaCl_2$ too.

Materials and methods

Reagents

1. Calcite saturated silver thiourea exchange solution: prepare 2L at a time, in a volumetric flask, following strict procedure (see Dohrmann 2006 b and c). The extraction solution should not be stored for more than 72h.
    - 15.2 g thiourea (M=76.1 $g.mol^{-1}$) in 1400 ml deionised water
    - 3.397 g $AgNO_3$ in 300 ml deionised water: add slowly (within 2 min) while stirring vigorously.
    - Add 200 ml ammonium acetate solution (c = 1 M)

- Fill the volumetric flask to 2 L.
- Transfer into a 2 L beaker. Add 1 g calcite. Stir vigorously for 2 hours.
- Leave to settle overnight. Filter to remove calcite undissolved.
- Use within 48 hours.

2. Nitric acid HNO_3 solution 0.5 M.

Procedure

A non-calcareous experimental soil, referenced 15D, is chosen from the NSRI soils archive. Its calcium carbonate content is checked qualitatively by dropping hydrochloric acid on sieved dry soil. The experimental soil 15D is a sandy loam of initial pH 5.6, and cation exchange capacity (CEC) measured when it was sampled in buffered $BaCl_2$ 0.058 $mol_c.kg^{-1}$.

To simplify its exchange complex the soil is washed repetitively in calcium chloride ($CaCl_2$ 10 mM), then sieved to 0.5 mm (see protocol in section 4.2.1).

To test the influence of $CaCO_3$ content of a soil on the accurate measurement of exchangeable calcium, the soil is spiked with known amounts of $CaCO_3$, according to Table C.1. Each sample contains the same amount of soil: 1g (+/- 0.0005g) accurately weighed into 85 ml centrifuge tubes, adjusted to contain 0, 1, 2, 5, 10, 20% $CaCO_3$, each treatment replicated three times. A blank, without soil or $CaCO_3$, is also prepared in triplicates.

After shaking for 2 hours on an end-over-end shaker in 50 ml of silver thiourea extraction solution, each tube is centrifuged 10 minutes at 4500 rpm. 100 μl of supernatant is diluted in 10 ml volumetric flasks already containing 1 ml HNO_3 (0.5 M), with deionised water. The calcium concentration in the diluted supernatant is measured by Atomic Adsorption Spectrophotometry (AAS).

Table C.1: *Composition of samples.*

Sample	Soil (g)	$CaCO_3$ ($mol.kg^{-1}$)
1	1	0.0
2	1	0.1
3	1	0.2
4	1	0.5
5	1	1.0
6	1	2.0

Additionally, the exchangeable cation content is measured in unamended soil (sample 1) following the British Standard method using a barium chloride ($BaCl_2$) extraction solution buffered at pH 8.2 with triethanolamine.

To check that no further calcite dissolution or precipitation prevents a correct measurement of exchangeable Ca^{2+}, the soil cake residual from the Ag-TU extraction is transferred into a sealed bottle, and 5 ml of HCl (1M) added with a syringe through the seal. The samples are then shaken for 15 minutes and the CO_2 in each bottle measured by gas chromatography (GC).

The soil cake is weighed prior to the addition of acid, to estimate the amount of calcite saturated extraction solution left after centrifugation, and calculate the exact amount of $CaCO_3$ there should be in the sample. The amount of CO_2 measured should correspond to the amount of calcium carbonate calculated for each sample.

Results and discussion

The exchangeable calcium content of the experimental soil, measured with barium chloride is 0.045 $mol_c.kg^{-1}$. The soil being non calcareous (checked with HCl prior extraction), this value is accepted as the accurate exchangeable calcium content of the soil.

The calcium content in the other samples is presented in table C.4 below, along with the

measurements of calcium carbonate in each sample after the extraction.

Table C.2: *Results.*

Sample	$Ca^{2+}_{exch.}$ ($mol_c.kg^{-1}$)	$CaCO_3$ ($mol.kg^{-1}$)
1	0.028 (± 0.009)	0.000 (± 0.006)
2	0.047 (± 0.008)	0.009 (± 0.004)
3	0.032 (± 0.006)	0.097 (± 0.008)
4	0.038 (± 0.008)	0.323 (± 0.011)
5	0.039 (± 0.006)	0.755 (± 0.022)
6	0.052 (± 0.007)	1.386 (± 0.025)

The output results for exchangeable calcium are not so different to completely dismiss the method. However, the variability is sufficient to doubt its use to get an accurate calcium balance on soil samples with increasing $CaCO_3$ amounts.

After the extraction $CaCO_3$ measured in the sample is expected to be over the amount added to the soil, because of the excess calcite saturated extraction solution that has not completely been removed from the soil cakes. However, according to Table C.4, the results are significantly underestimated. A partial dissolution by HCl is not considered as the reaction is instantaneous and HCl is added in considerable excess.

In sample 1 the minute amount of $CaCO_3$ added to the sample is more difficult to detect from the instrument background noise, which could account for the error found. All the calcium carbonate in sample 6 should however be recovered and detectable: it is on the contrary the sample relatively the most underestimated, with less than 70% of the total added $CaCO_3$ recovered after the extraction of exchangeable cations.

In his third paper (Dohrmann, 2006b), Dohrmann compares exchangeable calcium measurements in $CaCO_3$-bearing and $CaCO_3$-free bentonites and clayey sediments using the same Ag-TU extraction solution. He concludes that results are not significantly different for the calcareous

and non calcareous samples for either bentonites or clayey sediments. However, the scatter of result points around the fitted regression line is more dispersed for clayey sediments than for bentonites, and for exchangeable calcium than for any other exchangeable cation (Na^+, K^+ and Mg^{2+} were tested). It might be possible that some processes in live soils interfere with exchangeable Ca^{2+} measurements and have not been taken into consideration because the method was tested on mineral samples.

Summary

This test of Dohrmann's silver thiourea method for CEC and exchangeable cations measurement in soils found that, on the contrary to the hypotheses made, exchangeable Ca^{2+} output results for samples 1 to 6 do vary and do not correspond to the result of the standard $BaCl_2$ extraction method.

The calcite saturated silver thiourea extraction solution and method developed by Dohrmann does not give results for exchangeable calcium in soils that are accurate enough to be used in a calcium balance between samples with varying amounts of precipitated calcium carbonate.

Furthermore, an accurate estimation of solid $CaCO_3$ is of crucial importance in the main diffusion experiment. This method is however not adaptable to allow for samples to be used for such measurements.

Alternatively, the solid portion of the slices could be split after centrifugation to measure Ca^{2+}_{exch} and $CaCO_3$ independently. This has not been tested, but because of the limited size of the samples (barely more than 1 g), it is expected that the error found in Dohrmann's exchangeable calcium results would increase. This applies to precipitated $CaCO_3$: its precipitation being localised around a nucleation point, splitting the sample would lead to underestimating precipitated phases.

The calcite saturated silver thiourea method will thus not be used further as part of this study.

C.4 Method development - Acidified $BaCl_2$

Introduction

Despite its well known shortcomings for the analysis of calcareous samples, the barium chloride ($BaCl_2$) British Standard method (BS-7755) still is the most commonly used and accepted procedure to measure cation exchange capacity (CEC) and extract exchangeable cations from soils exchange complex.

Most methods described in the literature try to overcome the problem posed by the increased solubility of carbonate solid phases in electrolyte solutions such as are necessary to desorb exchangeable cations on soil particles. Adaptations of the method try and compensate the solubility increase by changing the extraction solution properties to limit the dissolution of solid phases.

In this section however, the approach tries to overcome the error introduced in exchangeable calcium by measuring the amount of $CaCO_3$ dissolved. The adapted method would thus allow for simultaneous measurement of $CaCO_3$ and exchangeable Ca^{2+} in the same experimental protocol. To dissolve all $CaCO_3$ present in the samples, this method uses an acidified $BaCl_2$ extraction solution as opposed to a buffered one.

The hypothesis is that the amount of exchangeable Ca^{2+} is the difference between final Ca^{2+} measurement in the supernatant and Ca^{2+} from $CaCO_3$ dissolution (measured by GC).

Materials and method

Reagents

1. Calibration stock solution: 5.0 ml calcium standard (1000 ppm) into a 100 ml volumetric flask. Fill to the mark with deionised water.
2. Extraction solution:
   - Barium chloride solution: 244 g $BaCl_2.H_2O$ in 1000 ml volumetric flask. Fill to the mark with deionised water
   - Hydrochloric acid 1 M: 83 ml concentrated acid ($\rho = 1.19$ g/ml) in 1000 ml volumetric flask. Fill to the mark with deionised water.
   - Mix equal volumes of the two solutions above.
3. Hydrochloric acid 1 M: 83 ml concentrated acid in 1000 ml volumetric flask. Fill to the mark with deionised water.

Procedure

This extraction solution is tested on the same soil as previously (15D) as well as four other soils (see Table C.3), calcareous and non calcareous. Samples are prepared in the same way as previously (see Table C.1), however sample 6, the highest addition of $CaCO_3$, was dropped. The initial presence or absence of $CaCO_3$ has been tested with hydrochloric acid, and soils CEC and exchangeable calcium content independently measured following the standard $BaCl_2$ extraction.

All samples are prepared in three replicates.

Table C.3: *Soils tested and CEC measured in triethanolamine buffered $BaCl_2$ extraction solution.*

Soil	Soil texture	CEC ($mol_c.kg^{-1}$)
15D	Sandy loam	0.058
8E	Sandy loam	0.230
T	Loam	0.149*
4E	Sandy clay loam	0.080
10G	Sandy loam	0.049

* T was sampled from Pegwell Bay, Kent. It sits on a chalky parent material, and has a high initial $CaCO_3$ content. This CEC value, measured with $BaCl_2$, is probably overestimated.

Each tube is sealed tight and 5 ml of acidified extraction added with a syringe through the seal. After shaking for an hour both as a first extraction step and to dissolve all precipitated calcium carbonate, the concentration in CO_2 in the headspace of the tubes is measured by GC.

All tubes are then centrifuged (10 min, 3000 rpm), and the supernatant transferred in 20 ml volumetric flasks. The extraction step is repeated twice, and the supernatant transferred each time in the same volumetric flask. After the third extraction, the volumetric flasks are filled to the mark with acidified $BaCl_2$ extraction solution. The extracts are then mixed and filtered.

After filtration, 1.0 ml of extract is into 10 ml volumetric flasks, 1.0 ml of hydrochloric acid solution (1 M) added and the flasks filled to the mark with deionised water. The total calcium concentration is measured by AAS.

the hypothesis is that the total calcium content comes from both the exchangeable soil complex and dissolved calcium carbonate.

The exact amount of calcium carbonate dissolved into solution is calculated from the GC measurements of CO_2, and subtracted from the total calcium content measured by AAS: the difference should correspond to the exchangeable calcium content of the soil.

Results and discussion

Only the results for 15D are presented here. Similar tables are presented in Appendix C.5 for the other soils.

Table C.4: *Results for soil referenced 15D.*

Sample	$Ca^{2+}_{exch.}$ ($mol_c.kg^{-1}$)	$CaCO_3$ ($mol.kg^{-1}$)
1	0.078 (± 0.002)	0.005 (± 0.001)
2	0.038 (± 0.010)	0.120 (± 0.006)
3	0.063 (± 0.010)	0.215 (± 0.006)
4	0.283 (± 0.011)	0.522 (± 0.012)
5	0.432 (± 0.007)	1.040 (± 0.031)

This method gives accurate results for calcium carbonate, in accordance with the amounts added to the soil.

However, the values for exchangeable calcium are more variable than with the silver thiourea extraction solution and are overestimated by an order of magnitude for $CaCO_3$ contents of 0.5 $mol.kg^{-1}$ and above. No explanation could be found for the scale of the error, so the same samples were measured by Inductive Coupled Plasma Atomic Emission Spectroscopy (ICP-AES) in the British Geological Survey (BGS) laboratories to double check the results. The results are shown in Table C.5.

Table C.5: *Exchangeable calcium in soil 15D measured by ICP-AES.*

Sample	$Ca^{2+}_{exch.}$ ($mol_c.kg^{-1}$)
1	0.046 (± 0.001)
2	0.037 (± 0.004)
3	0.038 (± 0.002)
4	0.039 (± 0.008)
5	0.075 (± 0.027)

The results are more consistent with each other and the initial exchangeable calcium content of soil 15D measured with the $BaCl_2$ standard extraction method. However, they still get elevated at higher $CaCO_3$ contents. This is verified with the other soils tested, especially those with a high initial calcium carbonate content (cf. Appendix C.5).

The high dilutions necessary to measure Ca^{2+} by AAS might partially explain the errors found previously.

The difference in techniques might further explain the better results measured by atomic emission spectroscopy (AES). In AAS, the electrons of an atom are excited to a higher electronic orbital by shining a ray of light on the solution nebulised in a flame at the wavelength corresponding to the atom of interest: calcium is measured at 455.77 nm. How much light has been absorbed from the light source when the electrons change orbital to an excited state is measured by a spectrometer on the other side of the flame. The cathode lamps used to provide the light have a very narrow bandwidth, limiting the overlapping of 2 different elements' absorption lines. However, bigger molecules have wider bandwidths that can overlap with a single element's. This could explain the large overestimation of Ca^{2+} in filtrates measured by AAS.

The overlapping is more limited in an AES, where, after exciting the electrons in the structure of the atom, it is the light emitted when they go back to a lower energy state that is measured by spectroscopy.

Summary

The method developed and tested here does give a way to accurately measure the calcium carbonate in a sample, but does not successfully address the issue of variability in the exchangeable calcium results.

To identify the cause of this variability and resolve the problems encountered, further work and time are necessary.

C.5 Conclusions

After testing the most recent calcite saturated silver thiourea extraction solution published in 2006 (Dohrmann, 2006a,b,c), this project tried and develop a method combining the measurement of $CaCO_3$, and exchangeable calcium.

The unreliability of the results for exchangeable calcium produced by either methods proved incompatible with the production of an accurate calcium balance sheet. Measuring calcium carbonate on the same soil sample following the extraction of exchangeable calcium in Dohrmann's method does not produce reliable enough data for either species, and while the acidified $BaCl_2$ extraction solution tested produces accurate results for $CaCO_3$, exchangeable calcium is still much overestimated. Splitting the soil samples to conduct both extractions separately was not feasible because of the limited amount of sample available from the main diffusion experiment for which these methods were investigated.

The development of a new method that would allow for the measurement of both calcium carbonate and exchangeable calcium in the same sample was thus abandoned for lack of time. The small amount of sample produced meant that only $CaCO_3$ could be measured: quantifying the amount f precipitation in a structured soil system is more important than exchangeable calcium for the validation of the mathematical model.